Review

Harnessing Transition Metal-Chalcogenides for Efficient Performance in Magnesium-Sulfur Battery: Synergising Experimental and Theoretical Techniques

Hassan O. Shoyiga * and Msimelelo Siswana

Posted Date: 27 October 2025

doi: 10.20944/preprints202510.1895.v1

Keywords: transition metal chalcogenide; Magnesium-sulfur batteries; DFT; artificial intelligence; energy storage

Review

Harnessing Transition Metal-Chalcogenides for Efficient Performance in Magnesium-Sulfur Battery: Synergising Experimental and Theoretical Techniques

Hassan O. Shoyiga * and Msimelelo Siswana

Faculty of Natural Sciences, Department of Applied Science, Walter Sisulu University, Old King William Town Road, Potsdam Site, East London 5200, South Africa

* Correspondence: hshoyiga@wsu.ac.za

Abstract

Magnesium-sulfur (Mg-S) batteries constitute a novel category of multivalent energy storage systems, including enhanced theoretical energy density, material availability, and ecological compatibility. Notwithstanding these benefits, practical implementation continues to be hindered by ongoing issues such as polysulfide shuttle effects, slow Mg^{2+} transport, and significant interfacial instability. This study emphasises recent progress in utilising transition metal chalcogenides (TMCs) as cathode materials and modifiers to overcome these challenges. We assess the structural, electrical, and catalytic characteristics of TMCs such as MoS_2, $CoSe_2$, WS_2, and TiS_2, highlighting their contributions to improving redox kinetics, retaining polysulfides, and enabling reversible Mg^{2+} intercalation. The review synthesises results from experimental and theoretical studies to offer a thorough comprehension of structure-function interactions. Particular emphasis is placed on morphological engineering, modulation of electronic conductivity, and techniques for surface functionalisation. Furthermore, we examine insights from density functional theory (DFT) simulations that corroborate the observed enhancements in electrochemical performance and offer predictive direction for material optimisation. This paper delineates nascent opportunities in AI-enhanced materials discovery and hybrid system design, proposing future trajectories to realise the potential of TMC-based Mg-S battery systems fully.

Keywords: transition metal chalcogenide; Magnesium-sulfur batteries; DFT; artificial intelligence; energy storage

1. Introduction

The rise in energy consumption, coupled with the ongoing depletion and carbon emissions associated with finite non-renewable energy sources, underscores the critical importance of energy production and storage from sources that are renewable for various contemporary innovations [1]. There is a growing emphasis on the development and investigation of innovative materials for energy storage systems, motivated by the advancement of sustainable development objectives. The limited availability of conventional energy sources, including oil, coal, and natural gas, drives this transition. Given the challenges outlined, the fact that their sources are renewable are recognised as a paradigm for decreasing our reliance on non-renewable energy sources. Nonetheless, the generation of sustainable energy is not constant; therefore, the implementation of renewable energy sources requires the utilisation of effective and dependable energy storage systems [2]. Contemporary smart and wearable electronics, including personal computers, mobile cell and various health and well-being monitoring apparatus, owe their existence to advances in electrochemical energy storage technologies, such as fuel cells, batteries, and supercapacitors [3]. An electrochemical device known

 doi:10.20944/preprints202510.1895.v1

as a fuel cell converts chemical energy directly into electricity, utilising hydrogen and oxygen as its fuel sources. When compared to alternative electrochemical (EC) energy storage (ES) devices, these demonstrate exceptionally high energy densities. In a supercapacitor, electrical energy is accumulated at the interface between the electrolyte and the electrode [4]. A significant benefit of a supercapacitor is its elevated specific energy; it also demonstrates encouraging specific power. Batteries utilise electrochemical reactions for energy storage and are distinguished by their remarkable energy density. Nonetheless, they face constraints due to low power densities [5]. Furthermore, each of these electrochemical storage technologies possesses a distinct mechanism for charge retention. Figure S1 illustrates a standard device structure for (a) the fuel cell, (b) the battery, and (c) the supercapacitor, highlighting the electrolyte, cathode, anodes, and separator, which constitute the primary components. The Ragone plot in Figure S2 (a) illustrates the comparison of different electrochemical storage devices based on their specific power density and specific energy. To ensure the effectiveness of electrochemical storage systems, it is crucial that the electrode material and electrolyte medium exhibit outstanding electronic and ionic transport properties.

The increasing need for efficient, renewable, and safe energy storage devices has led researchers to explore rechargeable batteries that exceed the capabilities of traditional Li^+-ion batteries. The potential of Mg-S batteries as a post-Li^+-ion battery solution is significant, considering the high availability of magnesium in the Earth's crust and seawater, thereby making it a more sustainable and scalable ES alternative. Additionally, Mg-S batteries present multiple benefits, such as elevated volumetric energy density, economic viability, and eco-sustainability [6]. Mg-S batteries have garnered considerable interest as a viable option for next-generation ES solutions. Sulfur provides advantages, including abundance, low cost, and non-toxicity, while magnesium serves as a safe metal anode, thereby increasing the value of this battery system. Additionally, the high theoretical capacity of the S cathode allows Mg-S batteries to attain notable gravimetric (1.68×10^3 Wh kg^{-1}) and volumetric energy densities (3.2×10^3 Wh L^{-1}) [7]. EC kinetics of conversion-type S cathodes are determined by two main features: the rate of charge transfer during S redox reactions and the specific surface area. The reduced electrical conductivity of sulfur (approximately 10-28 S cm^{-1}) necessitates the incorporation of substantial amounts of conductive additives to facilitate rapid redox reactions [8]. Carbon is the most frequently utilised additive, providing significant electronic charge transport and a high specific surface area. Previous works utilised different carbonaceous materials, including Ketjenblack [9, 10], activated carbon cloth (ACC) [11], CMK-3 [12]. Yu and Manthiram focus on CNT [13], Du et al. investigate graphene [14]. Due to the decreased attraction between non-polar carbon and polar polysulfides, there is a peril of polysulfide diffusion into the electrolyte during cycling, resulting in the irreversible depletion of active materials. Previous research indicates that the performance of magnesium-sulfur batteries can be enhanced by modifying the sulfur cathode through the incorporation of matrix materials characterised by high conductivity and specific structural properties. Numerous catalysts have been examined in Mg-S batteries, including heteroatom-doped carbon materials, metal oxides, metal nitrides, metal chalcogenides, and single-atom catalysts [15]. A great interest has been directed towards transition metal-chalcogenides (TMCs) among various cathode materials due to their exceptional EC properties. TMCs serve as prominent electrode materials in electrochemical ES systems, including Li^+-ion, Na^+-ion, and metal-sulfur batteries and supercapacitors. This results from their exceptional characteristics, including increased high reversible capacity, a substantial number of electroactive sites, thermal stability, and a stable structure that facilitates cyclability [16]. The deeper faradaic reaction of chalcogenides facilitates enhanced capacity, it is cost-effective, and can be regarded as an environmentally friendly material.

Numerous published studies have indicated progress in utilising metal chalcogenides (MC) as a promising material for improved EC storage systems, focusing on energy storage mechanisms, structural optimisation, and stabilisation. It has been suggested that a comprehensive understanding and enhancement of innovative materials for electrochemical applications can be achieved through the integration of computational and experimental studies [17]. In spite of the

 doi:10.20944/preprints202510.1895.v1

advancements made, numerous challenges continue to persist, which include but are not limited to redox degradation, the inability to accommodate large hydrated ions when used as cathode materials, and this requires attention. In addition to enhancing the characteristics of current cathode materials via systematic design, the investigation of novel cathode materials represents a significant focus in the advancement of Mg-S batteries. Consequently, density functional theory (DFT) calculations have demonstrated their effectiveness as a robust method for uncovering new materials and forecasting their electrochemical properties [18]. Given the extensive collection of MC compounds, it is quite probable that numerous additional promising cathode materials remain to be explored. Thus, integrating ab-initio calculations with machine learning (ML) and high-throughput experiments is expected to facilitate the discovery of innovative MC materials that possess structures and properties ideally appropriate for cathodes in Mg-S batteries. This review stresses the significant role of different transition metal chalcogenide-based materials in facilitating advancements in EC energy storage. This paper discusses the use of chalcogenide nanocrystals and innovative hybrid chalcogenide nanoarchitectures for the modification of cathodes in Mg-S battery technologies. This study emphasises the significance of emerging chalcogenide-based cathodes in overcoming the current limitations of energy storage technologies, analysed through both experimental materials and theoretical frameworks. The review concludes by presenting insights into the principle of charge transfer mechanisms in novel chalcogenide cathodes and the development of emerging advancements, including hybrid systems and AI/data-driven approaches, to fully realise the potential of Mg-S batteries.

2. Electrochemical Energy Storage Devices

Electrochemical energy storage devices are essential for renewable energy systems, providing options for sustainable grid integration, electric mobility, and portable power applications. Fuel cells, supercapacitors, and rechargeable batteries represent divergent methodologies, each possessing certain advantages and constraints. Fuel cells provide elevated efficiency, scalability, and negligible pollutant emissions, especially when utilising hydrogen as the fuel source. Nonetheless, their prolonged use is constrained by the elevated expenses of catalysts, difficulties in hydrogen storage, and inadequate infrastructure for fuel transport [19]. Supercapacitors serve as an intermediary between traditional capacitors and rechargeable batteries, providing elevated power density, rapid charging capabilities, and enhanced cycle longevity. Nonetheless, their very low energy density restricts their effectiveness for prolonged energy storage. Lithium-ion batteries (LiBs) prevail in the contemporary battery market, supporting portable devices, electric cars, and the integration of renewable energy [20]. Lithium-ion batteries with the structure and operation mechanism (Figure S2 b-c), provide elevated energy density, commendable cycle longevity, and cheap scalability; nonetheless, supply problems and safety issues present considerable constraints. Li-sulfur (Li-S) batteries have emerged as a possible next-generation alternative, possibly providing five times the energy density of lithium-ion batteries (LiBs). Nonetheless, Li-S technology encounters significant drawbacks, such as inadequate cycle longevity, restricted sulfur utilisation, and technical obstacles like the polysulfide shuttle phenomenon [21].

Magnesium-sulfur (Mg-S) batteries constitute an emerging category of non-lithium energy storage technologies characterised by increased theoretical volumetric energy density and considerable cost benefits attributable to the abundance of magnesium [22]. Their reduced volumetric expansion during cycling renders them comparatively safer, and the incorporation of multivalent ions such as Mg^{2+} augments the possibility for substantial storage capacity in compact systems. Resolving these impediments is essential for realising their complete potential. Contemporary research emphasises polysulfide stabilisation, electrolyte optimisation, and cathode architecture to reduce performance degradation [23].

3. Magnesium-Sulfur (Mg-S) Battery

 doi:10.20944/preprints202510.1895.v1

Given these limitations, focus has transitioned to alternative chemistries, especially multivalent metal-sulfur systems. Mg-S batteries are notable for their high theoretical volumetric energy density of 3218 Wh/L, significantly surpassing that of traditional lithium-ion batteries (LiBs) [24]. Moreover, the natural abundance and low cost of magnesium present significant economic benefits in comparison to lithium, cobalt, or nickel, which are facing growing supply chain challenges. Mg-S batteries exhibit improved safety relative to other non-lithium sulfur systems (Figure 10) due to their relatively low volumetric expansion of 36 % during cycling [25]. This characteristic reduces the significant mechanical instability seen in systems like aluminum- and potassium-sulfur batteries, which experience expansions exceeding 300 %. Despite these advantages, Mg-S batteries face significant challenges that restrict their practical implementation. The insulating properties of elemental sulfur limit electrochemical activity, whereas the dissolution of intermediate magnesium polysulfides results in the "shuttle effect," causing capacity degradation and reduced Coulombic efficiency [24]. Further obstacles comprise mechanical instability resulting from volumetric alterations of sulfur during cycling, low utilisation efficiency of polysulfide intermediates, and instability at the magnesium metal anode. In comparison to lithium-sulfur (Li-S) systems, Mg-S batteries face additional challenges due to the inherently slower kinetics of divalent Mg^{2+} ion transport, leading to reduced charge-discharge dynamics and suboptimal electrochemical performance [26]. These challenges necessitate the development of sophisticated electrode designs, electrolytes, and methods to inhibit polysulfide migration, thereby enhancing performance.

A notable issue is the inadequate comprehension and analysis of the shuttle effect in Mg-S batteries in the current literature. The detrimental impact is well established, evidenced by reduced cycle life, low sulfur utilisation, and the formation of inactive magnesium polysulfides; however, current evaluations provide limited mechanistic insights [27]. Similar to advancements in Li-S systems, Mg-S batteries may benefit from strategies including modified cathode architectures to confine active species, electrolyte additives to stabilise polysulfides, and protective interfacial coatings on the Mg anode. The slower diffusion kinetics of Mg^{2+} require solutions specifically designed for the distinct properties of Mg-S chemistry, rather than direct extrapolations from Li-S research [28].

Conclusively, Mg-S batteries offer a promising solution for next-generation, cost-effective, and high-density energy storage systems. They offer increased theoretical volumetric energy density, reduced material costs, and enhanced safety. However, practical challenges like sulfur insulation, polysulfide shuttle effects, and anode instability hinder commercialisation. Targeted research focuses on high-conductivity cathode frameworks, stable electrolytes, and protective modifications for the magnesium anode.

 doi:10.20944/preprints202510.1895.v1

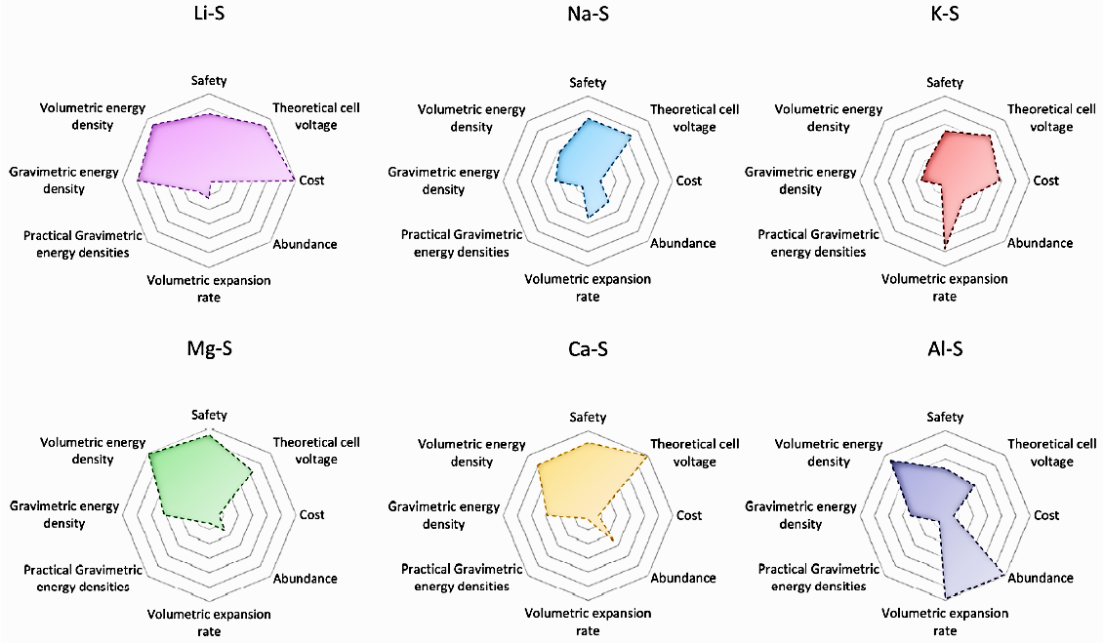

Figure 1. Evaluation of safety, estimated cell potential, cost, abundance, volumetric expansion rate, practical gravimetric energy densities at the cell level, gravimetric energy density, and volumetric energy density for Mg-S, Ca-S, Na-S, K-S, Al-S, and Li-S batteries [37].

4. Mg-S Battery Configuration and Mechanism of Operation

Magnesium (Mg) batteries represent intriguing contenders for the forthcoming production of ES devices, owing to their potential for high energy density, inherent safety attributes, and cost efficiency. The pairing of a Mg anode with a sulfur (S) cathode is a notable electrochemical coupling, providing an exceptional predicted volumetric energy density above 3,200 Wh L^{-1}. Nonetheless, due to the distinctive characteristics of Mg^{2+}-ion electrolytes, the surface passivation of Mg metal anodes and Mg polysulfides, the advancement of Mg-S batteries still encounters some obstacles. This section summarises the configuration and operational concepts of Mg-S batteries (Figure S2d) [38].

4.1. Electrolytes

The electrolyte in Mg-S batteries not only enables the transfer of Mg^{2+} ions but also significantly influences the compatibility, stability, and reversibility of the battery. The inaugural practical demonstration of a magnesium-sulfur battery in 2011 utilised a chloride-based complex electrolyte of magnesium hexamethyldisilazide (HMDS) and aluminium chloride ($AlCl_3$) [39]. This system exhibited reversible magnesium plating and stripping; nevertheless, the presence of chloride ions presented significant long-term stability challenges due to their corrosive nature. Subsequent innovations resulted in the creation of non-corrosive electrolytes, particularly fluorinated alkoxyborate salts like $Mg\backslash[B(hfip)_4]_2$, which demonstrate great oxidative stability (up to 4 V), little corrosivity, and enhanced Mg^{2+} transport [40]. This electrolyte demonstrated potential with carbon-sulfur cathodes, achieving capacities of about 400 mAh g^{-1} and a consistent discharge voltage of about 1.5 V. Nonetheless, despite these gains, challenges such as polysulfide solubility and the consequent shuttle effect continue to restrict long-term cycling performance. Researchers investigated gel polymer electrolytes (GPEs) formulated with $Mg/[B(hfip)_4]_2$, which encapsulate solvent molecules inside a polymer matrix, therefore inhibiting the migration of polysulfides. These GPEs exhibited consistent open-circuit voltages over prolonged periods and decreased self-discharge rates [41].

4.2. Separator

 doi:10.20944/preprints202510.1895.v1

Separators are essential yet frequently underrated elements in battery design. They must facilitate ionic conduction while electrically insulating the electrodes. In Mg-S batteries, their significance is heightened as they serve as both a physical and, at times, a chemical barrier to the polysulfide shuttle [39]. Contemporary research predominantly uses thick glass fibre separators, which, although efficient in laboratory evaluations, are impractical for commercial-scale applications due to their bulkiness and high electrolyte consumption. Researchers are investigating thinner functionalised separators to decrease cell volume while also preventing polysulfide migration. Polyoxometalate (POM)/carbon composites electrospun over glass fibre separators have demonstrated potential [42]. The carbon serves as a conductive matrix to immobilise polysulfides, while the vanadate clusters facilitate their transformation, hence inhibiting the shuttle effect and enhancing capacity retention. For example, copper phosphide (Cu_3P)-coated Celgard separators demonstrate catalytic activity that transforms long-chain polysulfides into short-chain MgS_2/MgS. These cells provided more than 500 cycles of consistent performance, setting a record for Mg-S batteries. The advancement of functional separators is crucial for performance and scalability [43].

4.3. Electrodes

4.3.2. Magnesium Anode

The magnesium (Mg) anode, while essential to the battery's energy density and safety, is frequently eclipsed by investigations into the cathode and electrolyte. The magnesium anodes have distinct problems absent in lithium-based systems. In contrast to lithium, which generates a solid electrolyte interphase (SEI) that facilitates ion transport, magnesium tends to develop passivating surface layers that entirely obstruct Mg^{2+} migration [44]. The blocking layers, typically generated by interactions with impurities or dissolved polysulfides, lead to elevated interfacial resistance and irregular Mg deposition/stripping, hence diminishing both cycle life and Coulombic efficiency [45]. Presently, the majority of Mg-S batteries utilise Mg foils or discs, which possess restricted surface area and require scraping before use to eliminate oxidation layers; this suboptimal procedure frequently results in surface irregularities and unequal current distribution. This non-uniformity intensifies passivation and generates hotspots for localised corrosion [38]. An effort to address these challenges involves employing 3D structured magnesium anodes, such as magnesium deposited onto activated carbon cloth (Mg@ACC) through electrodeposition, which produces a porous, high-surface-area configuration that guarantees uniform magnesium deposition, diminishes nucleation overpotential (approximately 0.16 V), and enhances cycle longevity [32].

4.3.3. Sulfur Cathode

Sulfur (S) cathode functions through a conversion-type redox reaction involving elemental sulfur and magnesium sulfide (MgS). The inherently low electronic conductivity of sulfur ($\sim 10^{-28}$ S cm^{-1}) presents a significant challenge, requiring the addition of conductive additives to enhance charge transfer efficiency. Carbon-based materials, including Ketjenblack, activated carbon cloth (ACC), CMK-3, carbon nanofibers (CNFs), carbon nanotubes (CNTs), and graphene, are extensively utilised as host matrices owing to their elevated surface area and electrical conductivity [40]. Traditional carbon hosts exhibit weak interactions with polar magnesium polysulfides due to their non-polar characteristics, resulting in the dissolution of active materials into the electrolyte, a primary factor contributing to the polysulfide shuttle effect. Alternative methods involve incorporating a catalytic composite framework comprising MXene and reduced graphene oxide (rGO), along with nanoconfined TiO_2 particles, which exhibited enhanced catalytic activity and redox kinetics, thereby improving the reversibility of S/MgS conversion [46]. The composite cathodes demonstrate potential in hybrid systems incorporating lithium ions; however, the objective is to achieve complete compatibility with magnesium. High-loading cathodes, although challenging to achieve, are crucial for converting laboratory success into commercial feasibility. Even though research on sulfur cathodes emphasises the enhancement of electrical conductivity, the suppression of polysulfide

 doi:10.20944/preprints202510.1895.v1

migration, the improvement of redox kinetics, and the augmentation of sulfur loading, these efforts are essential for achieving this goal. The advancement of functional and chemically interactive host matrices is a significant area of research which needs to be explored. Thus, the later sections explore the different modification techniques that have been employed to enhance the efficiency of the sulfur cathode [40].

4.4. Reaction Mechanism of Mg-S Batteries

While discharging, magnesium metal at the anode is oxidised to Mg^{2+}, releasing electrons, while sulfur at the cathode is reduced, resulting in the formation of MgS through a multistep conversion process [47]. Nonetheless, this ostensibly simple redox reaction encompasses intricate intermediate reactions, notably in the generation of soluble polysulfides (MgS_n, where n = 4-8). The intermediates induce a phenomenon known as the polysulfide shuttle effect, wherein dissolved polysulfides transfer between the electrodes, leading to the depletion of active materials, self-discharge, and electrode degradation. The shuttle effect poses a considerable problem in Mg-S batteries, similar to that in Li-S systems, although it is exacerbated by the characteristics of Mg^{2+} ions and their slow transport rates [33]. Furthermore, a combination of theoretical modelling and experimental investigations is recommended for establishing a fundamental understanding of the electrochemical mechanisms and depletion pathways in Mg-S batteries. The process in Mg-S batteries has three stages and involves the "shuttle effect" [34]. Mg-S batteries operate on the EC transformation of sulfur (S_8) into magnesium sulfide (MgS). In the discharge process, magnesium metal oxidises to produce magnesium ions and electrons, which travel to the sulfur cathode via the electrolyte and an external circuit, respectively. At the cathode, sulfur interacts with magnesium ions and electrons, undergoing reduction to produce MgS [36]. The reverse takes place during the charging process.

$$\text{Magnesium (Mg) anode (-): } Mg \rightarrow Mg^{2+} + 2e^- \quad (1)$$

$$\text{Sulfur (S) cathode (+): } S_8 + 8Mg^{2+} + 16e^- \rightarrow 8MgS \quad (2)$$

While the general discharge and charge processes, as presented in Eqs. (1) and (2) [37], are straightforward; the sulfur reduction process is significantly more complicated than that described in Eq. (2) and remains ambiguous to this day. Numerous studies have focused on examining the discharge mechanism of Mg-S batteries; nevertheless, inconsistencies exist within the literature [48, 49]. The reduction of sulfur is summarised in the following phases. The initial phase involves the solid-liquid biphasic reduction of sulfur to MgS8, subsequently followed by it dissolving into the electrolyte.

$$\text{Step A: } S_8 + 2e^- + Mg^{2+} \rightarrow 2MgS_8 \quad (3)$$

The reduction of straight-chain polysulfides occurs immediately, with the reaction taking place in the liquid phase and exhibiting rapid kinetics as described in processes (4) and (5).

$$\text{Step B: } 3MgS_8 + 2e^- + Mg^{2+} \rightarrow 4MgS_6 \quad (4)$$

$$\text{Step C: } 2MgS_6 + 2e^- + Mg^{2+} \rightarrow 3MgS_4 \quad (5)$$

MgS_4 is subsequently reduced to solid-phase MgS_2, which further reacts to yield the final product MgS. Alternatively, MgS_4 can be reduced to another solid-phase compound, Mg3S8, alongside MgS.

$$\text{Step D: } MgS_4 + 2e^- + Mg^{2+} \rightarrow 2MgS_2 \quad (6)$$

$$\text{Step E: } MgS_2 + 2e^- + Mg^{2+} \rightarrow MgS \quad (7)$$

Alt:

$$\text{Step D: } 2MgS_4 + 2e^- + Mg^{2+} \rightarrow Mg3S_8 \quad (8)$$

 doi:10.20944/preprints202510.1895.v1

$$\text{Step E: } Mg_3S_8 + 10e^- + 5Mg^{2+} \rightarrow 8MgS \quad (9)$$

The complex interactions within electrolyte systems significantly affect the electrochemical reaction paths of Mg-S cells. A comprehension of these routes requires consideration of key features, including thermodynamic characteristics, ionic strength, molarity, temperature, solvent dielectric constants, and counter-ionic features [50, 51]. The conversion of MgS_2 to MgS is observed in equation 9, while ex-situ XPS studies proved insufficient to accurately ascertain the dimension and chemical makeup of the intermediate MgS_x ($1 < x < 8$). However, the creation of MgS_4 and MgS_2 is indicated based on the observed capacity at each potential plateau or slope in the starting discharge curve.

4.5. Controlling Polysulfide Shuttle Effect in Mg-S Batteries

The polysulfide shuttle effect poses a considerable obstacle to the practical implementation of magnesium-sulfur (Mg-S) batteries, which are fundamentally distinct from lithium-sulfur (Li-S) batteries owing to the unique electrochemical properties of divalent magnesium ions (Mg^{2+}) [28]. In Mg-S batteries, the discharge process entails a multi-step reduction of elemental sulfur to form long-chain magnesium polysulfides (MgS_x, where x = 4-8), which exhibit solubility in ethereal electrolytes. Intermediate species migrate from the cathode to the magnesium anode, undergoing parasitic reduction reactions that result in shorter-chain polysulfides and ultimately magnesium sulfide (MgS). The ongoing migration leads to the shuttle effect, which results in the loss of active material, degradation of capacity, reduced Coulombic efficiency, increased self-discharge, and the formation of passivating layers on the magnesium anode. The shuttle effect is intensified due to the enhanced electrostatic interactions between the more highly charged Mg^{2+} ions and polysulfide anions, in contrast to Li^+ ions [29]. The interactions affect solvation behaviour, with different ethereal solvents such as dimethoxyethane (DME) and tetrahydrofuran (THF) exhibiting varying solvation capacities, subsequently influencing the mobility of polysulfides. The kinetics of magnesium polysulfide reduction are faster than those of lithium counterparts, resulting in increased side reactions and accelerated capacity degradation. Experimental findings underscore the enhanced importance of the shuttle effect in Mg-S systems compared to Li-S systems [30]. Operational simulations demonstrate that capacity loss can be accurately modelled by integrating these polysulfide shuttle mechanisms. The behaviour observed in the discharge plateau indicates variations in polysulfide species concentration, which directly influence electrochemical performance. Strategies to mitigate the polysulfide shuttle effect include the modification of separators. The modifications utilise physical blocking, chemical adsorption, and catalytic conversion to establish a barrier between cathodes and anodes, facilitating Mg^{2+} ion transport while inhibiting polysulfide migration [31]. Transition metal oxides such as MoO_2 and MnO_2 serve as effective separator modifiers owing to their chemical affinity for polysulfide species, resulting in improved electrochemical performance. The Mo_6S_8 Chevrel phase has demonstrated significant potential in recent developments, exhibiting enhanced polysulfide adsorption and catalytic efficiency, along with high capacity and cycling stability in Mg-S cells. Conductive polymers, such as polypyrrole (PPy) nanostructures, significantly improve the immobilisation of polysulfides, exhibiting notable capacities and durability. The development of advanced catalytic host materials signifies a transition towards the active management of polysulfides, with transition metal chalcogenides enhancing adsorption and conversion kinetics. Hierarchical nanostructured hosts enhance mass transfer and catalytic efficiency. Recent advancements in catalytic systems integrating polysulfide anchoring with dual conversion capabilities demonstrate significant progress in this field. The design of electrolytes is essential for controlling the polysulfide shuttle effect. Gel polymer electrolytes (GPEs) demonstrate high ionic conductivity and mechanical stability, while ionic liquid electrolytes offer additional benefits in managing polysulfides due to their low solubility for these compounds [32]. Electrolyte additives enable precise alterations in polysulfide behaviour, eliminating the necessity for extensive reformulations. Future perspectives suggest a trend towards integrated multi-component strategies

 doi:10.20944/preprints202510.1895.v1

for the collective management of polysulfides. Strategies for improvement involve the development of artificial solid electrolyte interphases to protect anodes and the application of cascade catalysis frameworks that regulate polysulfide conversion pathways [33]. Research is being conducted on solid-state electrolyte methods to address shuttling by eliminating liquid transport mechanisms. The successful development of Mg-S batteries will depend on the integration of various mitigation strategies, ensuring their effectiveness while addressing practical concerns such as cost, scalability, and manufacturing complexity.

5. Monitoring the Reaction Mechanism of Mg-S Batteries

The EC reaction steps involved in the transformation of Mg-S batteries is complicated, and keeping track of this procedure is essential in scientific studies. Traditional electrochemical methods are commonly employed to assess the battery reaction process; however, they fall short in accurately representing the alterations in the physical or chemical state of the electrode material throughout cycling. Ex-situ methods, including X-ray diffraction (XRD), scanning electron microscopy (SEM), X-ray photoelectron spectroscopy (XPS) and transmission electron microscopy (TEM), are capable of detecting various depths of discharges and states of charges; however, they may yield inaccurate information due to time delays and the need for post-processing. Recent advancements in in-situ and operando characterisation methods have been established to monitor the internal electrochemical reactions and degradation pathways of Mg-S batteries. In situ tracking entails the analysis of the battery at the location of use, whereas operando denotes continuous data collection throughout the battery's operation. The techniques listed, such as XRD, XANES, XPS, XRT, SEM, XRF, TEM, XRR, FT-IR, AFM, NMR, Raman spectroscopy, UV-vis absorption spectroscopy, and HPLC, serve as effective, sensitive, qualitative, and powerful instruments for monitoring rapid EC reactions and optimising the structural and compositional characteristics of Mg-S batteries [52].

6. Importance of Electrode Materials

The materials used for electrodes play a crucial role in determining the performance characteristics of energy storage devices, such as their capacity, cycle life, and charge/discharge rates. The effectiveness and efficiency of electrochemical energy storage devices, including batteries and supercapacitors, are fundamentally linked to the characteristics of their electrode materials. Electrodes serve as the centres for chemical reactions, allowing for the storage and release of electrical energy through the facilitation of electron flow during both charge and discharge cycles. The electrochemical properties and performance of energy storage devices are closely linked to the physicochemical characteristics of their electrode materials. Recent developments in electrode materials encompass metal-ion, carbon-based, tin oxide, and nanostructured materials, as well as organic electrode materials. The systematic design of electrode materials, encompassing structural modifications and compositional adjustments, is crucial for tackling issues like capacity degradation, limited voltage range, and inadequate rate performance. Organic electrode materials hold great potential, yet they encounter challenges such as stability and scalability that must be addressed before they can achieve widespread commercial adoption. Transition metals such as Nickel (Ni), copper (Cu) and silver (Ag), when paired with chalcogenides like sulfur (S) or selenium (Se), demonstrate improved conductivity and catalytic performance [52, 53]. As a result, TMCs have emerged as an innovative class of electrode materials, recognised for their exceptional electrochemical properties. The materials play a crucial role in the progress of energy storage technologies by improving conductivity, stability, and catalytic activity, all while addressing challenges and investigating future possibilities. TMCs exhibit enhanced performance in energy storage devices when compared to graphite, particularly in terms of capacity retention and overall capacity in Mg-S batteries, as indicated in Figure 2 [54].

 doi:10.20944/preprints202510.1895.v1

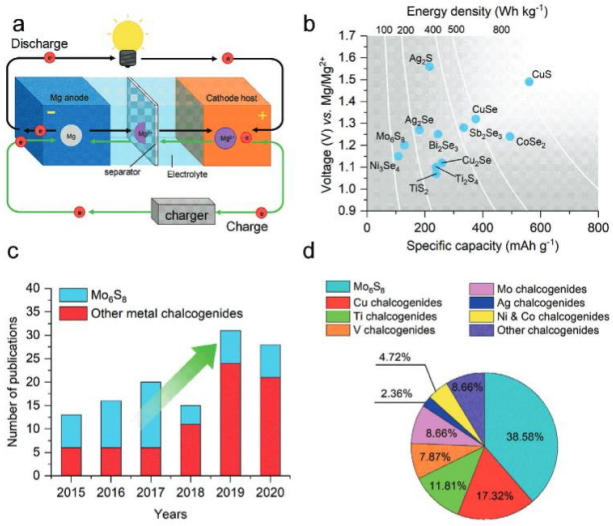

Figure 2. (a) Pictorial representation of a conventional rechargeable magnesium battery and its operational mechanism. (b) Estimated operational voltages with capacities relating to MC cathodes. (c) The increasing trend of research interest in MC for RMBs is demonstrated by the volume of published articles between 2015 and 2020. (d) A comparative analysis of diverse MC employed as cathode materials for RMBs across all publications [55].

7. Metal Chalcogenides-Based Cathode Materials for Mg-S Batteries

Sulfur is a promising cathode material for rechargeable batteries due to its improved theoretical specific capacity and economical nature. However, it has poor electrochemical performance due to low sulfur utilisation. This issue is common in magnesium batteries, where irreversible discharge products and dissolution of polysulfide into the electrolyte solution occur. Transition metal chalcogenides (TMC), such as Cu_{-x}, Ti_{-x}, Co_{-x}, Ni_{-x} and V_{-x}, have been investigated as potential cathode materials. These materials offer high specific capacity, favourable magnesium reaction kinetics, elevated electronic conductivity, and compatibility with various electrolytes. Nanostructured metal chalcogenides can enhance battery performance by increasing superficial area and reducing the diffusion path for Mg^{2+} ions in the solid phase. This review aims to provide a concise review of the application of nanostructured metal chalcogenides for Mg-S batteries and contribute to the advancement of cathode materials [51, 56].

7.1. Metal Chalcogenide Cathodes: Types and Structures

The diffusion kinetics of Mg^{2+} ions are a crucial factor that determines the electrochemical efficiency of Mg-S batteries. In contrast to the sluggish diffusion kinetics of Mg^{2+} in metal oxide ($M^{n+}O^{x-}$) lattices, accelerated Mg^{2+} transport has been noted when utilising MC (i.e., $M^{n+}S^{2-}$ and $M^{n+}Se^{2-}$) as cathode materials. Mao et al. demonstrated that Mg^{2+} mobility increases in layered MX_2 structures (where M = Ti, V; and X = S, Se, O) as the anion is systematically altered from O^{2-} to S^{2-} to Se^{2-} [57]. This has been ascribed to three key factors: i) augmentation of diffusion channel dimensions; ii) enhancement of electronic charge conductivity; and iii) reduction of Coulombic interactions between Mg^{2+} and more pliable host anions. The third factor is derived from Pearson's hard and soft acids and bases (HSAB) theory, which classifies Mg^{2+} as a hard acid, therefore indicating a stronger interaction with O^{2-}, a hard base [58]. The contact between cations and anions is diminished with the softer chalcogenide anions, resulting in a reduced barrier for Mg^{2+} diffusion. Thus, metal chalcogenides are gaining recognition as a viable cathode material due to their intrinsic capacity to enhance the kinetics of magnesiation, in Mg-S batteries . Metal chalcogenide cathodes are classified into intercalation-type and conversion-type, based on their redox mechanism during the cycling (charge and discharge) processes.

 doi:10.20944/preprints202510.1895.v1

Intercalation-type MC have a skeleton framework that experiences minimal structural perturbation upon integration of metallic ions, including Li^+, Na^+, and Mg^{2+} (Figure 3a). this type of metal chalcogenide facilitate the reversible intercalation of metal ions while maintaining structural integrity. The structure experiences a minor volume change during the insertion and extraction of metal ions, leading to elevated Coulombic efficiency and enhanced stability during cycling. Nonetheless, the intercalation materials generally exhibit limited Mn+: host stoichiometries (where M = metal; and n+ = oxidation state), which leads to a comparatively low capacity. The metal chalcogenides that have been experimentally tested as intercalation cathodes for Mg batteries are Mo_6S_8 [59], Ti_2S_4 [20], WSe_2 [60], Cu_2MoS_4 [61], VS_2 [62], Ni_3Se_4 [55], and Mg_xZrS_4 [59].

Conversely, metal chalcogenide compounds (MaXb, where M represents a metal and X denotes S, Se, or Te) react with Mg^{2+} to produce metallic nanoparticles embedded within the MgX matrix (Figure 3b), classifying them as conversion-type cathodes. In these conversion cathodes, the redox couple is M/M^{n+}, which provides enhanced capacity. Nonetheless, a primary challenge in employing conversion-type cathodes is that the associated conversion reactions typically result in significant structural, morphological, and volumetric alterations that compromise the integrity of the cathodes, ultimately causing capacity degradation [60]. The conversion cathode demonstrates significant voltage hysteresis between discharge and charge, leading to reduced energy efficiency [61]. The following MC viz are CuS [62], Ag_2S and Ag_2Se [63], $NiCo_2Se_4$ [64], Cu_{2-x} Se [65], CoS [66], FeS_2 [67], $CoSe_2$ [68], and $Ni_{0.75}Fe_{0.25}Se_2$ [69] have been experimentally investigated as a conversion cathode for Mg-S batteries.

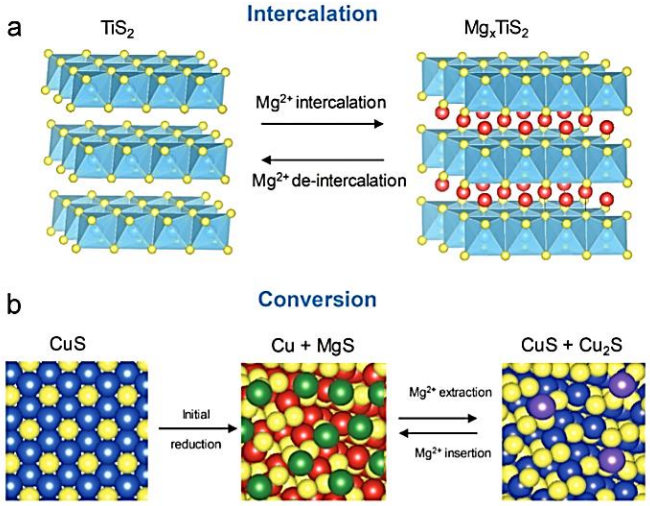

Figure 3. (a) Illustration of the intercalation process of Mg^{2+} ions into the layered TiS_2 cathode (blue: Ti^{4+}, yellow: S^{2-}, red: Mg^{2+}). (b) A schematic diagram of the conversion reaction occurring at the CuS cathode (yellow: S^{2-}, dark blue: Cu^{2+}, green: Cu°, violet: Cu^+, red: Mg^{2+}) [65].

7.2. Transition Metal-Dichalcogenides (TMDCs): Composition and Properties

The chemical formula of transition metal dichalcogenides (TMDCs) is expressed as MX_2, where M represents the transition metal from groups 4 to 10 of the periodic table, and X signifies the chalcogen, as illustrated in Figure 4a. TMD materials that include transition metals from groups 4 to 7 generally possess a layered structure, whereas specific transition metals from groups 8 to 10, such as pyrite, demonstrate a non-layered structure [70]. The atomic configuration in layered MX_2 produces polytypes, characterised by M, a transition metal atom coordinated by six (6) chalcogen atoms, X (Figure 4 b). In a transition metal dichalcogenide (TMD) monolayer (basal plane), robust covalent interactions between the transition metal and chalcogen lead to the emergence of stacking polytypes (stacking order) and polymorphs (metal coordination geometry). Figure 5a illustrates the conventional configurations of TMD structures: 1T, 2H, and 3R, corresponding to one, two, and three layers per stacked cell bound in tetragonal T, hexagonal H, and rhombohedral R phases, respectively.

 doi:10.20944/preprints202510.1895.v1

MoS_2 demonstrates all three polytypes, characterised by a consistent layered structure in which chalcogen atoms surround the Mo transition metal atoms (as shown in Figure 5b). 1T-MoS_2 is acknowledged as a metastable metallic phase, whereas 2H-MoS_2 and 3R-MoS_2 are well-established semiconductor phases noted for their thermodynamic stability. 1T- and 2H-MoS_2 demonstrate distinct characteristics concerning the lateral displacement of one amongst the two sulfur planes. The introduction of Mg^{2+} can induce the transition from the 2H phase to the 1T phase [71-73].

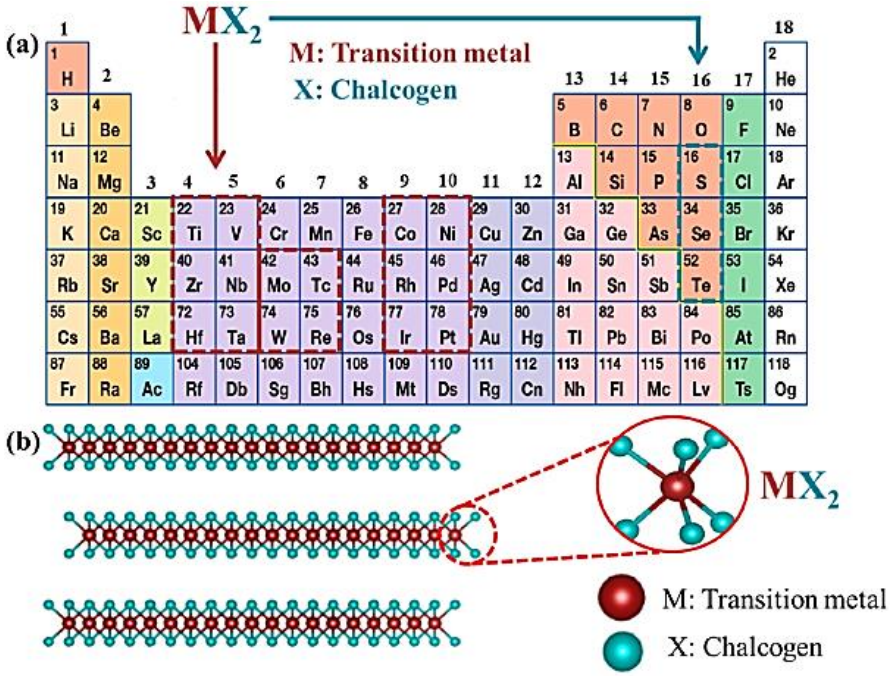

Figure 4. (a) TMDs having the MX_2 configuration, where M denotes one of the sixteen (16) transition metals (TM) highlighted by the dotted box in red, while X represents one of the three halogenic elements denoted by the dotted box in green, (b) layered architecture of MX_2.[74].

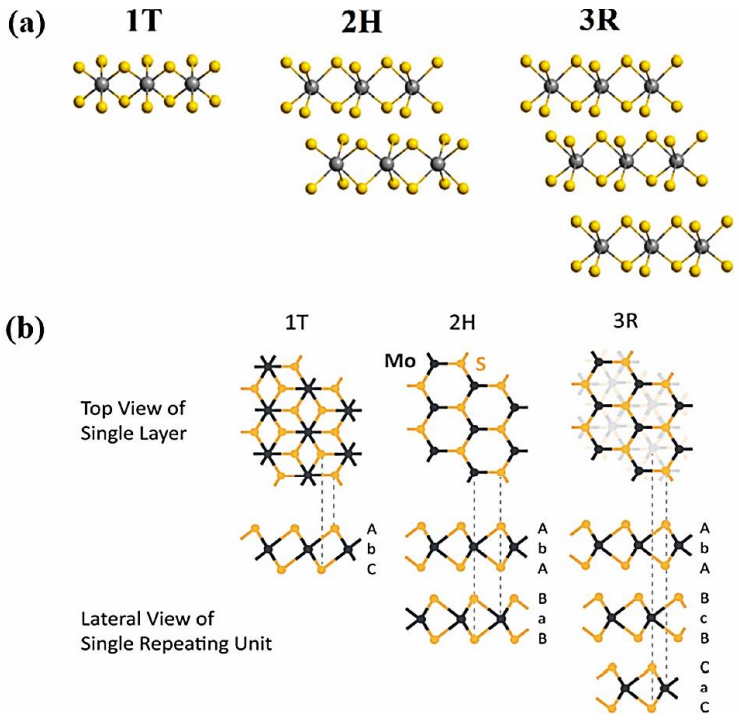

 doi:10.20944/preprints202510.1895.v1

Figure 5. (a)Polytypic structures of transition metal dichalcogenides (1T, 2H, and 3R). (b) Polytypic structure of MoS_2 [74].

The electrical configuration of graphene arises from the hybridisation of s and p orbitals, whereas the electronic characteristics of transition metal dichalcogenides (TMDs) are governed by the d orbital electrons of the transition metal. Graphene and transition metal dichalcogenides (TMDs) share structural similarities; nevertheless, the electrical characteristics of TMDs are influenced by the electron count in their non-bonding d orbitals and the spatial configuration of the transition metal atoms [75]. The extent of electron occupancy in the d orbital markedly affects the electrical characteristics of transition metal dichalcogenides (TMDs). A partially filled d orbital signifies metallic properties, while a filled d orbital is associated with semiconducting behaviour [70]. Thus, TM atoms exert a more significant impact on the electrical structure of TMDs than chalcogen atoms.

7.3. Advantages and Challenges of TMDs

Layered transition metal dichalcogenides (TMDs) exhibit significant potential for applications in energy storage, catalysis, and photonics. Graphene-like 2D transition metal dichalcogenides (TMDs) exhibit a large surface-to-volume ratio, facilitating enhanced interaction between the active material and electrolyte, making them highly beneficial for battery applications. The weak van der Waals (vdW) force enables rapid ion diffusion through the interlayer gap of the MX_2 layer. The significant interlayer distance within the MX_2 layer facilitates the accommodation of multivalent ions, including Zn^{2+}, Mg^{2+}, Al^{3+}, and Ca^{2+} [76, 77]. Figure 6 illustrates the interlayer distances and band gaps of different transition metal dichalcogenides (TMDs) frequently utilised in Mg-S batteries.

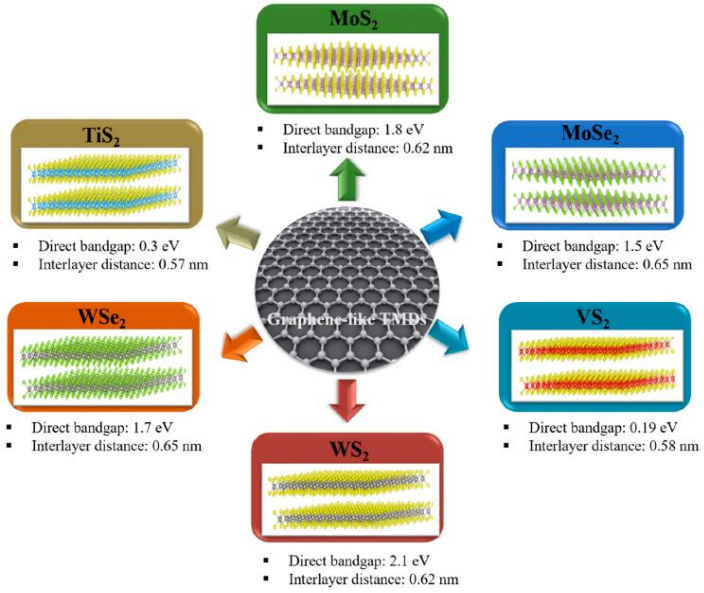

Figure 6. Direct energy bandgap and interlayer spacing of different forms of TMD [78].

Despite these advantages, the suboptimal rate performance and cyclic stability of TMDs, attributed to their low ionic conductivity and significant volume expansion, restrict their wide use as cathode materials in Mg-S batteries. The irreversible side effects occurring during the charging and discharging processes reduce the coulombic efficiency of the TMDs [79]. MoS_2 is regarded as an appropriate cathode for Mg^{2+} storage due to its significant interlayer distance of 0.62 nm, in contrast to its smaller size of 0.15 nm. According to Liu et al. [80], bulk MoS_2 exhibits a specific capacity of merely 40 mAh g^{-1} due to the absence of distinct redox peaks in electrochemical reactions. This indicates that the interlayer distance of MoS_2 is not the sole determinant of the high performance of Mg-S batteries. The critical issue is the efficient adsorption of ions on the electrode, which affects

 doi:10.20944/preprints202510.1895.v1

the electromigration characteristics of multivalent ions (M^{n+}) in aqueous solutions. Thus, the ionic radius in the hydrated state (i.e., $M^{n+}(H_2O)_n$) holds greater significance than the general ionic radius (i.e., M^{n+}) [74].

Table 1. Electrical conductivity for prevalent metal compounds at room temperature [78].

Objects	Metal compound	Conductivity (S cm^{-1})	Ref.
Sulfides	WS_2	3.7×10^{5}	[34]
	MoS_2 (1T edge)	2.0×10^{4}	[35]
	MoS_2 (2H)	2.0×10^{-3}	[36]
	CoS_2	6.7×10^{3}	[37]
Nitride	NbS_2	8.7×10^{3}	[38]
	MoN	2.3×10^{-1}	[39]
	Co_2N	2.1×10^{2}	[40]
	Cu_3N	2.5×10^{2}	[41]
Oxides	Fe_2O_3	2.0×10^{-1}	[42]
	TiO_2 (rutile)	1.1×10^{-1}	[43]
	ZnO	5.0×10^{-2}	[44]

Most transition metal sulfides (TMSs) exhibit a non-layered structure, similar to pyrite and marcasite. Pyrite is the most prevalent sulfide mineral in nature, primarily composed of coordination between TM from groups eight, 8 to twelve, 12 and sulfur [92]. It exhibits a stable structure, notable optical absorption, and an appropriate energy band gap, making it suitable for various applications in photovoltaics, energy storage, and electrocatalysis. Some transition metal dichalcogenides (TMDs) exhibit a layered structure, exemplified by WS_2, MoS_2, and VS_2. These materials possess a sandwich configuration comprising one layer of metal (M) bonded to two layers of sulfur (S), featuring both basal plane and edge site atomic arrangements (Figure 7a, and b) [74, 93]. The edge site facilitates the hydrogen evolution reaction, leading to the selective deposition of MgS at the edge sites of MoS_2. The differing electron filling states of the d orbital result in distinct band structures for sulfides formed with main group metals compared to those formed with transition metals, significantly affecting their electronic conductivity. The band structures of transition metal-based sulfides (TMSs) are complex owing to the presence of d electrons, leading to diverse properties. Semiconductors, such as FeS_2 and MnS_2, exhibit localised d-electrons situated between the valence and conduction energy bands. Table 1 summarises the conductivity of several typical metals at room temperature. Density functional theory (DFT) calculations elucidate the complex relationship between band structure and conductivity in layered materials (Figure 8a-g). Metal-metal bonds can enhance electrical conductivity, as seen in the case of metallic 1T MoS_2, which has distorted octahedral coordination [94]. This enhances electrochemical reactions and has led to increased interest in metal sulfides (MSs) for use in Mg-S batteries. MSs have been used in sulfur chemistry since the mid-20th century, serving as catalysts in hydrodesulfurization (HDS) due to their ability to cleave CeS bonds and facilitate the formation of CeH and HeS bonds. The EC conversion of high-valence state magnesium polysulfides (MgPSs) to low-valence MgS parallels the reduction process observed in hydrodesulfurization (HDS). Mg-S batteries with MSs demonstrate enhanced electrochemical performance compared to alternative heterogeneous catalysts, homogeneous promoters, or various metal compounds due to their superior electronic and ionic conductivity (Figure 9a-d) [78].

 doi:10.20944/preprints202510.1895.v1

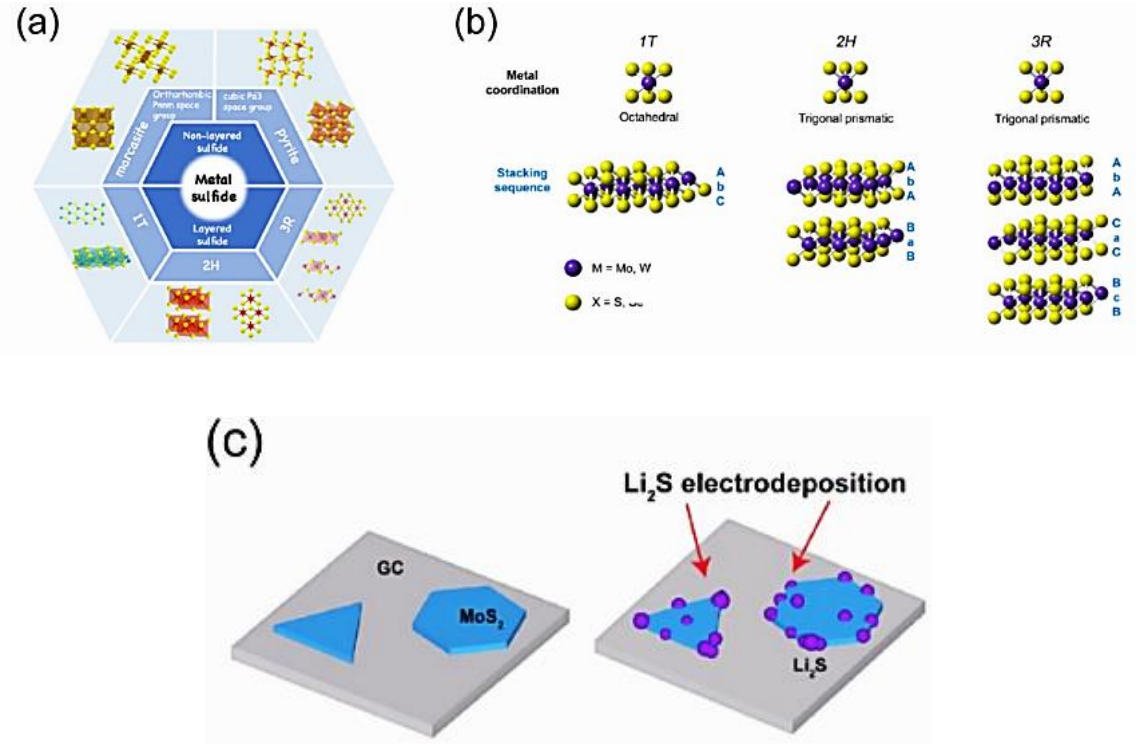

Figure 7. (a) A synopsis of conventional metallic sulfides exhibiting layered and non-layered crystalline structures. Layered transition metal dichalcogenides (WS_2, MoS_2) possess structural unit cells defined by octahedral or trigonal prismatic coordination. The hexagonal symmetry (2H) or rhombohedral symmetry (3R) is configured with two trigonal prismatic single layers. Illustration of Li_2S electrodeposition at the edge sites of MoS_2 sheets on a glassy carbon substrate. [93].

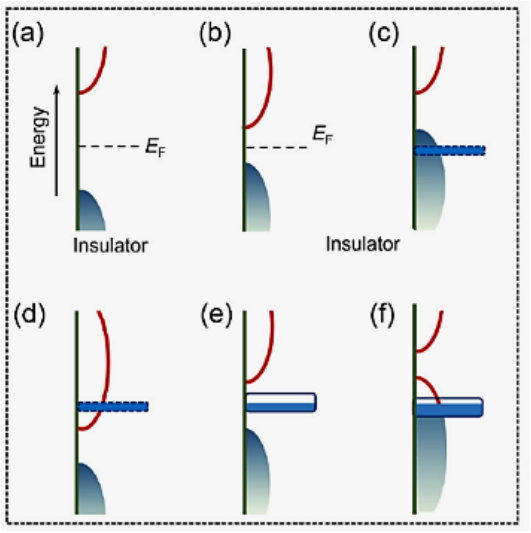

 doi:10.20944/preprints202510.1895.v1

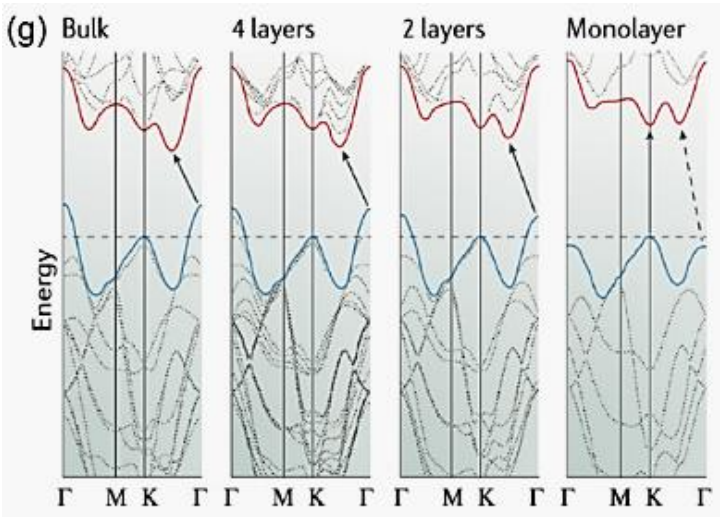

Figure 8. (a-f) Simplified band structures for metal sulfides (MSs) at absolute (0 K). Energy (E) denotes a function of the density of states (DOS). Occupied states are indicated in blue, denoting the valence band; unoccupied states are represented as open, with a red line signifying the conduction band. The localised d levels are depicted by the blue area and dashed lines, while Ey denotes the Fermi level. (a) Insulator composed of main group elements characterised by a wide band gap between the valence and conduction bands; (b) intrinsic semiconductor of main group elements exhibiting a reduced band gap; (c) semiconductors derived from TM elements; (d) p-type metallic conductor; and (e) n-type metallic conductor, featuring localised d levels of transition metals at varying positions; (f) transition metallic conductor with a low energy gap attributed to delocalised d electrons (oval blue block) and (g) The trend in the band structure of 2H-MoS_2 varies with reduced thickness [95].

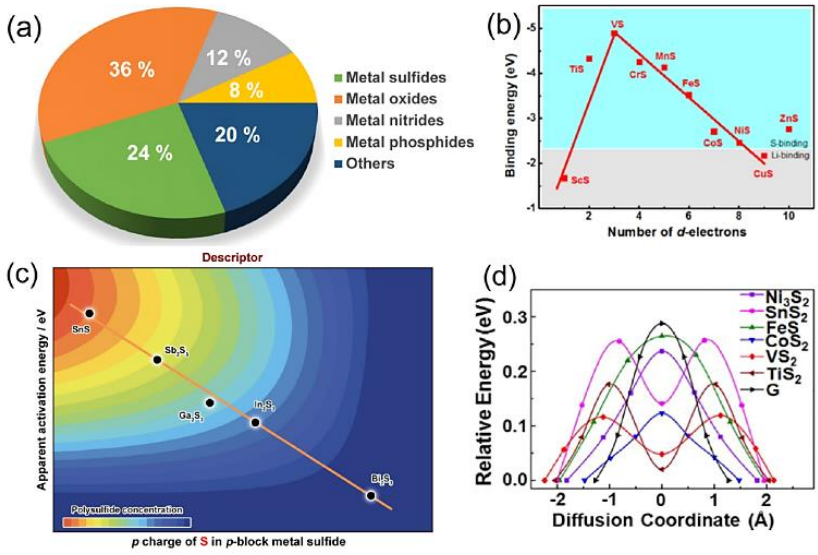

Figure 9. (a) The publications on metal sulfides and other metallic compounds in Mg-S batteries, as sourced from the WOS (Web of Science), (b) Pictorial representations of LiPSs anchored on the MS, guided by the periodic law of binding energy (BE). A linear relationship is observed between the p charge density of sulfur in MS and the apparent activation energy (Ea) of the sulfur reduction process. Energy profiles for the diffusion processes of Mg^{2+} on different catalyst surfaces [78].

8. Synthesis Methods

The synthesis of TMCs is critical for optimising their performance in electrochemical applications. TMCs, known for their anisotropy in electronic and crystallographic structure, are synthesised to improve their properties by adjusting interlayer spacing and microstructural

 doi:10.20944/preprints202510.1895.v1

morphology. Synthesis methods aim to achieve high yields, scalability, and energy efficiency while minimising costs. TMC synthesis techniques can be categorised into top-down and bottom-up approaches. Top-down methods start with bulk precursor material and achieve the desired morphology, while bottom-up methods construct atomic layers block-by-block or layer-by-layer. Top-down methods are cost-effective and produce significant material for electrochemical energy storage applications [96].

8.1. Hydrothermal Method

The hydrothermal technique employs an aqueous medium as the reaction system within sealed steel pressure containers lined with Teflon, which are subsequently heated to a specified temperature to facilitate the reaction. The temperature utilised frequently exceeds 100 °C to achieve vapour saturation pressure, hence generating autogenous pressure within a closed system. The reaction temperature significantly influences the pressure generated in situ within the reactor and is also contingent upon other experimental variables, including the volume of liquid introduced and the presence of dissolved salts Figure 10.

Figure 10. pictorial representation of Teflon-lined stainless-steel autoclaves of varying capacities [97].

Honma and Devaraju recently outlined the key benefits of hydrothermal and solvothermal techniques, which encompass rapid reaction kinetics, short processing times, phase purity, high crystallinity, and cost-effectiveness, among others [98]. The hydrothermal method has effectively enabled the synthesis of metal chalcogenides (MCs) exhibiting various nanostructures, such as ZnSe hollow microspheres [99], hollow cubic cages of MoS_2 [100], b-In_2S_3 nanoflowers [100], CuS microtubules [101], SnS_2 nanocrystals [102], NiSe nanowires, CoTe [103] and NiTe nanowires [104], as well as Ag_2Te nanotubes [105], and Ag_2Se nanoparticles [106]. In a hydrothermal process, a minimal number of organic ligands frequently influences the dimensions, forms, and architectures of the MCs. An exemplary case was presented by Zhao and colleagues [106]. The group detailed a one-step synthesis and assembly of copper sulfide nanoparticles using CuCl and thiourea as precursors via an organic amine-assisted hydrothermal process at moderate temperatures (90-110 °C). A modified hydrothermal method must be established to achieve the controlled synthesis of MCs with specific intrinsic features, such as ferro-magnetic MCs. Figure 11 demonstrates that the microrods of the ferrosulfide minerals greigite (Fe_3S_4) and marcasite (FeS_2) can be selectively synthesised through an in situ magnetic-field-assisted hydrothermal method [107, 108].

 doi:10.20944/preprints202510.1895.v1

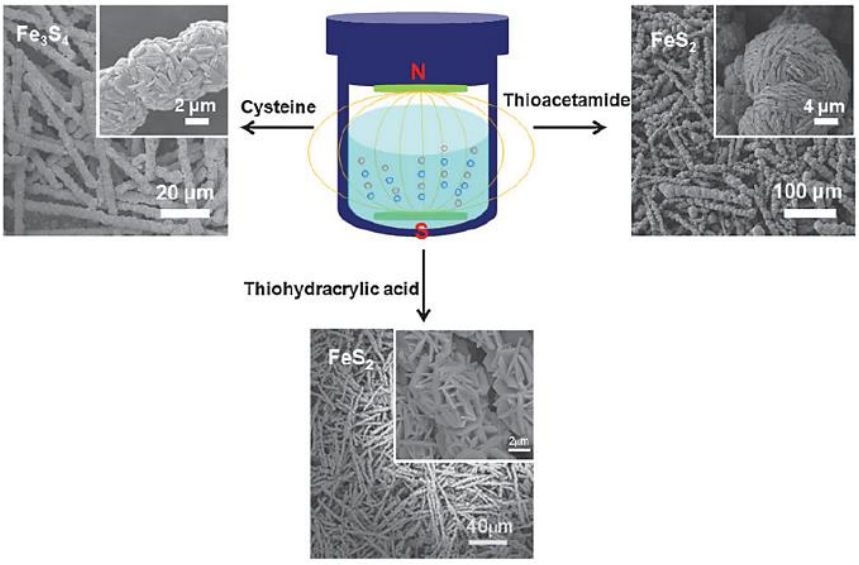

Figure 11. TEM micrographs of ferrosulfide microrods displaying different microstructures synthesised through an in-situ magnetic-field-assisted hydrothermal synthesis technique.

This synthesis method facilitates the creation of crystalline TMC materials while maintaining structural integrity and avoiding thermal decomposition. The method is also effective in the formation of layered TMCs like MoS_2, TiS_2, and VS_2, which are essential for magnesium-sulfur battery applications due to their capacity for magnesium ion intercalation [45]. Recent studies indicate that hydrothermally synthesised MoS_2/reduced graphene oxide (rGO) composites show remarkable efficacy as sulfur hosts in room-temperature sodium-sulfur batteries, attaining a reversible capacity of 190 mAh/g after 1000 cycles at a 2C rate. The hydrothermal process enables the formation of flower-like MoS_2 nanostructures, which exhibit enhanced conductivity and improved buffering of volume expansion during cycling. Moreover, a precise control of defect engineering is achieved by employing this method, as evidenced by the controlled defective MoS_2 nanosheets, which exhibit enhanced electrochemical performance due to optimised active sites and improved ion diffusion pathways [46, 47]. Generally, the mechanism of hydrothermal synthesis utilises surfactants, including but not limited to polyethene glycol (PEG) and polyvinylpyrrolidone (PVP), as structure-directing and stabilising agents. These agents create micelle-like structures that function as "microreactors" for the regulated nucleation and growth of TMC. This method produces uniformly distributed nanoflower-like structures with an average particle size of about 500 nm, demonstrating superior dispersion devoid of agglomeration. The improved electrochemical performance may be attributed to the creation of nitrogen-doped carbon matrices during subsequent annealing processes, which markedly enhance electron and ion transport at electrode interfaces [48].

8.2. Solvothermal Method

Given that the solvent characteristics, including polarity, viscosity, and softness, significantly influence the solubility and transport dynamics of precursors in liquid-based synthesis-thereby governing the reactivity, morphology, dimensions, and phases of the final products-various organic solvents may frequently serve as reaction media in place of water. This novel procedure is referred to as the "solvothermal method." In contrast to the hydrothermal approach, a broader selection of solvents with unique physicochemical features is available, and the reaction temperature can be significantly increased. Utilising the solvothermal method, numerous MC nanocrystals have been synthesised with precise control over size, shape distributions, and crystallinity. These include wire-like $Fe_{1-x}S_{(en)0.5}$ [109], FeS_2 [110], Cu_2Te [111], Ag_2Te [112], and Bi_2S_3 [113]; rod-like α-MnSe [114] and MnS [115]; belt-like ZnSe [116] and Bi_2S_3 [117]; flower-like $FeSe_2$ and $CoS_{1.097}$; sphere-like In_2S_3 [118] and Bi_2S_3 [119]; as well as FeS_2 [120] nanowebs and CoTe nanotubes [121], among others. Yu et al. [122] reported the synthesis of mesostructured wurtzite ZnS-nanowire/amine nanocomposites

 doi:10.20944/preprints202510.1895.v1

that display notable quantum size effects, employing various organic amines (including n-butylamine, ethylamine, and tetraethylene-pentamine) as solvents (Figure 12a). The amine ligands exhibit a preference for binding to the zinc atoms on the (002) face, resulting in the growth of ZnS nanocrystals along the *x*-axis. Using pyridine and xylene as solvents, Qian [120] and Cho [121] prepared ultrathin b-In_2S_3 nanobelts (Figure 12 b) and graphene-like MoS_2 nanoplates (Figure 12 c-d), respectively [123].

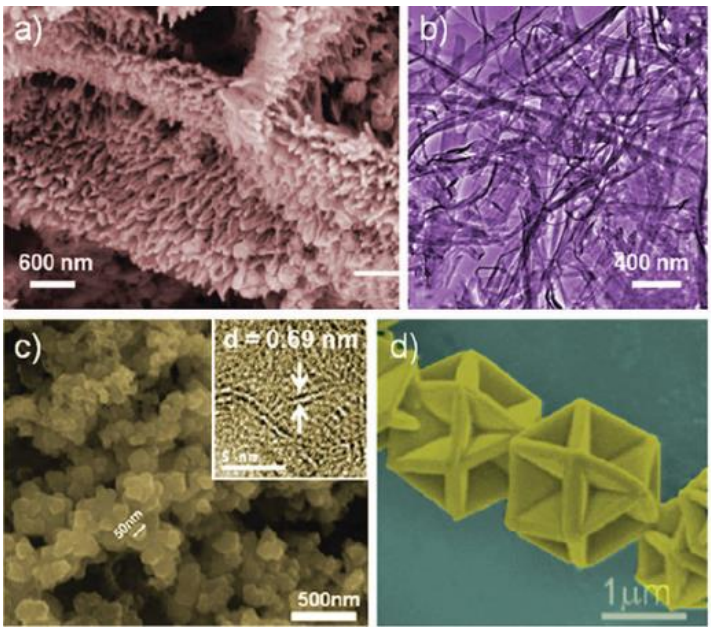

Figure 12. SEM/TEM micrographs of MCs synthesised via the solvothermal process using different solvents: (a) synthesised ZnS nanowire arrays in n-butylamine. (b) synthesised B-In_2S_3 nanobelts in pyridine. (c) prepared MoS_2 nanoplates in xylene (inset-magnified TEM micrograph). (d) prepared Cuboctahedral CuS crystals in EG [121, 122].

The solvothermal method is notably effective for the synthesis of quaternary chalcogenides and complex transition metal chalcogenide structures that are challenging to obtain via alternative methods [11]. Solvothermal synthesis demonstrates versatility through the successful preparation of compounds including $Cs_2CdGeSe_4$, $Cs_2Hg_2GeSe_5$, and $Na_3RbCu_8Ge_3S_{12}$, which display a range of crystal structures from one-dimensional chains to three-dimensional networks. The structural variations notably influence the photocurrent response and electrochemical properties of the materials, with certain compounds attaining photocurrent densities of 180 μA/cm^2, surpassing the performance of most germanium chalcogenides [49]. The mild reaction conditions used in solvothermal synthesis maintain the integrity of complex molecular structures and facilitate the incorporation of organic structure-directing agents. This method has enabled the synthesis of transition metal chalcogenoarsenates exhibiting various dimensionalities, ranging from one-dimensional chains to two-dimensional layers, by carefully selecting organic solvents and structure-directing agents. The materials produced demonstrate semiconducting characteristics with adjustable band gaps, rendering them appropriate for diverse energy storage applications [50].

8.3. Mixed solvent Method

The advancement of the hydrothermal/solvothermal method has led to the rapid development of a promising derivative strategy referred to as the "mixed solvent method." The mixed solvent typically consists of two or more components, allowing for the adjustment of its properties through variations in component selection and volume ratios, thereby facilitating the attainment of optimal synthetic conditions for the desired nanostructures. Recent advances indicate that employing a

 doi:10.20944/preprints202510.1895.v1

mixed solvent can effectively produce MC nanomaterials characterised by unique morphologies or novel nanoarchitectures. The preparation of monodisperse NiS_2 dodecahedrons, with a dimension of approximately. 6 mm in diameter, were carried out in a blended solvent (ethylenediamine, EDA and glycol (3:1, v/v)) using $NiCl_2{\cdot}6H_2O$ and sulfur as starting materials at 200 °C (Figure 13 a) [124]. Yu et al. [125, 126] demonstrated the successful synthesis of Fe_7Se_8 polyhedra featuring two (2) and twelve (12) facets through the heat treatment of $FeSO_4{\cdot}7H_2O$ in a combined solvent of DETA (diethylenetriamine) and water, incorporating Na_2SeO_3, (140 °C), as illustrated in Figure 13 b. The formation of the unique Fe_7Se_8 polyhedrons with exposed high-index facets occurs exclusively at a volume ratio of V_{DETA}/V_{water} = 1:2, highlighting the substantial impact of mixed solvents on the development of nanocrystals with novel structures and morphologies. The mixed solvent method demonstrates effectiveness in synthesising MCs characterised by unique 1D nanostructures, particularly when small organic amines are present. Small organic amine molecules can serve as efficient structure-directing molecules, facilitating anisotropic crystal development, and can as well integrate into the MC structure to create MC-amine inorganic-organic-organic hybrid composites. For the first time, $CoSe_2$-amine (DETA, TETA, or tetraethylenepentamine (TEPA)) hybrid nanobelts (amine =) with notable mesostructures have been synthesised in a binary solution of organic amines and water under mild solvothermal conditions [127]. Figure 14 a and 14 b demonstrate that the uniform and ultrathin nanobelts are single-crystalline, with widths ranging from 100 to 500 nm and lengths extending to several tens of micrometres. Multilayered nanostructures are distinctly observable along the thickness direction of the nearly transparent nanobelts (Figure 14 c). The formation of $CoSe_2$-amine nanobelts requires a specific volume ratio of amine to water, which is 2:1 (v/v). Figure 14 d illustrates that certain amine molecules undergo protonation upon reaction with water, resulting in the formation of positively charged NH^{4+} (ammonium ions). These ions are subsequently integrated into the adjacent $CoSe_2$ layers through binding with selenium [126, 128].

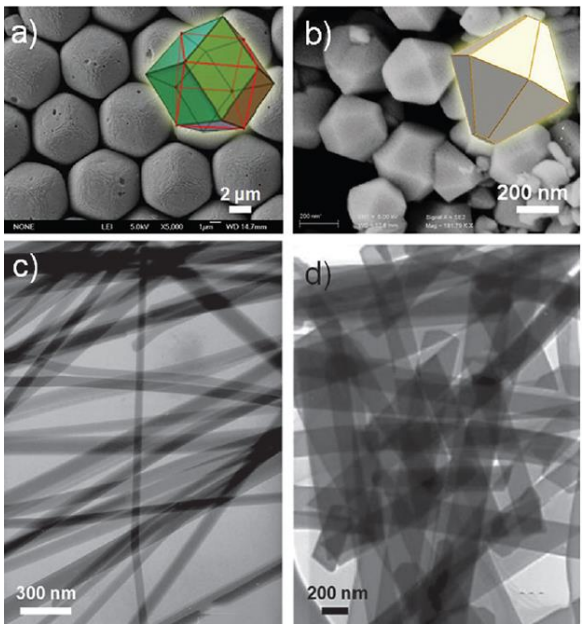

Figure 13. SEM/TEM micrograph of MCs synthesised using the blended solvent method. NiS_2 dodecahedra. (b) FeSeg polyhedra. (c) $[Fe_{18}S_{25}]$ $(TETAH)_{14}$ nanoribbons. (d) (ZnSe) $(DETA)_{0.5}$ nanobelts [97, 127].

 doi:10.20944/preprints202510.1895.v1

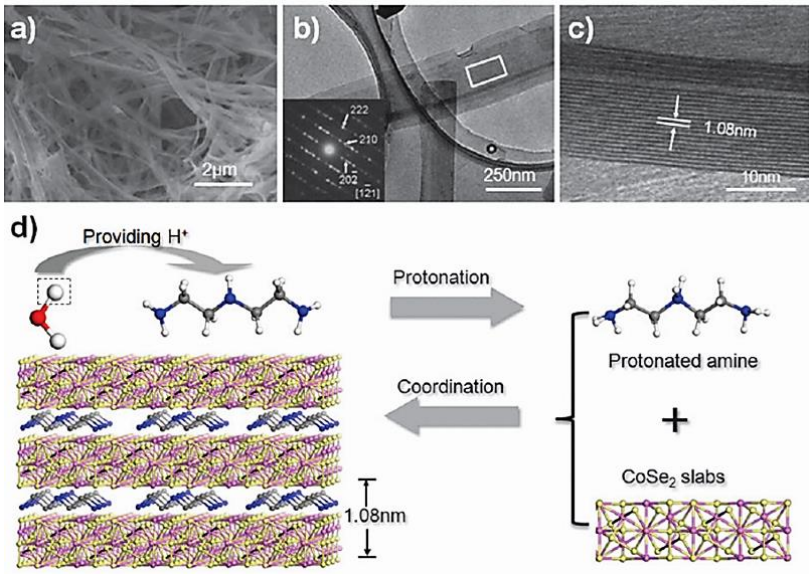

Figure 14. Images (a) SEM and (b) TEM illustrate the appearance of lamellar meso-structured $CoSe_2$-DETA nanobelts (in-set; matching SAED pattern). (c) ideal HRTEM micrograph observed along the lateral thickness direction. (d) Scheme illustrating the formation mechanism of mesostructured $CoSe_2$-DETA nanobelts [127].

8.4. Microwave Method

The heating of matter occurs efficiently through energy transfer via electromagnetic radiation in the frequency ranging from 0.3 to 2.45 GHz. The microwave dielectric thermal mechanism consists of two main processes, viz; dipolar polarisation and ionic conduction, which are distinct from the direct absorption of high-energy electromagnetic radiation necessary for initiating chemical reactions. Microwave-induced chemistry depends on the effective heating of materials. The selected microwave frequency of 2.45 GHz, corresponding to an energy of approximately 1 J mol^{-1}, is optimised for the conversion of microwave energy into thermal energy; however, this energy level is inadequate for breaking chemical bonds. Microwave stimulation has been employed to synthesise several MC nanomaterials [129]. The research conducted by Alonso-Vante [129] and Amini [130] indicates that carbon-supported Co_3S_4, $CoSe_2$, and CoSe nanoparticles, characterised by small dimansion and confined distributions, can be synthesised within 3-5 minutes using microwave stimulation. In contrast, the conventional heating method, which operates at a refluxing temperature of approximately 142 °C, requires several hours for a similar synthesis. Ramanath et al. [131] described a rapid and scalable microwave-induced solvothermal method for synthesising sulfurised Sb_2Se_3 nanowires and nanotubes at a rate of grammes per minute. Adjusting the microwave dose (i.e., microwave power multiplied by time) allows for the control of the diameter and length of these one-dimensional nanostructures. The authors observed a correlation between nanotube content and microwave exposure duration, with values of 7-10 % for 60 seconds, 15-17 % for 90 seconds, and 62-65 % for 120 seconds of synthesis, respectively (Figure 15). Microwave method utilises selective heating of conductive materials, like polypyrrole nanofibers, to deliver localised energy for chemical reactions while preserving mild overall reaction conditions [51]. The efficacy of microwave synthesis is notably demonstrated in the fabrication of TMCs for magnesium-ion battery applications. For example, $CuS_{0.96}Te_{0.04}$ nanosheets synthesised through microwave-assisted methods demonstrate superior performance as magnesium-ion battery cathodes, achieving a specific capacity of 394.5 mAh g^{-1} at a current density of 50 mA g^{-1}, in contrast to 305.4 mAh g^{-1} for pure CuS nanosheets produced under the same conditions. This enhancement is due to increased Mg-ion mobility and diffusion kinetics, which arise from the larger size and polarisability of Te anions, alongside improvements in redox reversibility behaviour [51]. Microwave synthesis also enables precise morphological tuning by varying heating parameters, leading to a range of

 doi:10.20944/preprints202510.1895.v1

nanostructures such as nanospheres, hollow nanospheres, and nanoflowers. The achievement of hollow nanospherical morphologies is crucial for battery applications, as these structures optimise surface area-to-volume ratios and offer resistance to volume changes during ion insertion and removal processes. Similarly, microwave-synthesised VS_4 hollow nanospheres exhibit enhanced performance, achieving specific capacities of 1226.7 mAh g^{-1} after 100 cycles and long-term cycling capacities of 1129.6 mAh g^{-1} after 1000 cycles [20, 51].

Additional synthesis techniques consist of: Liquid-phase synthesis, Hot-injection method, Single-source precursor approach, Electrospinning method, Electrodeposition method, Photochemical method, Cation exchange method, Kirkendall-effect-induced method, Template-directed method, and sonochemical method [129, 132, 133].

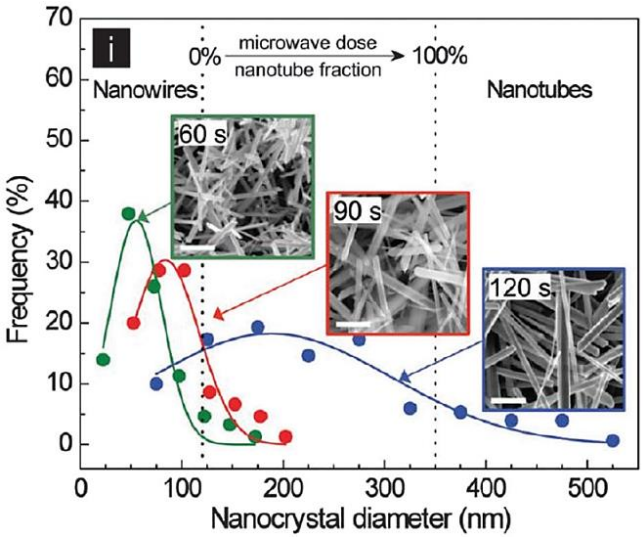

Figure 15. Size distribution graphs with SEM insets (scale bars = 1 μm) of the Sb_2Se_3 nanocrystals [134].

9. Morphology and Solvent Chemistry: Recipe for Improved Electrochemical and Battery Performance

The electrochemical performance of TMC cathodes in Mg-S batteries is closely related to their nanoscale morphology. Hollow and highly porous structures enhance the exposed surface area and offer numerous trapping sites for soluble polysulfides, thereby effectively mitigating the shuttle effect, which is a significant drawback to cycle stability. Nanoflower and nanosheet architectures provide increased interlayer spacings and vertically aligned channels, thereby reducing Mg^{2+} diffusion distances and enhancing rapid ion transport. Heterojunction structures, which involve the interfacing of two or more transition metal chalcogenides (TMCs) or TMC-carbon composites, facilitate significant polarisation effects. This enhancement leads to improved bidirectional catalytic conversion of polysulfides, thereby increasing both Coulombic efficiency and rate performance. The relationship among nanostructure, defect density, and pore volume is crucial: optimised morphologies enhance sulfur immobilisation and facilitate quicker magnesiation/demagnesiation kinetics and improved redox reversibility, resulting in increased reversible capacities and longer lifespans [52, 53]. The solvent environment employed in TMC synthesis serves as a significant factor in regulating material structure and the resulting battery performance. In hydrothermal and autoclave syntheses, pure water functions as a green, high-dielectric medium; nonetheless, solvent polarity, pH, and redox potential can be precisely adjusted through the addition of mineralisers, chelators, or surfactants. Additives influence nucleation rates, stabilise specific crystallographic facets, and promote oxygen- or sulfur-rich terminations, enhancing polysulfide anchoring and interface compatibility with magnesium salts. Autoclave conditions, characterised by high temperatures and saturated vapour pressures, facilitate the formation of large crystal domains and

 doi:10.20944/preprints202510.1895.v1

promote highly oriented growth. This process decreases grain boundary resistance and enhances overall cathode conductivity. Solvothermal synthesis employs organic solvents such as ethanol, ethylene glycol, and DMF, which exhibit a variety of coordinating and reducing properties. These solvents facilitate the stabilisation of metastable phases, promote atomically thin two-dimensional morphologies, and improve defect engineering, thereby creating numerous catalytic sites for sulfur redox reactions. Additionally, mixed-solvent systems that combine water with organic solvents or two immiscible solvents can produce spatial composition gradients or core-shell structures, thereby optimising the surface energy landscape for enhanced electrolyte wetting and polysulfide retention. This solvent engineering enhances electrode/electrolyte contact, reduces charge-transfer resistance, and results in improved cathode performance in Mg-S batteries.

Summarily, the role of diverse synthesis techniques on Mg-S battery performance demonstrates distinct trends. Hydrothermally synthesised TMCs typically exhibit well-aligned layered or nanoflower structures characterised by high crystallinity, which promote efficient Mg^{2+} intercalation and enhance cycle life. Microwave methods facilitate ultrafast heating and nucleation, producing nanomaterials characterised by numerous edge sites and surface defects. These features are essential for catalytic polysulfide conversion and improved electrolyte accessibility, leading to increased sulfur utilisation and extended cycling performance. Mixed-solvent approach optimises surface chemistry, pore size distribution, and facet exposure, thereby modifying the host–guest interactions essential for inhibiting the polysulfide shuttle and enhancing capacity retention. Solvothermal systems demonstrate adjustable polarity and donor properties of organic solvents, enabling precise control over crystal growth and phase composition, thereby optimising diffusion pathways for Mg^{2+} and enhancing electronic conductivity [51, 54]. The synthetic route and solvent environment are crucial factors, alongside composition, in determining the structure, morphology, and properties of Mg-S batteries. The selection of hydrothermal, microwave, mixed-solvent, and solvothermal methods, informed by the desired morphology and optimised through careful solvent design, facilitates the synthesis of chalcogenides characterised by strong sulfur anchoring, rapid Mg^{2+} diffusion, and superior cycle life. The integration of advanced nanostructure control and solvent engineering represents a significant advancement in the design of next-generation high-performance Mg-S battery cathode materials.

10. Modification of MC Nanomaterials

To meet the rigorous requirements of modern electrochemical storage devices, there is a pressing necessity for novel electrode and catalyst materials that demonstrate enhanced performance attributes. The ability to chemically modify an electrode or catalyst nanomaterial through the integration of additional functional nanomaterials offers an intriguing strategy for developing target materials with multifunctional properties or improved features. Recently, notable advancements have been achieved in the modification of MC nanomaterials with various functional materials (e.g., carbon materials, transition metals, metal oxides, and other MCs), revealing the full potential of these MC materials through their significantly enhanced performance.

10.1. Modification with Carbon Materials

Carbon materials, particularly CNTs (carbon, carbon nanotubes) activated carbon, , and graphene, have been the focus of extensive investigation as substrates for hosting diverse active nanomaterials in ECS applications, owing to their excellent conductivities and substantial surface areas. The incorporation of MC nanomaterials onto carbon materials has been effectively established. According to the findings of Gedanken et al. [135], 1D carbon-coated WS_2 (WS_2/C) nanocomposites can be synthesised through the thermolysis of $W(CO)_6$ with elemental sulfur in a sealed Swagelok reactor at 750 °C in an inert gas atmosphere. The WS_2-C particles resemble annelid-worms type , featuring a smooth surface with an average diameter of 25 nm and lengths measuring 180 nm. Similarly, WSe_2/C nanofibers measuring 50-100 nm in diameter and several micrometres in length were successfully produced through a 1-hour chemical reaction involving $W(CO)_6$ and Se at

 doi:10.20944/preprints202510.1895.v1

750 °C in a dry autoclave. Yan et al. [136] devised a straightforward method for synthesising FeS/C nanosheets in an oleylamine solution, utilising 1-dodecanethiol as both the sulfur source and surfactant [137-139]. This synthesis involves the reaction of $Fe(Acac)_3$ with sulfur atoms to produce narrowed layers of FeS, while the hydrocarbon ends of 1-dodecanethiol act as separators between these layers. Upon annealing in argon, the FeS layers are transformed into carbon. The synthetic approach described here can be adapted to produce FeS/C nanospheres and nanoplates through straightforward adjustments to the synthetic parameters. Carbon nanotubes are widely employed to enhance metal carbide nanomaterials due to their substantial surface area, superior thermal and chemical stability, and high electrical conductivity. Walton et al. reported their findings on the synthesis of WS_2/CNT composites via the pyrolysis of WO_3-coated multiwalled CNTs in an H_2S/N_2 atmosphere at 900 °C [140]. The distorted WO_3 coatings have been seen to transform into layered WS_2 nanotubular sheaths on the CNT surface, aligned with the basal carbon rings of the CNT. According to Park et al. [141], nanocrystals of b-Cu_2S can be synthesised in-situ on CNTs within an oleylamine medium through the reaction of $Cu(Acac)_2$ with elemental S at a temperature of 190 ℃. Chen et al. [142] have incorporated various MC nanomaterials onto graphene nanosheets (GNs). Layered MoS_2-graphene composites can be synthesised using an L-cysteine-enhanced solution-phase technique, followed by annealing in an H_2/N_2 gas atmosphere for 2 hours at 800 °C [143]. The L-cysteine-assisted approach was subsequently employed to create a few-layer SnS_2-graphene hybrid. Once more, L-cysteine serves as a complexing sulfide source and a reducing agent throughout the synthesis process. Through a one-step solvothermal reaction involving $(NH_4)MoS_4$ and hydrazine in DMF (N, N-dimethylformamide) solution containing mildly oxidised GO (graphene oxide) at 200 °C (Figure 16a), Dai et al. [144] successfully synthesised MoS_2/RGO hybrid nanostructured materials. The $(NH_4)MoS_4$ precursor underwent reduction to MoS_2 on GO, while the mildly oxidised GO was converted to reduced GO (RGO) through hydrazine reduction. Figure 16 b illustrates the uniform decoration of RGO sheets with MoS_2 nanoparticles. The HRTEM micrograph displays hexagonal atomic lattices within the MoS_2 basal planes, along with a significant presence of open edges in the nanoparticles (see inset in Figure 16 b). Conversely, the identical synthetic approach resulted in MoS_2 aggregating into 3D-like particles of differing sizes when GO sheets were not present (Figure 16c and inset). The remarkable morphological difference underscores the significant function of GO sheets in facilitating the nucleation and subsequent growth of MoS_2 [145].

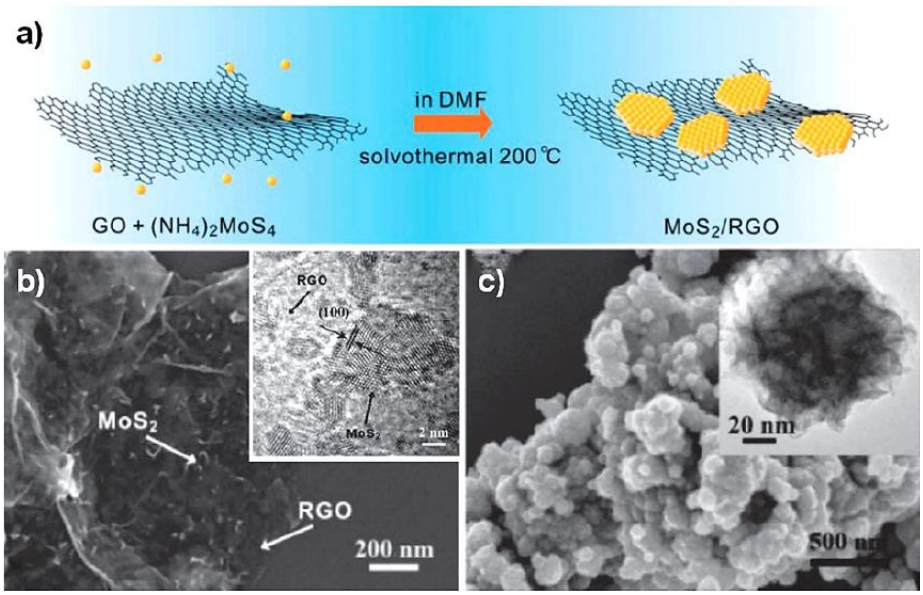

Figure 16. (a) pictorial representation of solvothermal method utilising GO thin sheets to produce the MoS_2/RGO hybrid. (b) SEM and HRTEM (inset) micrograph of the MoS_2/RGO hybrid nanomaterials. (c) SEM and (inset) TEM micrograph of the free MoS_2 nanoparticles synthesised, excluding any GO sheets [146].

 doi:10.20944/preprints202510.1895.v1

10.2. Tuning of MC Nanostructured Materials with Noble Metals

Noble metals have garnered significant attention due to their distinctive applications across multiple domains. For instance, Pt (Platinum) nanocrystals demonstrate significant catalytic and electrical properties, coupled with outstanding corrosion resistance. Gold (Au) nanoparticles possess unique physical, chemical, and biocompatible characteristics, resulting in broad applications in catalysis, sensing, imaging, and medicine. Silver (Ag) nanoparticles are applied in various oxidative coupling and oxidation reactions and are frequently used as substrates for near-field optical probing, Surface Enhanced Raman Scattering (SERS), and optical labelling. The strategic integration of noble metals with single-phase MC nanomaterials is expected to produce improved or novel advantageous properties in MCs. A range of noble-metal-modified MC nanostructures has been synthesised through various techniques, which can be classified into core-shell and heterostructures. Yu et al. [147] have presented a straightforward technique for the reduction of EG, enabling the in situ loading of Pt nanoparticles onto pre-synthesised $CoSe_2$/DETA nanobelts under moderate chemical conditions, eliminating the need for molecular linkers. The abundant surface amino moieties serve as nucleation sites, allowing for the homogeneous dispersion of Pt nanoparticles, approximately 8 nm in size, on $CoSe_2$/DETA nanobelts (Figure 17a). Furthermore, the configuration and surfaces of the loaded Pt nanoparticles can be altered by adjusting the reaction duration. The developed nanohybrid Pt-$CoSe_2$ exhibited a notable enhancement in ORR performance in acidic environments compared to the pure $CoSe_2$/DETA nanobelts. Wang et al. [148] synthesised Au-Ag-AuS nanomaterials with a cucumber shape (Figure 17) by hydrothermally treating Au nanorods, metal thiobenzoates, and $AgNO_3$, utilising cetyltrimethylammonium bromide (CTAB) as a surfactant. In this study, nickel thiobenzoate served as the sulfur source. The Au nanorods served a dual purpose: they acted as a sacrificial template guiding the formation of sea cucumber-shaped nanostructures, while also functioning as a initiator for the creation of Au-Ag-AuS nanostructures [149, 150]. Yang and Ying [151, 152] focused intently on the creation of heterogeneous semiconducting-noble metal composites. A general protocol was established for the transfer of transition metal ions from aqueous solutions to organic media through an ethanol-mediated approach, which has the potential to be applied in the preparation of various heterogeneous semiconductor/noble-metal hybrids [150]. Recently, this group introduced a straightforward aqueous approach for synthesising nanocomposites that incorporate Ag_2S alongside various noble metals [152]. Utilising the one-pot technique, 7 nm nanocrystals of Ag_2S were synthesised alongside sodium citrate and numerous noble-metal starting materials at temperatures of 105 °C for gold and 110 °C for other noble metals. This process resulted in the formation of noble-metal/Ag_2S heterostructures, including Au-Ag_2S (Figure 17c), Pt-Ag_2S (Figure 17d), and Os-Ag_2S (Figure 17e). The metals demonstrated a preference for nucleating on existing Ag_2S seeds rather than undergoing homogeneous nucleation in the presence of Ag_2S seeds. Au was found to deposit exclusively at a single site on each Ag_2S seed, while the nucleation and growth of Pt and Os occurred at multiple sites on each Ag_2S seed (Figure 17c-e). This is due to the presence of multiple facets in monoclinic Ag_2S, each exhibiting distinct lattice spacings. These variations may create advantageous sites that align with the lattice planes of different noble metals, facilitating their epitaxial development on the substrate. The synthesis utilised CTAB-embedded nanocrystals of Au as the initial reactants and metal-thiobenzoates as the precursors for metal-sulfides. The introduction of a minor concentration of Ag^+ ions or Cu^+ ions lead to the formation of Ag_2S/CuS, which serves as a wetting layer, facilitating the plating of additional metal sulfides onto the nanocrystals of Au. This approach enabled the successful production of various core-shell nanostructures, including Au/ZnS (Figure 17 f), Au/$Ni_{1-x}S$ (Figure 17 g), and Au/$Cu_{2-x}S$ (Figure 17 h). The straightforward one-pot approach is thought to be applicable for the synthesising core-shell nanostructures comprising nanocrystals of Au alongside metal Se (selenide) and Te (telluride) semiconductors [150, 152].

 doi:10.20944/preprints202510.1895.v1

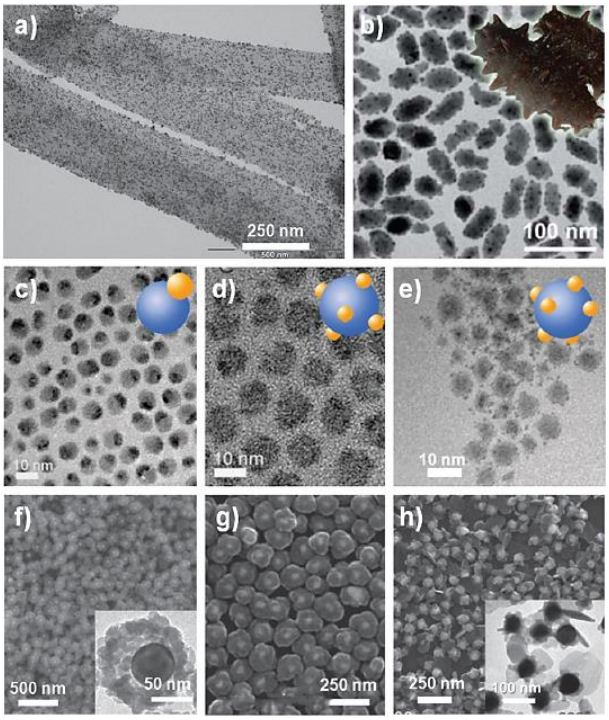

Figure 17. (a) TEM micrograph depicting Pt-$CoSe_2$ nanobelts. (b) TEM micrograph of Au/AgAuS nanohybrids (in-set; images of two sea cucumbers). (c-e) Transmission electron microscopy micrographs of Au/Ag_2S, Pt/Ag_2S, and Os-Ag_2S heterostructured materials, respectively. Insets represent configurations matching heterostructures. SEM micrographs of Au/ZnS, Au/$Ni_{1-x}S$, and Au/$Cu_{2-x}S$ core-shell structures are presented in panels (f-h), respectively. The insets in (f) and (h) display the corresponding TEM micrograph [97].

10.3. Tunning MC Nanomaterials Using Metal Oxides

Metal oxides serve as crucial active components in various EC charge-storage systems due to their combined electronic and ionic transport properties. For example, metal oxides frequently provide greater energy densities for supercapacitors compared to carbon materials, as well as enhanced electrochemical stability relative to polymer materials [153]. In light of this understanding, numerous research groups have extensively incorporated metal oxides to hybridise with MCs, aiming to enhance and expand the energy applications of MC nanomaterials [154]. Yu's [127] group chose pre-synthesised ultrathin lamellar mesostructured $CoSe_2$/DETA nanobelts as substrate materials, which were systematically tuned with various metal oxide NPs e.g., Fe_3O_4, and Mn_3O_4 (Figure 18), resulting in observed enhancements in electrocatalytic performances [155, 156]. The newly developed $CoSe_2$/DETA nanobelts exhibit numerous advantages, including a substantial specific surface area (BET = 77 m2 g^{-1}) and an abundance of amino groups on their surface, which enhance their potential for functionalisation. For example, through the thermal degradation of $Mn(Acac)_3$ in the TREG solution of $CoSe_2$/DETA nanobelts at 278 °C under nitrogen atmosphere resulted in the effective decoration of highly crystalline Mn_3O_4 nanoparticles, averaging approximately 15.7 nm in size, on the backbone of $CoSe_2$ nanobelts (Figure 18 a and b) [97, 157].

 doi:10.20944/preprints202510.1895.v1

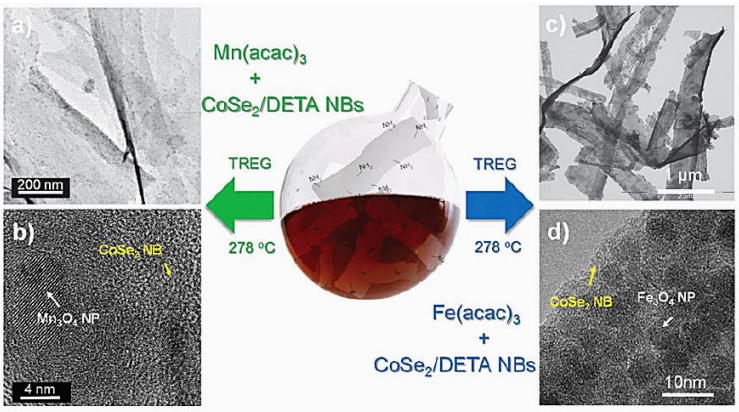

Figure 18. Metal oxides-$CoSe_2$ nanocomposites were synthesised using the polyol reduction method. TEM/HRTEM micrograph of Mn_3O_4-$CoSe_2$ composites synthesised at 278 ℃ for 1 hr are presented in (a) and (b), respectively. TEM/HRTEM micrograph of Fe_3O_4-$CoSe_2$ mposites synthesised at 278 ℃ for 30 min. are illustrated in panels (c) and (d), respectively [156, 157].

11. Application of Transition Metal-Chalcogenides in Mg-S Batteries

S cathodes generally engage in a conversion reaction that involves two electrons, exhibiting a theoretical capacity of up to 1684 Wh kg^{-1}. The actual energy density is considerably lower than the theoretical value, attributed to slow conversion kinetics and the low intrinsic conductivity of sulfur and its discharge product, magnesium sulfide. Researchers have suggested compositing the sulfur cathode with conductive carbon substrates to improve conductivity and conversion kinetics, and implementing partial doping of atoms like selenium, tellurium to extend covalent bonding lengths and increase the sulfur cathode's utilisation rate [158].

11.1. Copper (Cu)-Chalcogenide-Based Cathodes

Cu-chalcogenides (CuxTy, T = S, Se) have garnered significant interest owing to their substantial theoretical capacity, stable charge-discharge characteristics, and cost-effectiveness. Following the development of Mg-S batteries, numerous Cu-chalcogenides with superior morphology have been synthesised and utilised as cathodes in Mg-S batteries, establishing themselves as the predominant conversion cathodes [159]. Presently, the common CuxTy [160] compounds are CuS, $CuSe_2$, CuSe, Cu_2Se, Cu_2S, and so on. Earlier, Duffort et al. [161 previously investigated the application of CuS cathodes in Mg-S batteries and analysed their energy storage mechanism (Figures 19a-c). CuS nanoparticles were synthesised with particle sizes ranging from 5 to 10 nm through a multi-step heat treatment process involving Cu powder and S powder. Ex-situ XRD demonstrated the electrochemical processes associated with two stable discharge platforms, resulting in the formation of Cu_2S and MgS, respectively (Figure 19c). The capacities measured at room temperature were minimal, achieving only approximately 10% of the theoretical discharge capacity (60 mAh g^{-1}), even when the temperature was increased to 60 °C [161]. However, when the temperature was raised to 150 °C, an initial discharge capacity close to the theoretical capacity was obtained, indicating that the high temperature environment enhanced the rate of EC reaction (Figure 19a). It can be said that there remains significant potential to enhance the efficiency of CuS in Mg-S batteries, necessitating further research into its application as a cathode. By comparison, elemental Se (selenium) exhibits superior electrical conductivity and reduced diffusion energy barriers for Mg^{2+} in Se^{2-} materials. Additionally, the coulombic interactions between the anions and cations of MgSe intermediates formed by Mg embedded in Se^{2-} are less pronounced compared to MgS. This indicates that a lower energy threshold is necessary for the detachment of Mg^{2+} during the charging process, significantly improving the efficiency of Mg^{2+} insertion and de-insertion in these materials. Thus, CuS demonstrates broader application potentials. The performance of copper-based sulfides in Mg-S batteries is usually modified for device performance enhancement by partly employing the synthesis

 doi:10.20944/preprints202510.1895.v1

of materials with superior morphology, such as hollow structures and nanoflowers. This approach aims to increase the specific surface area and mechanical properties of the materials, thereby improving their EC properties [162]. For example, Xu et al. [163] studied the influence of particle dimension on the performance of magnesium ion batteries (MIBs) by utilising two (2) CuS (CuS-I, CuS-II) NPs of varying sizes. Both NPs exhibit a 100 nm NPs size; however, CuS-II demonstrates a comparatively larger average particle size of 148.9 nm. The reduced particle size resulted in a greater specific surface area (SSA) of 10.8675 $m^2\ g^{-1}$ and 6.6503 $m^2\ g^{-1}$ for CuS-I, and CuS-II respectively, facilitating the complete accessibility of active sites, thus improving reactivity (Figures 20 a and b). Cao's group [164] employed various solvents and conditions of reaction to synthesise typical CuS NPs and CuS exhibiting intricate nanoflower-like ball morphology by solvothermal technique, then examined the influence of morphology on the EC characteristics of the materials. Initially, CuS NPs were synthesised with no surfactants, utilising $Cu(NO_3)_2{\cdot}6H_2O$ as the Cu precursor, sulfur powder as the sulfur source, and ethylene glycol (EG) as the solvent. Exquisite single crystal CuS nanorods were synthesised utilising a blended solvent of acetone and water, with thiourea serving as the sulfur precursor, with the aid of bi-surfactants of PVP and CTAB (Figure 21 a). The extensive vertically stacked nanosheet arrays allowed the CuS nanoflower-shaped spheres to possess a substantial SSA (9.3 $m^2\ g^{-1}$, compared to 4.69 $m^2\ g^{-1}$, for CuS nanoparticles) together with numerous microporous and mesoporous structures. The CuS nanoflower spheres depicted in Figure 21 b demonstrated a high specific capacity of 252 mAh g^{-1} at a current density of 0.1 A g^{-1} and a reversible specific capacity of 171.2 mAh g^{-1} at 0.5 A g^{-1}, attributable to their structural characteristics. The CuS nanoflower spheres demonstrated a specific capacity of 91.7 mAh g^{-1} at a current of 1 A g^{-1} and exhibited stability over 500 cycles, achieving a capacity retention rate of 83.3%. In contrast, the CuS nanoparticles exhibited a discharge capacity of less than 100 mAh g^{-1} at a current density of 0.2 A g^{-1} (Figure 21c). The significant pores within the nanosheets of the CuS nanoflower spheres provide buffer capacity for the cathode material during cycling, thereby markedly improving its cycling stability [162].

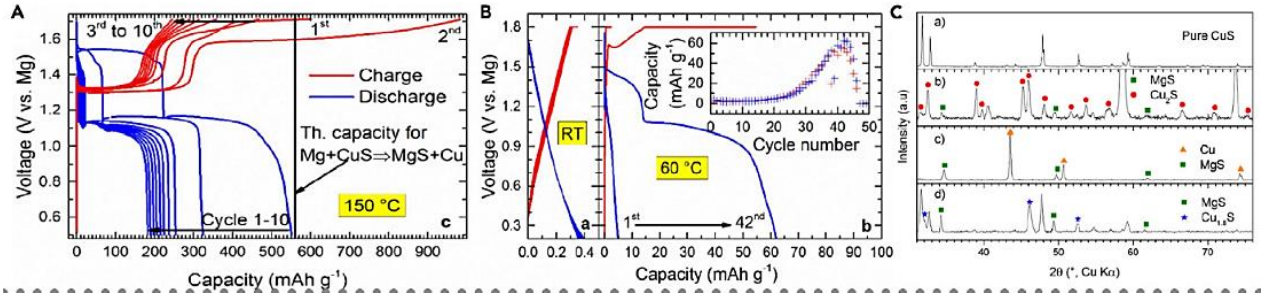

Figure 19. The design of nanoscale copper (Cu)-based chalcogenide cathodes for metal-ion batteries (MIBs). (a) GCD curves of CuS at each cycling stage: At 150 °C, the initial discharge nears the theoretical capacity of 550 mAh g^{-1}, (b) a comparison between room temperature and 60 °C, with a depiction of reversible capacity trend (inset), and (c) XRD spectra of the CuS cathode at various EC conditions [165].

 doi:10.20944/preprints202510.1895.v1

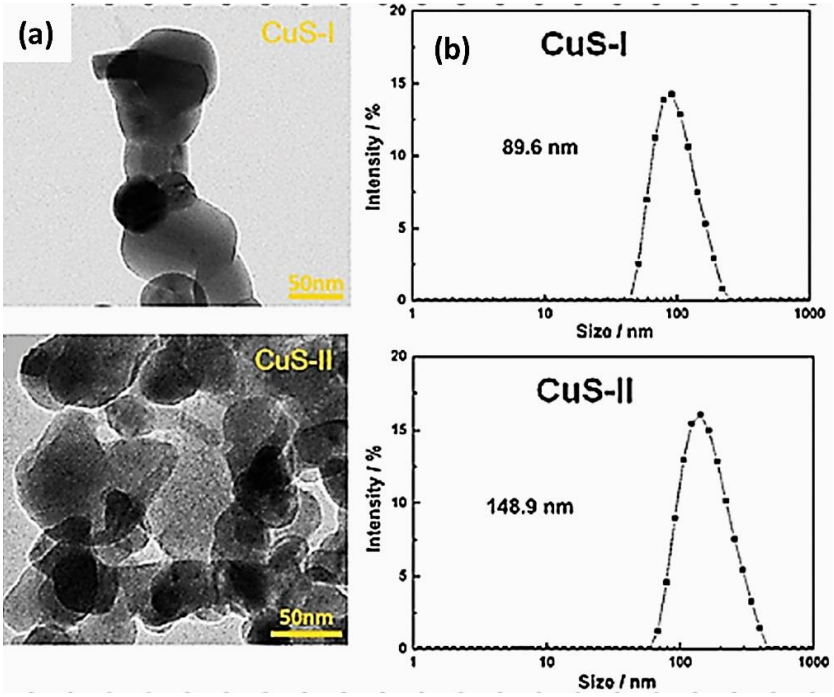

Figure 20. (a) Comparison of TEM micrographs and (b) Dynamic Light Scattering (DLS) results for CuS-I and CuS-II [166].

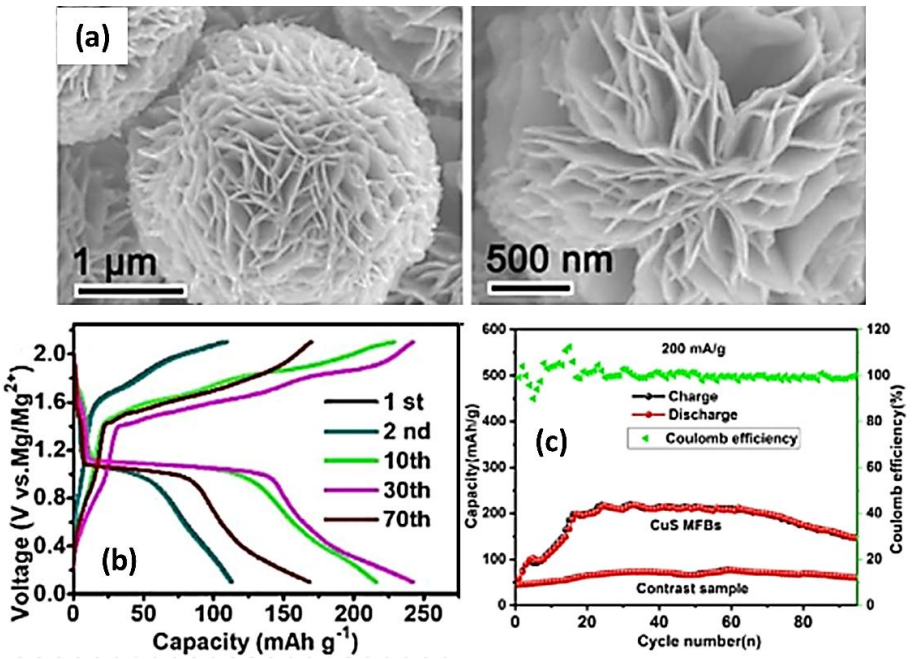

Figure 21. Self-assembly of nanoflower-shaped and nanosheet Cu chalcogenide cathodes for MgS is illustrated in (a) SEM micrograph, (c) selected electron diffraction images of CuS nano flowering spheres and (d) , rate performance, GCD curves, and cycling performance of CuS material [167].

11.2. Iron-Based Chalcogenide Cathodes

FeS_2, the primary constituent of pyrite, which is the most prevalent sulfide mineral globally, is considered a highly promising candidate for high-energy cathode materials. This is attributed to its high theoretical capacity of 894 $mAhg^{-1}$ and its excellent magnesium-ion storage performance in Mg-S batteries [168]. Magnesium metal ranks among the most abundant elements in the Earth's crust,

 doi:10.20944/preprints202510.1895.v1

resulting in its lower cost compared to lithium. The combination of Mg with FeS_2 results in a notable Mg-FeS_2 couple, characterised by a wealth of electrode materials and a high theoretical energy density that is comparable to that of Li-FeS_2 or Li-S. The battery system demonstrates significant potential for high-energy and sustainable electrochemical energy storage. The incorporation of $LiBH_4$ salt into the electrolyte of the Mg-Li hybrid battery facilitated enhanced performance, characterised by exclusive magnesium plating and stripping at the anode, while the FeS_2 cathode effectively reversibly stores lithium. Despite a noticeable decline in the capacity of FeS_2 cathodes during the initial cycles, a reversible capacity exceeding 200 mAh g^{-1} was sustained after 200 cycles (Figure 22a). The development of FeS_2 composites to address the volume changes of the cathode during cycling could enhance cycling stability [169]. Kovalenko et al. [170] addressed the limitations of magnesium storage kinetics and the rapid kinetics of alkali ion storage by developing a Mg-Na hybrid battery. This system utilises a magnesium salt-based electrolyte along with a $NaBH_4$ electrolyte additive. The constructed Mg-FeS_2 battery utilising hybrid Mg^{2+}/Na^+ storage exhibited an energy density of 210 Wh kg^{-1} (referencing the cathode). Nonetheless, the incorporation of sodium salt, which is cost-effective, aligns well with the development of a plentiful Mg-FeS_2 battery system. Despite the suboptimal magnesium storage kinetics of FeS_2, Suo et al. [40] reported the use of an ion-doping approach to prepare $Fe_{0.5}Co_{0.5}S_2$ solid solution, which exhibited a uniform elemental distribution of Fe, Co, and Si nanoscale regions (Figure 22 b), for magnesium storage. The as-prepared solid solution cathode material demonstrated an evident enhanced capability for reversible magnesium storage in the pure Mg-based electrolyte devoid of the incorporation of additional metal ions. A reversible capacity of approximately 200 mAh g^{-1} was achieved at a minimal current density of 20 mA g^{-1}, along with an energy density of around 240 Wh kg^{-1}, as reported in reference [171] (pertaining to the cathode). This study demonstrated that the $Fe_{0.5}Co_{0.5}S_2$ cathode material displayed intercalation-type magnesium storage during cycling. The four-electron conversion reaction remains unachieved. Furthermore, a capacity of 600 mAh g^{-1} is maintained after 50 cycles (Figure 22c), indicating a highly reversible electrode reaction. The mechanism study indicates that the FeS_2 cathode undergoes a two-step, four-electron conversion reaction for magnesium storage: $FeS_2 + Mg^{2+} \rightarrow FeS + MgS \rightarrow Fe + MgS$ (Figure 27d) [172]. The strategies for in-situ formation of conductive pathways in FeS_2 during cycling are advocated, given the formation of exceptionally small iron particles within the insulating MgS matrix during discharge.

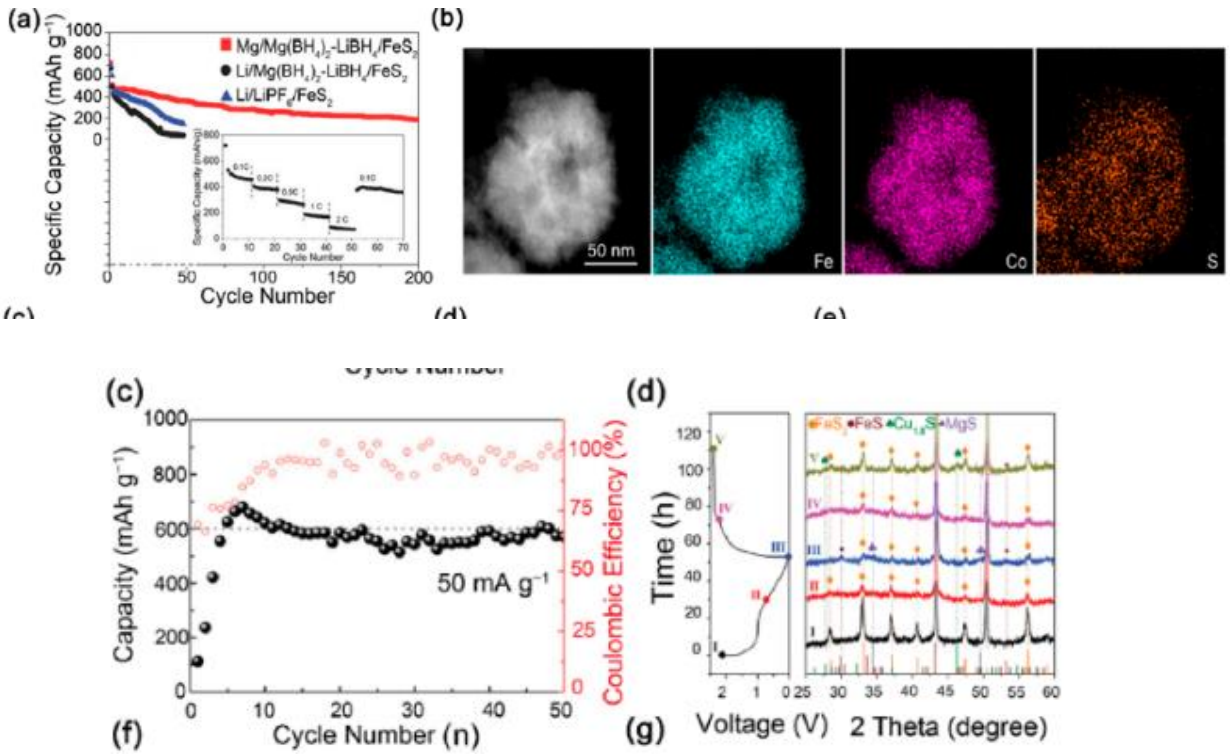

 doi:10.20944/preprints202510.1895.v1

Figure 22. (a) The discharge capacity and capability rate of Mg-FeS_2 in the $Mg(BH_4)_2$-iBH_4/DME electrolyte, (b) TEM mapping of Fe0.5 $Co_{0.5}S_2$ (scale bar: 100 nm), (c) Cycling performance and Coulombic efficiency of FeS_2 at a current density of 50 mA g^{-1}, (d) Galvanostatic discharge-charge curves of the FeS_2 cathode at 10 mA g^{-1} during the initial cycle, along with Exsitu XRD diffractograms of the FeS_2 cathodes in various EC states [162].

11.3. Cobalt-Based Chalcogenide Cathodes

Additionally, cobalt-based materials, alongside iron-based sulfides, exhibit significant potential for application in Mg-S batteries, attributed to their vast natural reserves and elevated electrical conductivity. The current focus in the advancement of electrode materials for cobalt-based sulfides is on nanosizing, surfactant-induced morphology formation, and the incorporation of carbon materials. Cai et al. [173] were the first to utilise spinel-structured Co_3S_4 in magnesium-sulfur batteries. They used the solvothermal reaction of Co $(OAc)_2.4H_2O$ with thioacetamide (TAA) to synthesise nanoflower spheres ($Co_3S_{4\text{-}F}$) in a laminated nanosheet self-assembled structure, and the thickness of the nanosheets was small at only 10 nm, which significantly reduced the diffusion path for Mg^{2+}(Figure 23a). The heat-treatment strategy applied to the sulfurised Co_3O_4 precursor facilitated the synthesis of layered mounted nanorods ($Co_3S_{4\text{-}T}$) and allowed for an independent exploration of the Mg storage properties (Figure 23b). Figure 23 c-d illustrates that the $Co_3S_{4\text{-}F}$ electrode achieved an initial discharge capacity of 779.8 mAh g^{-1} in the APC/LiCl electrolyte system at a current density of 100 mA g^{-1}. After 100 charge/discharge cycles, it retained a capacity of 399.5 mAh g^{-1}, resulting in a capacity retention rate of 51.2 %. The capacity of $Co_3S_{4\text{-}T}$ was measured at 16.9 mAh g^{-1} following 100 cycles. Zhao et al. [174] introduced a Co_3S_4@MXene heterostructure designed to serve as a sulfur host for reversible Mg-S batteries. The interaction between the decorated Co_3S_4 nanocrystals and polysulfide intermediates may facilitate the absorption and catalysis of polysulfide conversion, thereby enhancing the EC reduction-oxidation kinetics, as indicated by XPS measurements. The MXene matrix has the potential to significantly improve Mg ion transport dynamics. The Mg-S batteries utilising Co_3S_4@MXene-S as the cathode material demonstrated high sulfur utilisation, achieving a specific capacity of 1220 mAh g^{-1} and a capacity of 528 mAh g^{-1} after 100 cycles, alongside satisfactory rate performance at 2C. This study presents a unique cathode design for reversible high-energy Mg-S batteries.

Given the weaker Co-Se bond relative to the Co-S bond, $CoSe_2$ may demonstrate superior reaction kinetics compared to CoS_2, despite possessing a reduced theoretical capacity. Xu's [175] team. Given the weaker Co-Se bond relative to the Co-S bond, $CoSe_2$ may demonstrate superior reaction kinetics compared to CoS_2, despite possessing a lower theoretical capacity. Xu's team developed three distinct $CoSe_2$ nanostructured materials exhibiting nano polyhedral, hollow microsphere or nanorod morphologies, which displayed significant variations in electrochemical properties. The $CoSe_2$ nanorods demonstrated a maximum reversible capacity of 233 mAh g^{-1} at 50 mAg^{-1} and a rate capability of 116 mAh g^{-1} at 0.5 Ag^{-1}, attributed to their one-dimensional structure that facilitates extensive contact surface for Mg^{2+} pseudocapacitive storage. In contrast, the $CoSe_2$ hollow microspheres exhibited superior cycling performance due to their stable hierarchical micro/nanostructure. A subsequent investigation integrated $CoSe_2$ with an MXene material to establish a conductive network within the composite material (Figure 24a-e). The MXene material is capable of reversibly storing Mg^{2+} ions. Therefore, the composite cathode facilitates both intercalation and conversion reactions, enabling reversible magnesium storage. $CoSe_2$ demonstrates notable enhancements in charge and discharge performance through various structural and compositional modifications. Nonetheless, the experimental energy density remains significantly lower than that of CoS_2. The electrochemical performance data of cobalt-based chalcogenides for Mg metal-based batteries are outlined in Table 2 [97].

 doi:10.20944/preprints202510.1895.v1

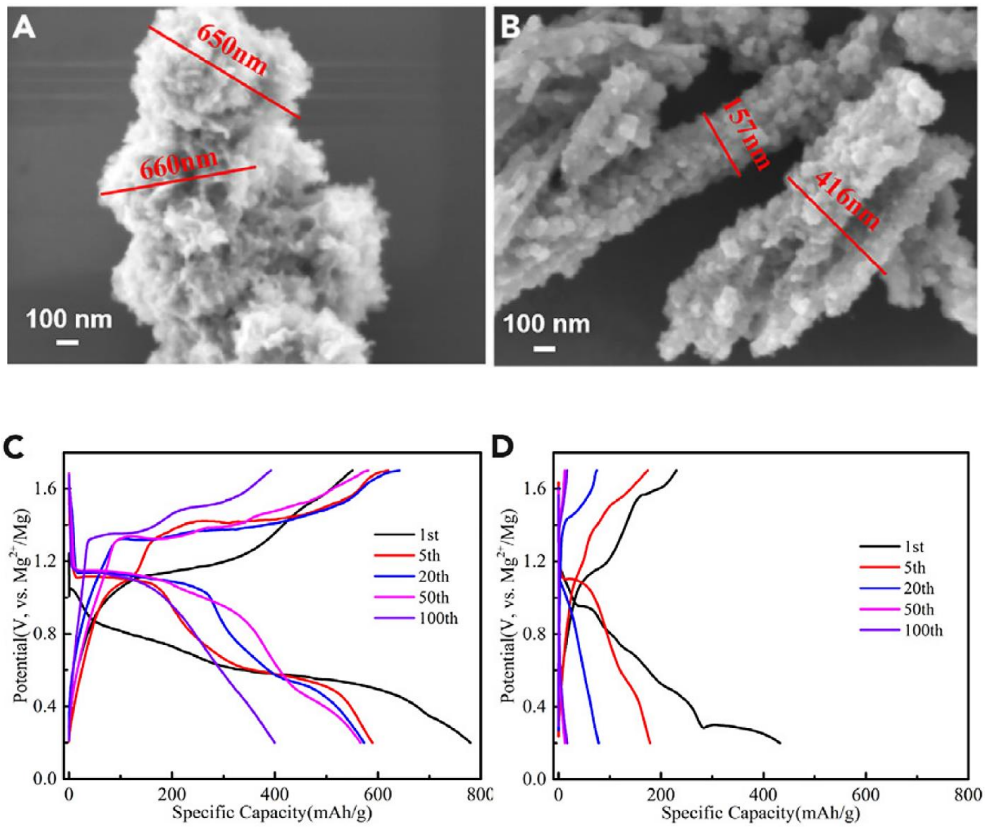

Figure 23. The integration of cobalt-based sulfide cathode in MgS batteries: (a-b) SEM micrograph of granular $Co_3S_{4\text{-}F}$ and rod $Co_3S_{4\text{-}T}$ materials, respectively. (c-d) GCD plots of granular $Co_3S_{4\text{-}F}$ and rod-shaped $Co_3S_{4\text{-}T}$ nanomaterials, respectively [162].

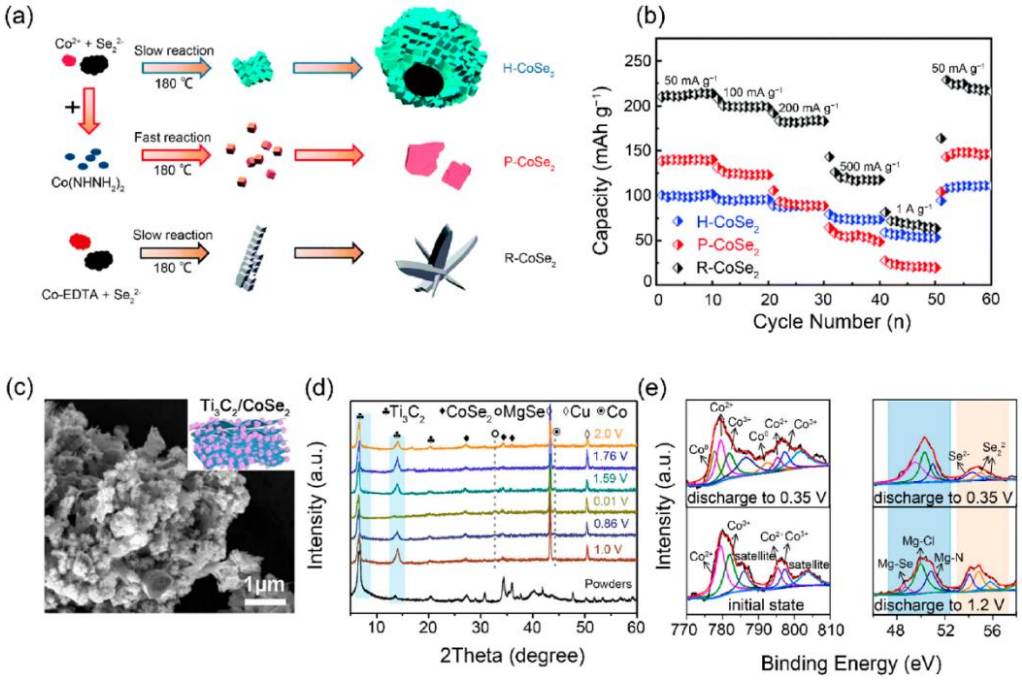

Figure 24. (a) Diagrammatic representation of the synthesis of $CoSe_2$ materials exhibiting various morphologies and (b) their performance in terms of rate capability across the different morphologies of $CoSe_2$. (c) SEM micrograph depicting the morphology of $Ti_3C_2/CoSe_2$. (d) Exsitu XRD diffractograms of $Ti_3C_2/CoSe_2$ after achieving a discharge and recharging of 0.01 V and 2.0 V, respectively. (e) Exsitu XPS spectra of $CoSe_2$ cathodes [176].

 doi:10.20944/preprints202510.1895.v1

11.4. Nickel-Based Chalcogenide Cathodes

In contrast to iron and cobalt sulfides, nickel sulfides and/or selenides utilised in Mg-metal-based batteries have been less frequently documented in comparison to iron and cobalt sulfides and/or selenides. Nickel sulfides and selenides undergo irreversible phase transformations during redox reactions, in contrast to iron and cobalt disulfides and diselenides. Mai et al. [40] prepared $Ni_{0.75}Fe_{0.25}Se_2$ flower-like microspheres by doping Fe into the $NiSe_2$ material. Fe-doped $Ni_{0.75}Fe_{0.25}Se_2$ demonstrates a greater number of active redox sites and enhanced Mg^{2+} diffusion kinetics, nearly double that of pure $NiSe_2$. The elemental analysis indicated that the Ni to Fe ratio was maintained at 3:1 after 30 cycles (Figure 25 a); however, a decrease in Se content was observed. Charging the cathode to 2.0V during the initial cycle resulted in the formation of $Ni_{0.75}Fe_{0.25}Se$, rather than the original $Ni_{0.75}Fe_{0.25}Se_2$, indicating an irreversible phase transformation. The redox processes that occur in the subsequent cycles are characterised as

$$Ni_{0.75}Fe_{0.25}\ Se + 1 - 0.75\chi)Mg^{2+} + (2 - 1.5\chi\ )e^{-} \leftrightarrow 0.25\ Fe + 0.75NiSe\chi + (1 - 0.75\chi)MgSe\ (0 < \chi < 1) \quad (10)$$

The sequential reaction order of Fe and Ni cations in the reduction process of $Ni_{0.75}Fe_{0.25}Se_2$ results in the exposure of additional active sites, enhancing the diffusion kinetics of Mg^{2+} and leading to a twofold increase in capacity relative to undoped $NiSe_2$. The Fe-doped electrode material demonstrates a discharge capacity of 190 mAh g^{-1} at a current density of 20 mA g^{-1}, sustaining a discharge capacity of 148 mAh g^{-1} after 500 cycles (Figure 25 b). An analogous irreversible phase transformation is observed in nickel sulfide materials. Yu et al. [147] developed two NiS@C materials with carbon cladding and improved their ion transport kinetics through a Mg-Li hybrid system to mitigate strong electrostatic interactions between the host anion and Mg^{2+} (Figure 25 c-d) [177]. For example, developed two NiS@C materials with carbon cladding and improved their ion transport kinetics through a Mg-Li hybrid system to mitigate strong electrostatic interactions between the host anion and Mg^{2+} (Figure 25 c-d) [177]. The ultra-fine carbon-covered self-supported NiS_2 nanoparticles (NiS_2@CNPs/CC) were synthesised through the carbonisation and sulfurization of a benzoic acid anion-inserted $Ni(OH)_2$ precursor, which was deposited on carbon cloth. The absence of the binder and metallic collector enhances the energy density of the battery. The assembled cathode materials demonstrated a reversible capacity of 437 mAh g^{-1} at 100 mA g^{-1}, with 214 mAh g^{-1} retained at 200 mA g^{-1} after 250 cycles. The enhanced electrochemical performance can be attributed to the small average grain size of 13.2 nm for NiS_2, which reduces the ion transport distance, along with the synergistic improvement in electrical conductivity facilitated by carbon confinement and a carbon cloth matrix. Zhang et al. anchored NiS_2 onto Ni-based carbon nanotubes, resulting in improved charge transfer kinetics of the composites and reduced volume change of NiS_2 during cycling [178]. The synthesised NiS_2 cathode demonstrated a discharge capacity of 244.5 mAh g^{-1} at a current rate of 50 mA g^{-1}, and a rate performance of 94.7 mAh g^{-1} at 1 A g^{-1}. The assembled battery is capable of operating for more than 2000 cycles at a current density of 200 mA g^{-1} (Figure 25e). Yang et al. [179] developed ultrathin, freestanding nanoporous NiSx amorphous films (Figure 25f) and demonstrated their potential for magnesium storage. The electrochemical performance data of selected nickel sulfide/selenide cathodes for magnesium metal-based batteries are highlighted in Table 2.

 doi:10.20944/preprints202510.1895.v1

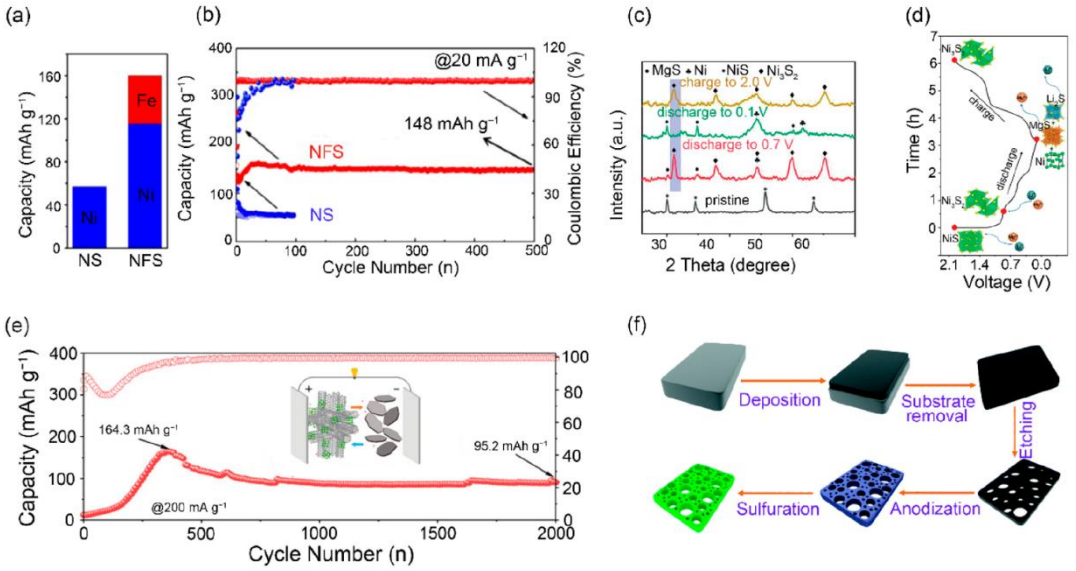

Figure 25. (a) The proportions of capacity contribution from the Ni and Fe species in the two electrodes. (b) The cycling efficiency of the NS and NFS electrodes was assessed at room temperature, yielding a rate of 20 mA g^{-1}. (c) Ex-situ XRD diffractograms of the NiS@C NPs/CC electrode under different EC conditions. (d) Pictorial representation of the reaction mechanism for NiS. Long-term cycling of the NiS_2/NCNTs electrode was conducted at a current density of 200 mA g^{-1}. (f) Schematic representation of the fabrication process for a nanoporous NiS layer [176].

In another report, Gao et al. [180] utilised a straightforward hydrothermal method to synthesise 1T-VSe_2 nanoparticles, which were combined with reduced graphene oxide (1T-VSe_2@rGO) composite in an APC electrolyte environment, serving as the cathode material for the second-generation rechargeable MIB. The 1T-VSe_2@rGO composite cathode material exhibited a reversible capacity of 235.5 mAh g-1 at a current density of 50 mA g-1 and maintained 62.7% of its initial capacitance after 500 cycles at the same current density. An initial capacitance rate capability of 46% was observed, corresponding to a current density of 1000 mA g^{-1} [180]. Also, layered TiS_2 has been demonstrated as a promising cathode material, providing 115 mAh g^{-1} stabilised capacity in a Mg-S battery [22]. Chen et al. have synthesised a highly exfoliated, graphene-like MoS_2 cathode for MIBs, and the MIB exhibited an operating voltage of 1.8 V and a well-reversible capacity of 170 mAh g^{-1} [181, 182].

Table 2. Chalcogenides for batteries.

Cathode material	Synthesis techniques	Voltage range (V)	Cycling performance (mAhg-1/No. of cycles	Maximum rate capacity (mAhg-1)	Current density (A/g/mAg-1	Ref
MoS_2/N-doped carbon Nanowall/carbon cloth	Solvothermal	0.01-3	619.2/100	235	2	[55]
MoS_2/carbon fiber @MoS_2@C	Electrospinning	0.01-2.5	332.6/1000	233.6	10	[56]
MoS_2/CF	Vaccum infiltration	0.05-3	240/500	171	5	[57]
MoS_2/single-wall carbon nanotubes	Liquid phase exfoliation	0.1-3	390/100	192	20	[58]
N-doped hollow MoS_2/C Nanospheres	Hydrothermal	0.01-3	128/5000	242	5	[59]
MoS_2/graphene	Ball milling/exfoliation	0.01-2.7	421/250	201	50	[60]
MoS_2/S-doped graphene	Hydrothermal	0.005-3	309/1000	264	5	[61]

 doi:10.20944/preprints202510.1895.v1

Fe_3O_4/MoS_2 graphite paper	Modified hydrothermal	0.01-3	388/300	231	3.2	[62]
1T MoS_2/graphene tube	Solvothermal	0.01-3	313/200	175	2	[63]
MoS_2/cotton-derived carbon fibers	Electrospinning	0.01-3.0	323.1/150	355.6	2	[64]
NBT/C/MoS_2 NFs	Hydrothermal	0.01-3	448.2/600	2000	200	[65]
N-doped amorphous micron-sized carbon ribbons /MoS_2	One-pot hydrothermal	0.01-3.0	305/300	302	2	[66]
Hollow flower-like MoS_2/C-RGO	Facile acid precipitation	0.01-3	637/50	467	1	[67]
amorphous MoS_3/carbon nanotube	Solvothermal	0.05-2.8	565/100	2350	20	[68]
$MoSe_2$/N, P-rGO	One-step hydrothermal	0.01-3	378/1000	216	15	[69]
$MoSe_2$/MWCNT	In-situ hydrothermal	0.01-3	459/90	385	2	[70]
VS_4-rGO	Hydrothermal	0.01-3	540/50	123	20	[71]
VS_4-rGO	Facile hydrothermal	0.01-2.2	241/50	219.9	0.5	[72]
CogSg/C nanospheres	Facile solvothermal	0.01-3	305/1000	297	5	[73]
CoS_2/multichannel carbon nanofibers		0.4-2.9	315.7/1000	201.9	10	[74]
$CoSe_2$MWCNT	Simple hydrothermal	1-2.9	568/100	550.5	0.8	[75]
Sb_2S_3 nanorods/C	Facile hydrothermal	0-2	570/100	337	2	[76]
Sb_2S_3/S-doped graphene sheets	Ultrasonication	0.01-2.5	524.4/900	591.6	5	[77]
ZnSeSb_2S_3/C	Sulfurisation reaction	0.01-1.8	630/120	390.6	0.8	[78]
Sb_2Se_3/C rods	Self-assembly reaction	0.01-2.5	485.2/100	311.5	2	[79]
$Sb2se_3$ nanowire-based membrāne	Hydrothermal/vaccum filtration	0.01-2	296/50	153	1.6	[80]
SnS/3D N-doped graphene	Facile, self-assembly method	0.01-25	509.9/1000	404.8	6	[81]
NiS_2/CoS_2/N-doped carbon coreshell nanocubes	Co-precipitation method	0.01-3	600/250	560	5	[82]

12. Comparative Structure-Properties Performance Evaluation of TMCs in Mg-S Battery

The electrochemical performance of transition metal chalcogenides (TMCs) in magnesium-sulfur batteries is fundamentally influenced by their electronic structure, which varies significantly among different materials and directly affects their effectiveness as cathode modifiers. TiS_2 is notable for its unique semi-metallic characteristics, demonstrating significant electronic conductivity between 222 and 208 m Scm^{-1} at temperatures from 25 to 60°C, and exhibiting a remarkably low resistivity of 5×10^{-3} Ω·cm. Metallic conductivity arises from unoccupied d-orbitals and the band structure, placing it at the boundary between semiconducting and metallic behaviour. The Group VI dichalcogenides MoS_2 and WS_2 display intrinsic semiconductor properties with significantly high resistivities: MoS_2 shows approximately 10 Ω·cm, while WS_2 exhibits similar values around 10 Ω·cm. The unique electronic structure of TiS_2 results in improved charge transport properties, enabling efficient electron transfer in polysulfide conversion reactions and contributing to its exceptional rate capability in Mg-S systems [83-85]. The hierarchy of electronic conductivity includes selenide-based materials, with $CoSe_2$ demonstrating superior performance compared to its sulfide counterparts, attributed to enhanced metallicity and an optimised d-band structure. The introduction of selenium,

 doi:10.20944/preprints202510.1895.v1

which has a larger atomic radius and lower electronegativity compared to sulfur, leads to enhanced delocalised electronic states and improved charge transfer properties. The electronic advantage is markedly improved in bimetallic systems such as (CuCo)Se_2, where the incorporation of copper modifies the d-band centre of cobalt, leading to optimal binding energies for polysulfide species while maintaining excellent catalytic activity. The electronic structure optimisation results indicate significantly lower Tafel slopes (66-82 mV/dec) compared to pure $CoSe_2$ systems (180-293 mV/dec), which correlates directly with enhanced polysulfide conversion kinetics [86, 87].

The relationship between interlayer spacing and electrochemical performance in transition metal chalcogenides (TMCs) is noteworthy. MoS_2, despite its favourable van der Waals spacing of 6.15-6.37 Å, consistently exhibits inferior performance when compared to materials with similar or even smaller interlayer distances. This seemingly contradictory situation results from complex interactions among structural, electronic, and kinetic elements that extend beyond simple geometric considerations. The layered structure of MoS_2 provides adequate space for Mg^{2+} intercalation; however, its semiconducting characteristics and strong interlayer interactions present significant obstacles to ion diffusion and electron transport [88, 89].

The main limitation of MoS_2 lies in its electronic structure, which creates energy barriers for ion intercalation and electronic conduction that cannot be overcome solely by modifying interlayer spacing. Density functional theory calculations reveal that pure MoS_2 exhibits Mg^{2+} diffusion barriers between 0.20 and 0.22 eV, which are considerably higher than those observed in metallic transition metal chalcogenides. The mechanism of conversion reactions in MoS_2 during extensive lithiation and magnesiation leads to structural breakdown and the formation of amorphous phases, which considerably compromise the integrity of the electrode and its cycling stability. The progressive accumulation of sulfur-rich intermediates leads to the emergence of electrically insulating regions that effectively isolate the active material from the conductive framework, resulting in a rapid decrease in capacity despite seemingly favourable structural parameters [90]. The performance limitation has led to extensive research on modification strategies for MoS_2, including interlayer expansion through molecular intercalation (resulting in spacing of up to 9.38 Å with CO_2 molecules), defect engineering, and the creation of heterostructures. The increase in MoS_2 interlayer spacing to 9.8 Å through various intercalation methods leads to a substantial enhancement in the Mg^{2+} diffusion coefficient, increasing by 12-14 orders of magnitude. This observation suggests that the initial interlayer spacing, while seemingly adequate, functioned as a limiting factor alongside the material's intrinsic electronic properties [90, 91]. $CoSe_2$ demonstrates exceptional catalytic efficiency in polysulfide conversion reactions, significantly outperforming sulfide-based transition metal compounds due to its optimised electronic structure, surface chemistry, and morphological characteristics. The improved performance is due to selenium's larger atomic radius (1.16 Å versus 1.04 Å for sulfur) and its lower electronegativity (2.55 compared to 2.58). This combination leads to enhanced polarisability of bonds and improved electronic delocalisation within the crystal structure. This electronic environment improves interactions with polysulfide species while maintaining moderate binding energies that facilitate effective adsorption-catalysis-desorption cycles [87, 92].

The catalytic efficiency of $CoSe_2$ is evidenced by its significantly lower energy barriers for polysulfide conversion reactions. Research on surface characteristics indicates that different $CoSe_2$ crystal facets exhibit varying catalytic performances, with the (200) surface showing the highest activity for Li_2S oxidation and polysulfide reduction. The material exhibits Tafel slopes as low as 66 mV/dec, compared to the 180-293 mV/dec recorded for CoS_2, indicating markedly improved reaction kinetics. $CoSe_2$ demonstrates a Li_2S nucleation capacity of 180.59 mAh/g, exceeding that of other transition metal compounds, and maintains a Li_2S decomposition capability of 364.72 mAh/g, underscoring its dual catalytic performance [86, 93]. The exceptional performance of $CoSe_2$ is evident in its structural stability and morphological versatility. Unlike MoS_2, which undergoes destructive conversion reactions, $CoSe_2$ maintains its structural integrity during cycling and provides numerous active sites for polysulfide anchoring. The material can be synthesised in different morphologies, including cubic nanoparticles, hollow spheres, and nanosheet arrays, each offering

 doi:10.20944/preprints202510.1895.v1

distinct advantages for specific battery applications. The incorporation of $CoSe_2$@carbon composites into carbon matrices demonstrates significant cycling stability, with a capacity retention exceeding 80% after 1000 cycles, surpassing that of sulfide counterparts [92].

12.1. Performance Metrics Analysis

The assessment of TMCs in Mg-S systems reveals distinct hierarchies based on multiple performance metrics: The sequence is TiS_2, $CoSe_2$, VS_2, WS_2, and MoS_2, which is directly related to their electronic band structures and charge transport characteristics. TiS_2 exhibits significant areal capacities of 9 mAh/cm², maintaining consistent performance over 200 cycles and enduring high current densities of up to 10 mA/cm². This performance results from its unique ability to function concurrently as an intercalation host and as a conductive framework for sulfur conversion reactions [94, 95]. Materials based on $CoSe_2$ demonstrate outstanding performance in polysulfide anchoring and conversion catalysis, due to their optimised binding energies and electronic structure. The material exhibits capacities exceeding 1000 mAh/g at moderate current densities and demonstrates exceptional rate performance of 838 mAh g^{-1} at 4C. $CoSe_2$ exhibits the lowest impedance during charge-discharge cycling, indicating superior kinetic properties relative to other transition metal compounds. VS_2 exhibits significant efficacy as a catalyst for polysulfide conversion, particularly when augmented by the incorporation of sulfur vacancies, achieving initial capacities of 1492 mAh g^{-1} and demonstrating remarkable long-term stability with a decay rate of merely 0.07% over 1000 cycles [86, 87]. The hierarchy of structural stability and cycling performance is as follows: $TiS_2 \approx CoSe_2 > VS_2 > WS_2 > MoS_2$, underscoring the importance of maintaining structural integrity during multiple Mg^{2+} insertion and extraction cycles. TiS_2 demonstrates remarkable stability attributed to its intercalation mechanism, which effectively avoids the detrimental conversion reactions that impact other transition metal chalcogenides. The material demonstrates an 82% capacity retention after 500 cycles at high current densities, indicating one of the highest long-term stability performances recorded for TMC-based Mg-S systems. WS_2 occupies an intermediate position, exhibiting enhanced performance relative to MoS_2 due to its unique electronic structure; however, it encounters similar fundamental limitations associated with its semiconducting properties [96, 97]. The performance variations among TMCs are linked to fundamental material properties: the electronic structure impacts charge transport efficiency, the d-band positioning influences catalytic activity, and structural stability is vital for long-term cyclability. TiS_2 exhibits notable metallic conductivity and stable intercalation chemistry. $CoSe_2$ is notable in catalytic applications owing to its optimised electronic structure and moderate binding energies. MoS_2 and WS_2, despite their beneficial layered structures, encounter constraints stemming from their semiconducting properties and vulnerability to detrimental conversion reactions. This comprehensive understanding provides specific design principles for future TMC materials in Mg-S battery applications, emphasising the need to balance electronic conductivity, catalytic activity, and structural stability for optimal performance. A comparative overview of various TMC-modified Mg-S cathodes, emphasising the range of performance improvements, including initial capacity enhancements, cycling stability, and rate capability, achieved through diverse compositional, structural, and defect engineering strategies, is presented in Table 3 [98].

Table 3. A comparative overview of different TMC-modified Mg-S cathodes and performance enhancements [98].

TMC/Cathode Composite	Initial Capacity (mAh g^{-1})	Sustained Capacity/Retention	Rate Capability mA g^{-1}	Cycle Life/Retention	Ref.
2H–MoS_2	100–150	~100 after 50 cycles	100	50 cycles	[99, 100]
1T–VS_2	133	95% after 100 cycles	100	100 cycles	[101]
$V_0.63Mo_0.46S_2$ (VMS)	211	82.7% after 500 cycles (1000 mA/g)	100–1000	500 cycles	[99]
Expanded TiS_2	239	>80% after 200 cycles	24	200 cycles	[99]

 doi:10.20944/preprints202510.1895.v1

Mo_6S_8 (Chevrel phase)	~120	Stable >2000 cycles	20	>2000 cycles	[102]
MoS_2/rGO composite	160–190	95% after 100 cycles	20-50	100 cycles	[99]
VS_4@rGO (pillar ext.)	268	—	50	—	[99]
N-doped MoS_2	120–132	—	100	—	[103]
TiS_2/VS_2 hetero	Not specified	Predicted stable	—	— (DFT-guided)	[104]
MoS_2-$CoSe_2$ hybrids	200–240	—	100	—	[105]
$MgMo_6S_{8-y}Se_y$ (Se-doped)	140–154	—	—	—	[106]
WS_2 nanosheets	98	—	100	—	[107]
TiS_2/MoS_2 composites	>220	Good after >100 cycles	50	>100 cycles	[99]
VS_2 (defective)	Up to 160	—	100	—	[99]
NiS_2	120–170	—	50-100	—	[103]
$CoS_2/CoSe_2$ hybrids	225	—	100	—	[103]
TiS_2/MgO composite	200	—	80	—	[102]
VSe_2	178	—	100	—	[102]
$NiCo_2S_4$	185	Cycle stability enhanced	100	—	[103]
$MoWS_2$	950	—	—	—	[108]
CoS_2-$CoSe_2$ in carbon nanofibers	749	-	1000	200	[109, 110]

TMC and TMC-based materials show exceptional performance in magnesium-sulfur (Mg-S) cathode applications, attributed to their high electronic conductivity, intrinsic catalytic activity for polysulfide conversion, and engineered morphologies that enhance Mg^{2+} diffusion. In contrast, metal-carbon composites have notable conductivity but fall short in catalytic efficiency, failing to adequately address the polysulfide shuttle problem and suffering from capacity degradation. Metal oxides are limited by low electronic conductivity and sluggish Mg ion kinetics, adversely affecting their rate performance and cycle life. Metal nitrides offer moderate performance but lack the strong interactions with polysulfides and catalytic advantages of TMCs. Sulfides such as NiS_2 and FeS_2, while chemically similar, often show reduced structural stability and rate performance compared to chalcogenides featuring mixed metal compositions or heterostructured designs. Other materials like phosphides and fluorides exhibit even lower performance metrics due to material limitations, as highlighted in Table 4. This analysis highlights the superior electrochemical properties of transition metal chalcogenides, establishing them as the premier class of cathode materials for next-generation magnesium-sulfur batteries.

Table 4. The performance of TMC cathode materials over other significant classes of cathode materials utilised in Mg-S batteries [98].

Material Class	Specific Material/Composite	Initial Capacity (mAh/g)	Cycle Life/Capacity Retention	Rate Capability	Key Advantages of TMC Over Others	Ref.
Transition Metal Chalcogenides (TMC)	$CoSe_2$, N-doped $CoSe_2$, TiS_2, VS_2, MoS_2/rGO	1200–1500	>80% retention after 500–1000 cycles	Up to 2C or higher	Superior Mg^{2+} diffusion, strong polysulfide binding & catalytic activity	[86, 111]
Metal-Carbon Composites	Sulfur/Graphene, N-doped Carbon/S	500–900	Moderate, ~60–70% after 100 cycles	Up to 1C	Lower catalytic activity and polysulfide anchoring	[46, 103]

 doi:10.20944/preprints202510.1895.v1

					compared to TMCs	
Metal Oxides	MnO_2, MoO_3, TiO_2	~400–900	Good, but fast capacity decay at high current	Up to 1C	Lower electronic conductivity and slower Mg^{2+} diffusion than TMCs	[112]
Metal Nitrides	VN, MoN, TiN	600–1100	Moderate cycle retention	Up to 2C	Generally lower catalytic activity for polysulfides compared to TMCs	[112]
Metal Sulfides (non-TMC)	NiS_2, FeS_2	1100–1300	Fair cycling stability (~70% after 200 cycles)	Up to 1–2C	Often less structural stability and poorer rate capabilities	[113]
Metal Phosphides	FeP, CoP	400–1000	Moderate, typically 50–70% retention	Limited (<1C)	Lower polysulfide affinity, worse cycling stability	[114]
Metal Fluorides	FeF_3	<400	Poor cycling due to insulating nature	Low	Poor conductivity and polysulfide conversion	[115]

13. Computational Perspectives

13.1. Materials/Device Simulation

Density functional theory (DFT) studies offer insights into electronic structures and reaction pathways, thereby informing strategies for material optimisation. Investigating the charge conductivity properties in MgS and MgS_2 is essential for the development of an effective Mg-S battery with extended cycle life. The mechanism of charge transport in MgS and MgS_2 remains inadequately understood. While there are limited experimental and computational studies on MgS, the investigation of charge transport in MgS_2 has not yet been conducted. Most experimental studies on charge transport in MgS have been conducted at elevated temperatures (900K), whereas ambient temperature conductivity is more relevant for battery applications. The absence of electrical conductivity measurements for MgS at room temperature likely arises from challenges in assessing its low conductivity, attributed to its insulating properties. Numerous computational studies have examined charge transport in MgS through the application of empirical interatomic potentials. Puntambekar et al. [116] determined the migration energies of Mg^{2+} (approximately 2.6 eV) and S^{2-} (approximately 3.4 eV) ions in MgS. Chen et al. [117] employed DFT to determine a migration barrier of 1.2 eV for Mg^{2+} in MgS. The studies primarily concentrated on ion transport, with minimal attention given to electronic transport. First-principles DFT calculations employing hybrid functional theory were utilised to elucidate the charge transport mechanism in MgS and MgS_2. Research focuses on ionic and electronic conductivity resulting from the movement of charged point and polaronic defects, including hole and electron polarons. The formation energies and

 doi:10.20944/preprints202510.1895.v1

equilibrium concentrations of various point and polarons defects are estimated to determine the predominant anomalies. A study on the migration barrier for the predominant defects was conducted. The determined energy barrier is utilised to calculate the highest thickness of MgS and MgS_2 layers necessary for achieving feasible discharge rates. The study examined the transfer mechanism in non-equilibrium states, focusing on the introduction or extraction of polarons and Mg^{2+} from the positive (+) electrode material, utilising ab initio molecular dynamics (AIMD) for analysis. The study indicated that MgS_2 can facilitate electronic conduction through dual-electron polarons above 3μm within practical battery functioning conditions, generally at discharge rates of 1C. This transport mechanism facilitates additional reduction, ultimately leading to the production of MgS. Conversely, MgS_2 is noted to exhibit no feasible electronic or ionic transportation. The study underscores the necessity of inhibiting the oxidation of MgS_2 to MgS, advocating for the development of experimental approach to resolve this adverse EC process. The atomistic structure and reactivity of TMCs have been extensively analysed through DFT methods. The DFT method was employed to simulate cells comprising several hundred to a few thousand atoms, while empirically fitted interatomic potential models were utilised for atomistic simulations of significantly larger systems. Computational studies focus on creating precise structural models of cathode, electrolyte, or anode materials, utilising this understanding to interpret experimental outcomes, including Mg ion conductivity and voltage profiles during charging and discharging [118-121]. Modelling across multiple scales enhances the comprehension of both constraining and advantageous processes in Mg-S batteries, thereby significantly facilitating and expediting experimental investigation. As an illustration, stabilities and structures of species in different electrolytes were analysed, including MgS_n intermediates [122]. Atomistic modelling has been utilised to examine materials that can effectively adsorb polysulfides, thereby reducing detrimental shuttle effects and/or facilitating polysulfide conversion [123]. Conversely, limited methodologies exist for characterising Mg coating and stripping, along with complete Mg battery cells on a continuum scale. The initial continuum simulations were documented in 2015, concentrating on the three-dimensional morphology of magnesium deposition [124]. Subsequently, Chadwick et al. [125] introduced a one-dimensional model for magnesium plating and stripping on a transition metal substrate. The objective was to achieve an adequate parameterisation, particularly concerning electrochemical kinetics, by aligning simulated cyclic voltammograms with experimentally obtained cyclic voltammograms. While early continuum simulations offer significant insights, the models rely on numerous simplifications. Transport in the electrolyte was characterised exclusively by diffusion and the principles of dilute solution theory. The latest continuum models are founded on a thermodynamically coherent transport theory and do not presuppose an ideal solution devoid of reactions among dissolved species. Latz et al and Drews et al. [126, 127] overtly examined Mg-characteristic phenomena, including ion accumulation and desolvation preceding electron transport, along with the advanced electrolyte based on $Mg[B(hfip)_4]$. The impact of polysulfides on the charge transfer properties and EC kinetics of magnesium deposits remains inadequately explored.

The initial continuum model of a complete Mg-S battery was introduced merely three years prior. Richter et al. [128] expanded upon a well-known Li-S model and examined the differences in self-discharge and degradation effects between the Mg-S and Li-S systems. The study concentrated on the behaviour of the S species; thus, no significant differences in the dissolution/deposition kinetics of Mg and Li were noted, and it was assumed that ions were fully dissociated in the electrolyte. The model integrated the intricate transformation and precipitation process of S species with their conductivity in the electrolyte, while also accounting for side reactions on the anode (-) surface and the consequent passivation effects. The impact of spatial confinement via sulfur encapsulation in a porous carbon structure was examined using a 1+1D approach, focusing on conductivity and reactions at both the macroscopic cell and the microscopic particle level. The kinetics of unwanted side reactions were observed to be considerably more rapid for magnesium compared to lithium, resulting in an accelerated self-discharge during storage at open circuit voltage and the swift, irreversible formation of passivating magnesium sulfide during the initial cycle. One possible

 doi:10.20944/preprints202510.1895.v1

explanation is the lack of a protective solid electrolyte interphase (SEI) on the magnesium metal. The development of an appropriate artificial solid electrolyte interphase (SEI) represents an effective approach to reducing the adverse impacts of the polysulfide shuttle. Numerous instances demonstrate the mutual enrichment of theory and experiments, with the collaborative synergy among experiments, DFT calculations, and continuum simulations enhancing the understanding of critical processes in Mg-S batteries [129-131].

Furthermore, the DFT technique enables precise evaluation of diffusion barriers, interfacial binding energies, and electronic state characteristics, which are crucial for guiding experimental efforts in materials selection and engineering. Modern DFT calculations go beyond basic ground-state analysis, routinely incorporating advanced functionals such as HSE06 to investigate intrinsic point defects, interfacial phenomena, and vibrational enthalpy effects at relevant operational temperatures. Computational methods systematically reveal how minor lattice distortions, chemical modifications, and the formation of heterostructures can modify essential material properties to improve battery performance [132]. Theoretical studies have identified significant factors affecting the mobility of Mg^{2+} ions in TMC hosts, especially within spinel and layered structures. Periodic DFT studies of spinel chalcogenides, including TiS_2, MoS_2, WS_2, and $CoSe_2$, indicate that trigonal distortions and covalent bonding within the structure significantly influence magnesium site preference and overall ion mobility. The barriers for Mg^{2+} diffusion in selenide-spinel frameworks is notably diminished, at times approaching those found in lithium-ion systems. The incorporation of selenium or the application of mixed-anion strategies may enhance rate performance while preserving stability. DFT calculations demonstrate that defect engineering, specifically through the intentional introduction of sulfur or selenium vacancies, creates negative charge centres and additional electronic carriers. This process effectively lowers migration energy and provides additional diffusion pathways. This mechanistic insight facilitates the targeted advancement of defect-rich TMCs, as evidenced by recent experiments showing enhanced capacities and improved rate capabilities in vacancy-modified materials [8, 102]. The application of DFT has elucidated the intricate relationship between the binding energies of polysulfide species and the electronic structures of TMC cathode hosts, offering important insights for the development of catalytic and anchoring materials. Simulations on MoS_2, WS_2, and $CoSe_2$ surfaces indicate that optimal polysulfide binding occurs when the surface possesses appropriate polarity and electronic density near the Fermi level, thereby enhancing both anchoring strength and charge transfer efficiency. Research utilising hybrid and interface DFT on heterostructures, such as 1T-TiS_2/WSe_2, clarifies how band alignment and interfacial charge densities affect the distribution and reactivity of adsorbed species, leading to improved sulfur utilisation and a diminished shuttle effect. The migratory barriers for electron polaritons may reach as low as 0.45 eV in certain crystalline orientations, promoting rapid redox kinetics essential for high-rate cycling [133, 134].

DFT quantifies the stabilisation energy of point defects, offering insights for the synthesis of chalcogenide materials with customised electronic states. The analysis of point defect formation energies and density of states for MoS_2 and WS_2 indicates that sulfur vacancies enhance conductivity and generate new anchoring sites, thereby aiding experiments in optimising defect density for desired performance trade-offs. Experimental data confirm these predictions, indicating that defect-rich surfaces achieve higher reversible capacities and longer cycle lives than their pristine equivalents [135]. Table 5 provides a summary of diffusion barriers, binding energies, electronic conductivity, and experimental performance parameters such as capacity, cycle life, and rate capability, based on reported examples of MoS_2, WS_2, $CoSe_2$, TiS_2, and related materials with diverse morphologies and defect engineering. The findings integrate insights from computational predictions alongside key metrics for experimental validation. The convergence of theory and experiment validates DFT-guided design and facilitates the rational discovery and optimisation of next-generation Mg-S battery cathode materials.

Maps generated from DFT concerning diffusion, binding, and electronic structure offer essential insights into multiple aspects of Mg-S battery material engineering. DFT elucidates the connections

 doi:10.20944/preprints202510.1895.v1

between migration barriers and material composition, guiding the choice of host materials and dopants to improve Mg^{2+} mobility. This approach steers synthesis towards selenide-rich frameworks or lattice-distorted structures. The calculations of binding energy aid in the selection or design of surface coatings and cathode host morphologies that achieve a balance between anchoring strength and catalytic turnover, thereby preventing overbinding that could impede kinetics or trap active species [134]. Furthermore, the insights obtained from DFT provide substantial explanations for experimental defect engineering. Increased vacancy concentrations, deliberate heterointerface formation, and modifications in electronic structure have all demonstrated correlations with performance enhancements in real batteries. The integration of computational findings into synthesis and device optimisation will continue to accelerate the development of next-generation TMC cathodes for magnesium-based energy storage, linking theoretical potential with experimental realisation [45].

Table 5. Correlation between computational parameters, experimental prediction, and battery performance [135].

Material/System	DFT Predicted Mg^{2+} Diffusion Barrier (eV)	DFT Predicted Binding Energy (eV)	Relevant DFT Electronic Feature	Experimental Capacity (mAh g^{-1})	Rate/Retention/Remark	Ref.
2H–MoS_2	0.47	-0.97 (centre hex)	Semiconducting (bandgap)	~100 at 100	Poor Mg-ion mobility, poor rate, low retention	[99, 100]
1T–VS_2	0.41	-1.36 (centre hex est.)	Metallic, low Eg.	~133 at 100	Higher Mg-ion mobility, stable	[99]
$V_0.63Mo_0.46S_2$ (VMS)	~0.44	–	Defected, expanded layer	211 at 100	82.7% after 500 cycles (1000 mA/g)	[99]
TiS_2 (expanded)	0.35	–	Semi-metallic, expanded	239 at 24	Good rate and reversibility	[99]
Mo_6S_8 (Chevrel phase)	<0.2	–	Metallic, strong Mg^{2+} affinity	~120 at 20	Best cycling cathode, >2000 cycles	[8, 102]
MoS_2/rGO composite	0.47	–	Interlayer-coordinated	160–190 at 20–50	Improved by a graphene conductive matrix	[99]
VS_4@rGO (pillar ext.)	0.61 (Zn)–0.47 (Mg)	–	Open, flexible structure	268 at 50	Excellent initial activity	[99]
N-doped MoS_2	Lowered barrier by 0.05 - 0.1	Up to -1.1	Fermi level upshift	120–132 at 100	Improved via dopants	[103]
TiS_2/VS_2 hetero	0.33	–	Heterointerface, metallic	Not stated	Predicted best for alkali-experimental data pending	[101]
MoS_2–$CoSe_2$ hybrids	0.42–0.45	-1.0 to -1.4 (composite)	Band alignment, dual redox	200–240 at 100	Synergy effect, stable	[102]
$MgMo_6S_8$-ySey (Se-doped)	~0.14 for y=1	–	Band narrowing, higher DOS	140–154 (DFT-based)	Improved by Se substitution	[104]
WS_2 nanosheets	0.50	-0.62	Larger bandgap (pristine)	98 at 100	Lower rates than MoS_2	[105]
TiS_2/MoS_2 composites	0.41–0.44	–	Expanded band, mixed valence	>220 at 50	Fast Mg diffusion	[99]
VS_2 (defective)	<0.40 (vacancy, DFT)	–	More active sites	Up to 160 at 100	Enhanced by sulfur vacancies	[99]
MoS_2 (1T phase)	0.34	–	Metallic after Li/Na insertion	Not stable for Mg	Phase change is hindered for Mg	[100]

 doi:10.20944/preprints202510.1895.v1

NiS_2	0.39	-1.22 (center hex)	Conductive	120–170 at 50–100	Rapid Mg^{2+} uptake	[103]
$CoS_2/CoSe_2$ hybrids	0.28–0.35	-1.30 ($CoSe_2$)	High redox eletcronic density	225 at 100	Excellent cycling, catalyst [211]	[103]
TiS_2/MgO composite	<0.3–0.4 (surface)	–	Grain-boundary assisted	200 at 80	Improved by grain boundary	[102]
VSe_2	0.37	-1.05 (center hex)	Metallic, open structure	178 at 100	High rate and stability	[102]
$NiCo_2S_4$	0.40	-1.15	Multiple redox	185 at 100	Cycle stability enhanced	[103]

There is a lack of reports on joint theoretical and experimental studies, especially regarding adequate continuum models and comprehensive simulations for the Mg-S system. A collaborative approach is necessary to address the existing obstacles. DFT approaches grounded in quantum mechanics offer high precision and predictability; however, their computational cost limits application to small simulation cells and idealised model systems. Thus, a novel technique proposed to mitigate this challenge is the rapid and accurate development of interatomic potentials using machine learning (ML), based on quantum-mechanical reference data. This methodology is particularly relevant for battery research, enabling a thorough investigation of intercalation mechanisms in electrode materials. The deployment of artificial intelligence (AI) and machine learning (ML) is crucial for investigating machine learning-based interatomic potentials, discovering novel alternative cathode materials for Mg-S batteries, and enhancing the understanding of the structures and properties of battery materials [136, 137].

13.2. Machine Learning Approaches

Recent reviews have shown that various emerging machine learning algorithms are being increasingly utilised in the field of energy materials, particularly in battery research. Machine learning (ML) represents the fourth paradigm of science, focused on deriving insights from extensive datasets. Recent years have seen considerable interest due to the availability of extensive data. Interatomic potentials based on machine learning represent a supervised learning problem, wherein the optimal fit is achieved using a dataset of precisely calculated energies and forces at specific points on a potential-energy surface (PES). In contrast to empirically fitted interatomic potential models, machine learning potentials do not pre-establish the interaction shape, necessitating learning from reference data or model development. Machine learning potentials facilitate the examination of significantly larger systems, such as 1000-atom cells, which characterise materials that exhibit graphite-like properties but are highly disordered. Machine learning potentials can now effectively simulate systems comprising tens of thousands of atoms, with simulation-cell lengths nearing the dimensions of nanostructures in devices [138, 139].

Enhancing the efficiency of practical Mg-S batteries necessitates more effective knowledge extraction from their intricate chemistries. A comprehensive framework or platforms, including BEEP, VerticaPy, PyBaMM, and additional methods [140-142], have demonstrated efficacy in data-driven battery prognosis. Currently, the majority of these applications utilise black-box models to achieve sufficient accuracy in the prognosis of commercialising Mg-S batteries with established chemistries (Figure 26a). Improving models' robustness to handle field data in dynamic real-world applications is crucial; concurrently, utilising machine learning to expedite the development of next-generation cathode materials and magnesium-sulfur batteries is also important [143].

An intelligible hybrid machine learning framework may integrate time series decomposition with an RNN (recurrent neural network) to elucidate declining capacity chemistries in magnesium-sulfur batteries (Figure 26b). The hybrid model, developed through the pretraining engineering of dynamic features that address battery variances and the integration of static features that group individual batteries, effectively predicts battery and cathode degradation with a remarkably low prediction error of 8.9% for end-of-life forecasts. Moreover, in contrast to traditional machine learning for battery prognosis, which typically employs obscure models and offers restricted insights,

 doi:10.20944/preprints202510.1895.v1

the hybrid machine learning framework prioritises the enhancement of physical comprehension. No prior report has provided a comprehensive mechanistic analysis utilising feature importance ranking of the performance metric (the ratio of electrolyte quantity to high-voltage-area capacity during the initial discharge) to characterise the cycling efficiency of Mg-S batteries, which is highly effective than the commonly accepted index, the electrolyte-to-sulfur (E/S) ratio. The rational development and parameter optimisation of feasible cathode materials in Mg-S batteries can thus be addressed. These occurrences demonstrate the efficacy of interpretable machine learning in revealing concealed patterns within intricate cathode materials and battery chemistries, as well as in converting learnt patterns into comprehensible knowledge. Consequently, the significant potential of the interpretable hybrid machine learning framework to enhance the validation and development of innovative cathode materials, especially TMC-based cathodes for practical magnesium-sulfur batteries and other advanced complex systems, can be demonstrated.

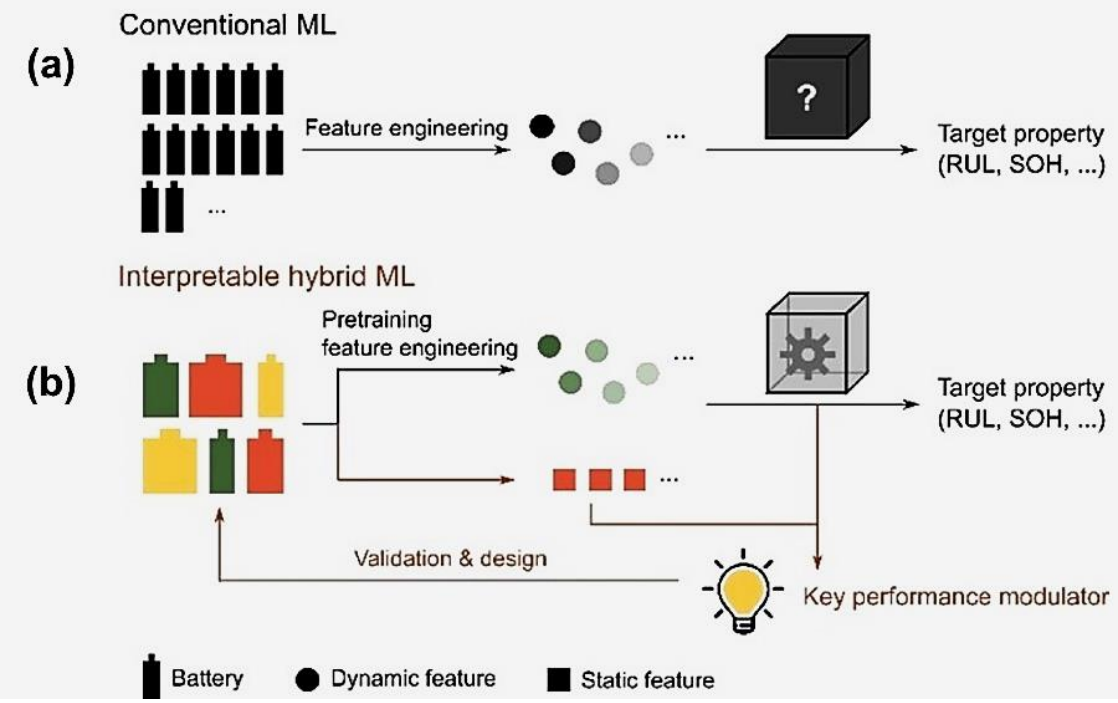

Figure 26. Scheme comparing traditional and interpretable hybrid machine learning techniques; (a) Traditional machine learning often derives data from extensive datasets utilising commercial batteries. Temporal dynamic variables (e.g., voltage curves, internal resistance, and temperature) are frequently input into a black-box model to produce forecasts for various target attributes (e.g., remaining usable life (RUL) and state of health (SOH). (b) The interpretable hybrid machine learning approach seeks to derive greater physical insights from the model. In addition to the dynamic data, static features such as active material loading and electrolyte quantity are also input into the ML model. This architecture enables predictions for less developed battery systems with intricate chemistries (e.g., Li-S batteries) and subpar dataset quality, while still extracting essential performance characteristics to clarify future battery validation and design [144].

13.3. Catalysis of Materials Discovery

Artificial intelligence (AI) and machine learning (ML) have markedly enhanced the speed and quality of research on cathode modification for magnesium-sulfur (Mg-S) batteries. These platforms, especially those utilising crystal graph convolutional neural networks (CGCNNs), enable the screening of tens of thousands of candidate compounds, identifying promising Mg cathode materials with excellent voltage and ionic conductivity from extensive datasets. Furthermore, data-driven screening techniques, including knowledge graphs, enable the visualisation and mapping of correlations across doping combinations, redox potentials, capabilities, and energy densities across

 doi:10.20944/preprints202510.1895.v1

material sets. Researchers may now instantly observe the impact of compositional alterations on battery parameters, significantly minimising expensive and labour-intensive experimental cycles [145]. This methodology shifts materials research from a trial-and-error framework to a hypothesis-driven, data-informed discovery process.

For example, Okamoto et al. demonstrated that spinel Mn_2O_4 achieves an average discharge voltage of 2.9 V, facilitated by its three-dimensional Mg diffusion channels and the redox activity of Mn^{3+}/Mn^{4+} [4]. Zeng et al. identified NASICON-structured $V_2(PO_4)_3$ as an effective high-voltage intercalation host for Mg-S battery, demonstrating a stable voltage plateau near 2.5 V [5]. Orikasa et al. reported that ion-exchange $MgFeSiO_4$ demonstrates a voltage of 2.4 V, which is attributed to redox activity involving Fe 3d states and O 2p hybridisation within the polyanion host structure [6]. Although the above work showcases recent advancements in voltage optimisation, the practical use of M-S batteries is still constrained by slow Mg diffusion kinetics and restricted capacity [146].

ML frameworks excel at identifying and assessing essential characteristics that affect vital cathode properties, such as entropy, electronegativity, ionic radius, and molecular mass. Recursive feature removal and interpretable modelling elucidate the synthesis and structural variables that influence cycle stability, high energy density, and rate capability in modified Mg-S cathodes. Advanced virtual prototyping and inverse design are other techniques that facilitate inverse design pipelines, wherein defined electrochemical results are computationally deduced to determine appropriate material compositions. This has enabled the swift suggestion and experimental verification of innovative cathode materials with customised features, directing researchers to pertinent systems.

However, conventional cathode development in Mg-S batteries encounters ongoing challenges: slow Mg^{2+} diffusion, polysulfide shuttle phenomena, and inadequate cycling stability. AI/ML-based models currently replicate the effects of compositional and microstructural alterations on these bottlenecks, directing cathode engineering to address sluggish ion movement and improve sulfur utilisation. Digital frameworks for microstructure optimisation facilitate the identification of optimal processing parameters, hence enhancing performance outcomes. Recent case studies and experimental validation confirm that engineered Mg-S cathode materials show enhancements in reversible capacity and cycling durability relative to empirically obtained alternatives. Machine learning-driven suggestions for dopant kinds and production methods have produced electrodes exhibiting elevated redox potentials, enhanced conductivity, and diminished shuttle effect. AI/ML-driven materials research is advancing broader battery development, encompassing various multivalent ion chemistries (Na, Ca, Zn) and high-entropy systems, promoting cross-pollination and methodological progress throughout the industry. Strategic collaboration between experimentalists and computational scientists will guarantee that these data-driven advancements result in real, significant developments for global energy storage systems.

13.4. AI-Driven Discovery Workflow for Electrode Materials of Mg Batteries

An AI-driven workflow is illustrated in Figure 27, indicating an end-to-end workflow for materials discovery. At ab-initio, a universal CGCNN model designed to predict the voltage of all intercalation-type electrodes was developed. In contrast to previous studies employing transfer learning to address the limitations of small datasets [14], the CGCNN model in Figure 28 leverages shared characteristics of intercalation-type electrode materials, allowing for simultaneous training of all electrodes with varying working ions. The mean average error (MAE) of the voltage for Li, Mg, Na, Al, K, Ca, and Zn cathodes is reduced to 0.32, 0.29, 0.32, 0.33, 0.30, 0.29, and 0.25 V, respectively. The predictions closely match the target voltages and experimental data for Mg cathode materials, thereby validating the model's accuracy and its potential to inform high-voltage Mg cathode design via predictive screening as depicted in Figure 29 (a-c). Subsequently, this model was implemented on stable magnesium compounds sourced from the Materials Project (MP) dataset and the Graph Networks for Materials Exploration (GNoME) AI database [147], identifying magnesium cathode candidates that exhibit a voltage exceeding 3.0 V and a volumetric capacity greater than 800 mA

 doi:10.20944/preprints202510.1895.v1

h/cm^3, this is represented in Figure 30 (a-c). First-principles calculations are subsequently employed to validate the prediction. This is then followed by Neural Equivariant Interatomic Potentials (NequIP) to conduct machine learning molecular dynamics (MLMD) simulations and assess the Mg ionic conductivity of the chosen high-voltage materials [148]. This AI-driven workflow is valuable in addressing the constraints of small datasets, allowing for the identification of 23 promising candidates from a total of 15,308 options for new intercalation-type sulfur cathode materials characterised by high energy density and ionic conductivity. This facilitates additional experimental research and industrial advancement of Mg batteries.

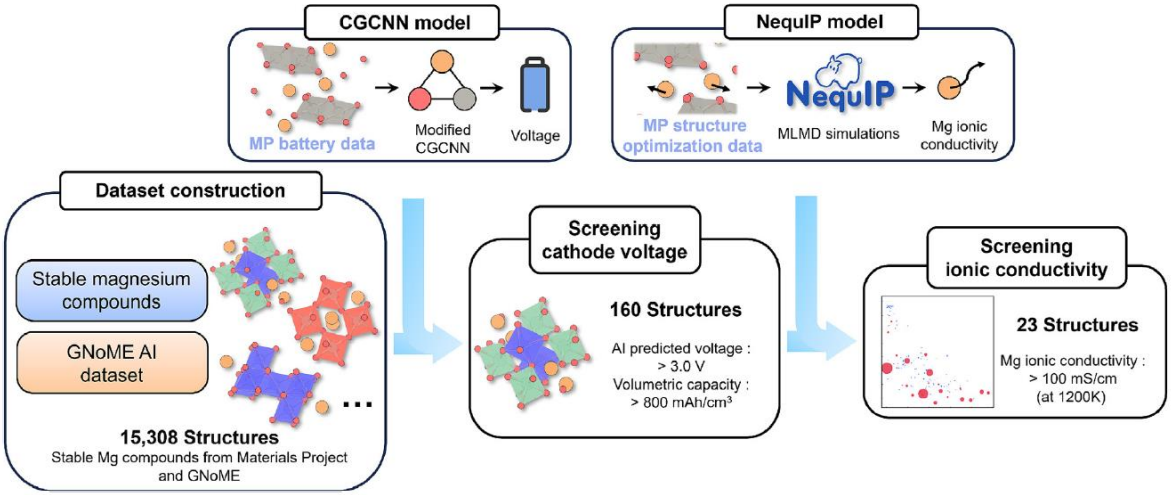

Figure 27. Depiction of the comprehensive artificial intelligence workflow for predicting cathode voltage in a battery using battery data obtained from the Materials Project to train a CGCNN model. The prediction highlights twenty-three (23) materials with high voltage and ionic conductivity as potential candidates for Mg-S battery cathodes [146].

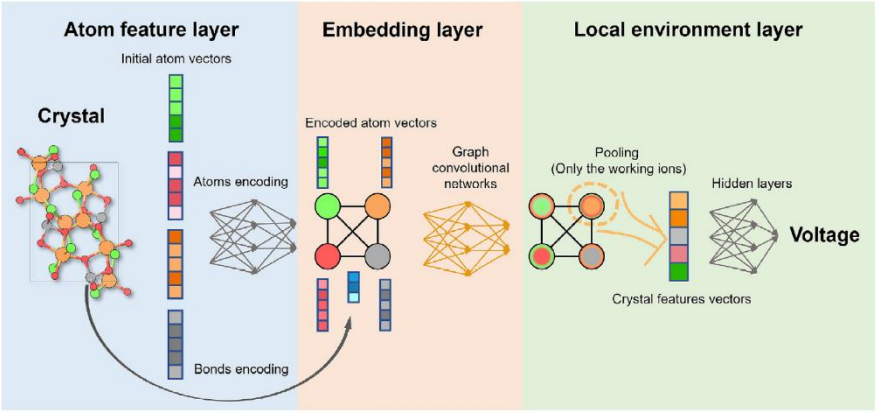

Figure 28. Depiction of the altered CGCNN model for voltage forecasting. A crystal is represented as a multigraph, with atoms embedded in the nodes and the relationships between atoms represented by the edges. Only functional ions are aggregated and utilised to predict the electrode voltage [146].

 doi:10.20944/preprints202510.1895.v1

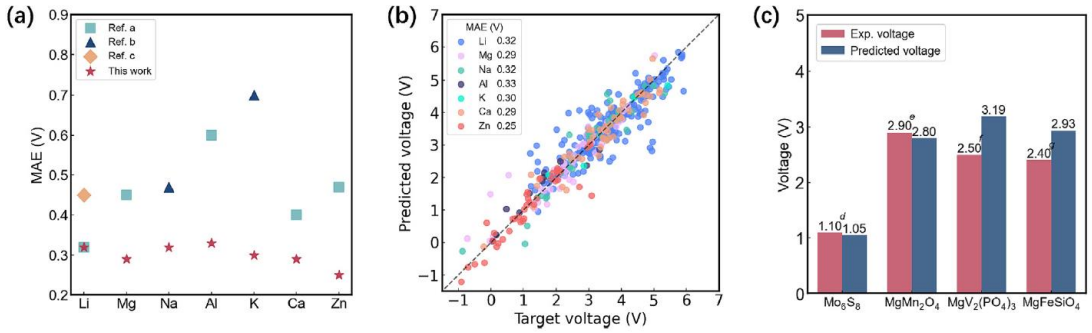

Figure 29. ML performance. (a) Assessment of the MAE for all working ions with prior research findings, (b) Plots illustrating the predicted potential versus the target voltage within the test data, (c) Evaluation of estimated voltages and experimental voltages for typical magnesium cathode materials [146].

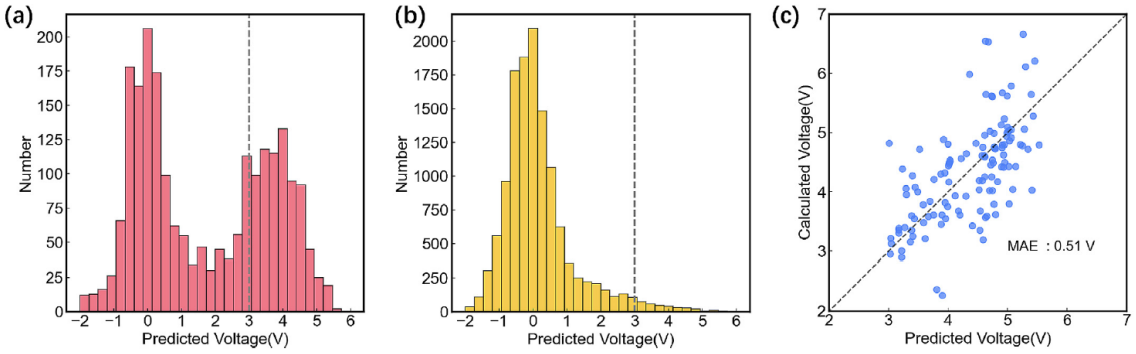

Figure 30. Voltage assessment and first-principles validation of high-voltage Mg cathode materials. Estimated voltage spectrum for compounds sourced from (a) the Materials Project, (b) the GNoME database and (c) *Ab-initio* validation conducted for materials of choice exhibiting predicted voltages exceeding 3 V [146].

14. Challenges and Limitations

Although transition metal chalcogenides provide numerous advantages for Mg-S battery systems, some limits remain. The intrinsic conductivity of numerous transition metal compounds (TMCs) is often inadequate, particularly in their pure or stoichiometric states, hence hindering rapid electron transport during charge-discharge cycles. Secondly, TMCs frequently experience structural and volumetric alterations during cycling, especially in conversion-type processes, resulting in electrode fragmentation and capacity degradation. Third, whereas TMC-based materials have robust polysulfidesulfide adsorption capabilities, they may undergo surface passivation or reduced active site availability over prolonged cycles, hence compromising their long-term efficacy. Furthermore, the sluggish kinetics of Mg^{2+} diffusion, attributed to its elevated charge density and robust solvation shell, present an additional impediment that even catalytically active materials find challenging to surmount completely. Ultimately, numerous high-performing TMC synthesis pathways entail intricate, non-scalable procedures or ecologically detrimental chemicals, posing obstacles to commercial implementation and sustainability. These constraints highlight the imperative for ongoing advancement in material design and process engineering.

15. Future Directions and Opportunities

To fully harness the promise of TMCs in Mg-S batteries, future research must focus on three interrelated strategies: compositional tuning, structural engineering, and interface optimisation. Elemental doping, heterostructure creation, or defect engineering can adjust electronic characteristics and improve catalytic activity. Structural improvements, such as the creation of hollow, layered, and hierarchical nanostructures, can manage volume fluctuations while enhancing the available

 doi:10.20944/preprints202510.1895.v1

surface area and ion transport pathways. At the interface level, coating or combining TMCs with conductive polymers, carbon frameworks, or ionic sieving membranes can further inhibit polysulfidesulfide migration and enhance electrode-electrolyte interactions. Moreover, subsequent research should utilise sophisticated in situ and operando characterisation methods to observe phase changes, interfacial interactions, and ion dynamics in real time. Integrating these initiatives with machine learning and high-throughput DFT simulations may expedite the identification of next-generation TMC materials designed for Mg-S systems. The incorporation of TMCs into Mg-S battery frameworks has many distinctive prospects. Tunable electronic architectures and many active sites render TMCs optimal hosts for multivalent ion storage and polysulfide conversion catalysis. The collaboration between TMCs and hybrid systems such as TMC-graphene composites or TMC-MXene hybrids can produce multifunctional platforms that concurrently enhance conductivity, mechanical strength, and chemical containment. Furthermore, the versatility of TMCs across many synthesis scales and the potential for utilising solution-based or green chemistry methods facilitate sustainable manufacturing. The insights derived from TMC research extend beyond conventional battery applications and may also be pertinent to other electrochemical systems, such as Mg-air, Na-S and Zn-S batteries, hence enhancing the significance of this material class. The coupling of TMC-based battery technology with circular economy principles through resource recycling, waste valorisation, and renewable energy integration generates significant commercial and environmental value propositions.

16. Conclusions

TMC have emerged as a critical material for tackling the significant problems in magnesium-sulfur batteries, providing a diverse foundation for enhancing conductivity, redox kinetics, and polysulfide confinement. Their distinctive characteristics, resulting from stacked crystal configurations, pronounced polarity, and catalytic capabilities, provide multifunctional applications as cathode hosts, separator interlayers, and electrolyte-compatible interfaces. However, to realise their complete potential, coordinated efforts are required to address challenges associated with structural stability, Mg^{2+} transport, and processing scalability. This analysis has consolidated recent advancements in TMC-based design methodologies, while highlighting distinct potential for innovation via compositional tailoring, hierarchical structure, and computationally assisted material discovery. This roadmap integrates practical advancements with theoretical insights, establishing a robust framework for future enhancements in Mg-S battery performance. The strategic integration of TMCs may significantly influence the development of sustainable, high-performance, and economically viable multivalent battery systems.

Supplementary Materials: The following supporting information can be downloaded at: https://www.mdpi.com/article/doi/s1, Figure S1: title; Table S1: title; Video S1: title.

Author Contributions: MS conceptualised, contributed to the manuscript's writing, and proofread the final draft. HS prepared the original draft, data curation and proofreading of the final manuscript.

Funding: This research and APC were funded by the research office of the Walter Sisulu University, Mthatha, South Africa.

Data Availability Statement: All data and figures used in this work have been adequately referenced.

Acknowledgments: HS and MS express their gratitude to the research directorate of Walter Sisulu University for their generous financial support for the postdoctoral fellowship and provision of research facilities.

Conflicts of Interest: The Authors declare no conflict of interest.

Abbreviations

The following are some of the abbreviations used in this manuscript:

 doi:10.20944/preprints202510.1895.v1

PVP	Polyvinylpyrolidone
CTAB	Cetyltrimethylammonium bromide
DFT	Density Functional Theory
POM	Polyoxometalate
ACC	Activated carbon cloth
CNFs	Carbon nanofiber
RMB	Rechargeable magnesium battery
HSAB	Hard and soft acids and bases
TMDs	Transition metal dichalcogenides
TMSs	Transition metal-based sulfides
HDS	Hydrodesulfurisation
DOS	Density of states
TEPA	Tetraethylenepentamine
ECS	Electrochemical storage
CNTs	Carbon nanotube
GO	Graphene oxide
SERS	Surface-enhanced Raman scattering
MC	Metal chalcogenide
TAA	Thioacetamide
GPE	Gel polymer electrolyte
DETA	Diethylenetriamine
PEMFCs	Proton exchange membrane fuel cells
DMFCs	Direct methanol fuel cells
GNS	Graphene nanosheet
DMF	Dimethyl formamide

References

1. Bielecki, A., S. Ernst, W. Skrodzka, I. Wojnicki, *The externalities of energy production in the context of development of clean energy generation,* Environmental Science and Pollution Research, 27 (2020) 11506-11530
2. Mensah-Darkwa, K., D. Nframah Ampong, E. Agyekum, F.M. de Souza, R.K. Gupta, *Recent advancements in chalcogenides for electrochemical energy storage applications,* Energies, 15 (2022) 4052
3. Dai, M. ,R. Wang, *Synthesis and applications of nanostructured hollow transition metal chalcogenides,* Small, 17 (2021) 2006813
4. Galek, P., A. Mackowiak, P. Bujewska, K. Fic, *Three-dimensional architectures in electrochemical capacitor applications–insights, opinions, and perspectives,* Frontiers in Energy Research, 8 (2020) 139
5. Budde-Meiwes, H., J. Drillkens, B. Lunz, J. Muennix, S. Rothgang, J. Kowal, D.U. Sauer, *A review of current automotive battery technology and future prospects,* Proceedings of the Institution of Mechanical Engineers, Part D: Journal of Automobile Engineering, 227 (2013) 761-776
6. Besenhard, J.O. ,M. Winter, *Advances in battery technology: Rechargeable magnesium batteries and novel negative-electrode materials for lithium ion batteries,* ChemPhysChem, 3 (2002) 155-159
7. Zu, C.-X. ,H. Li, *Thermodynamic analysis on energy densities of batteries,* Energy & Environmental Science, 4 (2011) 2614-2624
8. Li, Z., J. Häcker, M. Fichtner, Z. Zhao-Karger, *Cathode materials and chemistries for magnesium batteries: challenges and opportunities,* Advanced Energy Materials, 13 (2023) 2300682
9. Häcker, J., D.H. Nguyen, T. Rommel, Z. Zhao-Karger, N. Wagner, K.A. Friedrich, *Operando UV/vis spectroscopy providing insights into the sulfur and polysulfide dissolution in magnesium–sulfur batteries,* ACS Energy Letters, 7 (2021) 1-9
10. Ji, Y., X. Liu-Théato, Y. Xiu, S. Indris, C. Njel, J. Maibach, H. Ehrenberg, M. Fichtner, Z. Zhao-Karger, *Polyoxometalate modified separator for performance enhancement of magnesium–sulfur batteries,* Advanced Functional Materials, 31 (2021) 2100868

 doi:10.20944/preprints202510.1895.v1

11. Gao, T., M. Noked, A.J. Pearse, E. Gillette, X. Fan, Y. Zhu, C. Luo, L. Suo, M.A. Schroeder, K. Xu, *Enhancing the reversibility of Mg/S battery chemistry through Li+ mediation,* Journal of the American Chemical Society, 137 (2015) 12388-12393
12. Gao, T., S. Hou, K. Huynh, F. Wang, N. Eidson, X. Fan, F. Han, C. Luo, M. Mao, X. Li, *Existence of solid electrolyte interphase in Mg batteries: Mg/S chemistry as an example,* ACS applied materials & interfaces, 10 (2018) 14767-14776
13. Yu, X. ,A. Manthiram, *Performance enhancement and mechanistic studies of magnesium–sulfur cells with an advanced cathode structure,* ACS Energy Letters, 1 (2016) 431-437
14. Du, A., Z. Zhang, H. Qu, Z. Cui, L. Qiao, L. Wang, J. Chai, T. Lu, S. Dong, T. Dong, *An efficient organic magnesium borate-based electrolyte with non-nucleophilic characteristics for magnesium–sulfur battery,* Energy & environmental science, 10 (2017) 2616-2625
15. Yin, L.-C., J. Liang, G.-M. Zhou, F. Li, R. Saito, H.-M. Cheng, *Understanding the interactions between lithium polysulfides and N-doped graphene using density functional theory calculations,* Nano Energy, 25 (2016) 203-210
16. Yuan, H., L. Kong, T. Li, Q. Zhang, *A review of transition metal chalcogenide/graphene nanocomposites for energy storage and conversion,* Chinese Chemical Letters, 28 (2017) 2180-2194
17. Yan, Z., M. Ji, J. Xia, H. Zhu, *Recent advanced materials for electrochemical and photoelectrochemical synthesis of ammonia from dinitrogen: one step closer to a sustainable energy future,* Advanced Energy Materials, 10 (2020) 1902020
18. Sun, X., P. Bonnick, V. Duffort, M. Liu, Z. Rong, K.A. Persson, G. Ceder, L.F. Nazar, *A high capacity thiospinel cathode for Mg batteries,* Energy & Environmental Science, 9 (2016) 2273-2277
19. Ponnambalam, S. ,M. Ilampoornan, *Integration of Renewable Energy Technologies and Hybrid Electric Vehicle Challenges in Power Systems*, in *Hybrid Electric Vehicles and Distributed Renewable Energy Conversion: Control and Vibration Analysis*. 2025, IGI Global Scientific Publishing. p. 157-186.
20. Jin, L., *Energy storage in multi-energy carrier communities: Li-ion batteries and hydrogen multi-physical details for integration into the planning stage,* (2024)
21. Yang, Q., Y. Su, X. Wang, K. Xiao, T. Chen, J. Fu, *Emerging Strategies for Sustainable Holistic Recycling of Spent Lithium-Ion Batteries,* Advanced Functional Materials, (2025) e14524
22. Sheng, L., *High-performance cathode design and safety evaluation of magnesium-sulfur batteries*. 2022, UCL (University College London).
23. Yao, W., K. Liao, T. Lai, H. Sul, A. Manthiram, *Rechargeable metal-sulfur batteries: key materials to mechanisms,* Chemical Reviews, 124 (2024) 4935-5118
24. Razaq, R., P. Li, Y. Dong, Y. Li, Y. Mao, S.H. Bo, *Practical energy densities, cost, and technical challenges for magnesium-sulfur batteries,* EcoMat, 2 (2020) e12056
25. Betz, J., G. Bieker, P. Meister, T. Placke, M. Winter, R. Schmuch, *Theoretical versus practical energy: a plea for more transparency in the energy calculation of different rechargeable battery systems,* Advanced energy materials, 9 (2019) 1803170
26. Salama, M., R. Attias, B. Hirsch, R. Yemini, Y. Gofer, M. Noked, D. Aurbach, *On the feasibility of practical Mg–S batteries: practical limitations associated with metallic magnesium anodes,* ACS Applied Materials & Interfaces, 10 (2018) 36910-36917
27. Montenegro, C.T., J.F. Peters, M. Baumann, Z. Zhao-Karger, C. Wolter, M. Weil, *Environmental assessment of a new generation battery: The magnesium-sulfur system,* Journal of Energy Storage, 35 (2021) 102053
28. Zhao, J., Y.Y. Xiao, Q. Liu, J. Wu, Z.C. Jiang, H. Zeng, *The rise of multivalent metal–sulfur batteries: advances, challenges, and opportunities,* Advanced Functional Materials, 34 (2024) 2405358
29. Sheng, L., J. Feng, M. Gong, L. Zhang, J. Harding, Z. Hao, F.R. Wang, *Advances and challenges in electrolyte development for magnesium–sulfur batteries: a comprehensive review,* Molecules, 29 (2024) 1234
30. Zhou, X., T. Xu, M. Guo, H. Zhang, C. Li, W. Wang, M. Sun, G. Xia, X. Yu, *Vertically Aligned Mesoporous Arrays Catalyzing Long-Chain Polysulfide Conversion to Unlock High-Energy Magnesium–Sulfur Batteries,* ACS nano, (2025)
31. Guan, Q., J. Zhang, Y. Zhang, X. Cheng, J. Dong, L. Jia, H. Lin, J. Wang, *Prospect of Cascade Catalysis in Magnesium-Sulfur Batteries from Desolvation to Conversion Reactions,* Advanced Science, (2025) e70008

 doi:10.20944/preprints202510.1895.v1

32. Bai, X., X. Bai, T. Li, T. Li, U. Gulzar, U. Gulzar, R.P. Zaccaria, R.P. Zaccaria, C. Capiglia, Y.J. Bai, *Comprehensive Understanding of Lithium-Sulfur Batteries: Current Status and Outlook,* Advanced Battery Materials, (2019) 355-398
33. Flatscher, F., *Lithium dendrites in solid-state batteries-Where they come from and how to mitigate them,* (2023)
34. Eng, A.Y.S., A. Ambrosi, Z. Sofer, P. Simek, M. Pumera, *Electrochemistry of transition metal dichalcogenides: strong dependence on the metal-to-chalcogen composition and exfoliation method,* Acs Nano, 8 (2014) 12185-12198
35. Tan, S.M., A. Ambrosi, Z. Sofer, Š. Huber, D. Sedmidubský, M. Pumera, *Pristine basal-and edge-plane-oriented molybdenite MoS2 exhibiting highly anisotropic properties,* Chemistry–A European Journal, 21 (2015) 7170-7178
36. Jayabal, S., J. Wu, J. Chen, D. Geng, X. Meng, *Metallic 1T-MoS2 nanosheets and their composite materials: Preparation, properties and emerging applications,* Materials today energy, 10 (2018) 264-279
37. Yuan, Z., H.-J. Peng, T.-Z. Hou, J.-Q. Huang, C.-M. Chen, D.-W. Wang, X.-B. Cheng, F. Wei, Q. Zhang, *Powering lithium–sulfur battery performance by propelling polysulfide redox at sulfiphilic hosts,* Nano letters, 16 (2016) 519-527
38. Shao, F., Z. Tian, P. Qin, K. Bu, W. Zhao, L. Xu, D. Wang, F. Huang, *2H-NbS2 film as a novel counter electrode for meso-structured perovskite solar cells,* Scientific Reports, 8 (2018) 7033
39. Li, Y., Z. Zhou, S. Zhang, Z. Chen, *MoS2 nanoribbons: high stability and unusual electronic and magnetic properties,* Journal of the American Chemical Society, 130 (2008) 16739-16744
40. Chen, P., K. Xu, Y. Tong, X. Li, S. Tao, Z. Fang, W. Chu, X. Wu, C. Wu, *Cobalt nitrides as a class of metallic electrocatalysts for the oxygen evolution reaction,* Inorganic Chemistry Frontiers, 3 (2016) 236-242
41. Du, Y., A. Ji, L. Ma, Y. Wang, Z. Cao, *Electrical conductivity and photoreflectance of nanocrystalline copper nitride thin films deposited at low temperature,* Journal of crystal growth, 280 (2005) 490-494
42. Kaya, A.I., *Determination of thermal conductivity and physical properties of Fe2O3 doped rigid polyurethane materials,* Science of Advanced Materials, 12 (2020) 1790-1793
43. Stozhko, N.Y., E.I. Khamzina, M.A. Bukharinova, A.V. Tarasov, *An electrochemical sensor based on carbon paper modified with graphite powder for sensitive determination of sunset yellow and tartrazine in drinks,* Sensors, 22 (2022) 4092
44. Zhou, Z., K. Kato, T. Komaki, M. Yoshino, H. Yukawa, M. Morinaga, K. Morita, *Effects of dopants and hydrogen on the electrical conductivity of ZnO,* Journal of the European Ceramic Society, 24 (2004) 139-146
45. Muthu, P., S. Rajagopal, D. Saju, V. Kesavan, A. Dellus, L. Sadhasivam, N. Chandrasekaran, *Review of transition metal chalcogenides and halides as electrode materials for thermal batteries and secondary energy storage systems,* ACS omega, 9 (2024) 7357-7374
46. Reddy, B., M. Premasudha, N. Reddy, H.-J. Ahn, J.-H. Ahn, K.-K. Cho, *Hydrothermal synthesis of MoS2/rGO composite as sulfur hosts for room temperature sodium-sulfur batteries and its electrochemical properties,* Journal of Energy Storage, 39 (2021) 102660
47. Zhu, F., H. Zhang, Z. Lu, D. Kang, L. Han, *Controlled defective engineering of MoS2 nanosheets for rechargeable Mg batteries,* Journal of Energy Storage, 42 (2021) 103046
48. Liu, W., S. Yang, D. Fan, Y. Wu, J. Zhang, Y. Lu, L. Fu, *PEG–PVP-assisted hydrothermal synthesis and electrochemical performance of N-doped MoS2/C composites as anode material for lithium-ion batteries,* ACS omega, 9 (2024) 9792-9802
49. Cui, C., H. Pan, L. Wang, M. Baiyin, *Transition Metal Germanium Chalcogenide Materials: Solvothermal Syntheses, Flexible Crystal, Structures, and Photoelectric Response Property,* Crystal Growth & Design, 24 (2024) 1227-1234
50. Tian, X.-Y., C.-X. Du, G. ZhaoRi, M. SheLe, Y. Bao, M. Baiyin, *The solvothermal synthesis and characterization of quaternary arsenic chalcogenides CsTMAsQ 3 (TM= Hg, Cd; Q= S, Se) using Cs+ as a structure directing agent: from 1D anionic chains to 2D anionic layers,* RSC advances, 10 (2020) 34903-34909
51. Liu, Z., L. Zhang, R. Wang, S. Poyraz, J. Cook, M.J. Bozack, S. Das, X. Zhang, L. Hu, *Ultrafast microwave nano-manufacturing of fullerene-like metal chalcogenides,* Scientific reports, 6 (2016) 22503
52. Aslam, M.K., I.D. Seymour, N. Katyal, S. Li, T. Yang, S.-j. Bao, G. Henkelman, M. Xu, *Metal chalcogenide hollow polar bipyramid prisms as efficient sulfur hosts for Na-S batteries,* Nature communications, 11 (2020) 5242

 doi:10.20944/preprints202510.1895.v1

53. Wang, J., T. Ghosh, Z. Ju, M.-F. Ng, G. Wu, G. Yang, X. Zhang, L. Zhang, A.D. Handoko, S. Kumar, *Heterojunction structure of cobalt sulfide cathodes for high-performance magnesium-ion batteries,* Matter, 7 (2024) 1833-1847
54. Szkoda, M., A. Ilnicka, K. Trzciński, Z. Zarach, D. Roda, A.P. Nowak, *Synthesis and characterization of MoS2-carbon based materials for enhanced energy storage applications,* Scientific Reports, 14 (2024) 26128
55. Li, P., J.Y. Jeong, B. Jin, K. Zhang, J.H. Park, *Vertically oriented MoS2 with spatially controlled geometry on nitrogenous graphene sheets for high-performance sodium-ion batteries,* Advanced Energy Materials, 8 (2018) 1703300
56. Cui, C., Z. Wei, J. Xu, Y. Zhang, S. Liu, H. Liu, M. Mao, S. Wang, J. Ma, S. Dou, *Three-dimensional carbon frameworks enabling MoS2 as anode for dual ion batteries with superior sodium storage properties,* Energy Storage Materials, 15 (2018) 22-30
57. Zhao, Z.-H., X.-D. Hu, H. Wang, M.-Y. Ye, Z.-Y. Sang, H.-M. Ji, X.-L. Li, Y. Dai, *Superelastic 3D few-layer MoS2/carbon framework heterogeneous electrodes for highly reversible sodium-ion batteries,* Nano Energy, 48 (2018) 526-535
58. Liu, Y., X. He, D. Hanlon, A. Harvey, J.N. Coleman, Y. Li, *Liquid phase exfoliated MoS2 nanosheets percolated with carbon nanotubes for high volumetric/areal capacity sodium-ion batteries,* Acs Nano, 10 (2016) 8821-8828
59. Cai, Y., H. Yang, J. Zhou, Z. Luo, G. Fang, S. Liu, A. Pan, S. Liang, *Nitrogen doped hollow MoS2/C nanospheres as anode for long-life sodium-ion batteries,* Chemical Engineering Journal, 327 (2017) 522-529
60. Sun, D., D. Ye, P. Liu, Y. Tang, J. Guo, L. Wang, H. Wang, *MoS2/Graphene nanosheets from commercial bulky MoS2 and graphite as anode materials for high rate sodium-ion batteries,* Advanced Energy Materials, 8 (2018) 1702383
61. Li, G., D. Luo, X. Wang, M.H. Seo, S. Hemmati, A. Yu, Z. Chen, *Enhanced reversible sodium-ion intercalation by synergistic coupling of few-layered MoS2 and S-doped graphene,* Advanced Functional Materials, 27 (2017) 1702562
62. Kong, D., C. Cheng, Y. Wang, Z. Huang, B. Liu, Y. Von Lim, Q. Ge, H.Y. Yang, *Fe 3 O 4 quantum dot decorated MoS 2 nanosheet arrays on graphite paper as free-standing sodium-ion battery anodes,* Journal of Materials Chemistry A, 5 (2017) 9122-9131
63. Geng, X., Y. Jiao, Y. Han, A. Mukhopadhyay, L. Yang, H. Zhu, *Freestanding metallic 1T MoS2 with dual ion diffusion paths as high rate anode for sodium-ion batteries,* Advanced Functional Materials, 27 (2017) 1702998
64. Li, X., Y. Yang, J. Liu, L. Ouyang, J. Liu, R. Hu, L. Yang, M. Zhu, *MoS2/cotton-derived carbon fibers with enhanced cyclic performance for sodium-ion batteries,* Applied Surface Science, 413 (2017) 169-174
65. Wang, L., G. Yang, J. Wang, S. Peng, W. Yan, S. Ramakrishna, *Controllable design of MoS2 nanosheets grown on nitrogen-doped branched TiO2/C nanofibers: toward enhanced sodium storage performance induced by pseudocapacitance behavior,* Small, 16 (2020) 1904589
66. Pang, Y., S. Zhang, L. Liu, J. Liang, Z. Sun, Y. Wang, C. Xiao, D. Ding, S. Ding, *Few-layer MoS 2 anchored at nitrogen-doped carbon ribbons for sodium-ion battery anodes with high rate performance,* Journal of Materials Chemistry A, 5 (2017) 17963-17972
67. Zhang, Y., S. Yu, H. Wang, Z. Zhu, Q. Liu, E. Xu, D. Li, G. Tong, Y. Jiang, *A novel carbon-decorated hollow flower-like MoS2 nanostructure wrapped with RGO for enhanced sodium-ion storage,* Chemical Engineering Journal, 343 (2018) 180-188
68. Ye, H., L. Wang, S. Deng, X. Zeng, K. Nie, P.N. Duchesne, B. Wang, S. Liu, J. Zhou, F. Zhao, *Amorphous MoS3 infiltrated with carbon nanotubes as an advanced anode material of sodium-ion batteries with large gravimetric, areal, and volumetric capacities,* Advanced Energy Materials, 7 (2017) 1601602
69. Niu, F., J. Yang, N. Wang, D. Zhang, W. Fan, J. Yang, Y. Qian, *MoSe2-covered N, P-doped carbon nanosheets as a long-life and high-rate anode material for sodium-ion batteries,* Advanced Functional Materials, 27 (2017) 1700522
70. Zhang, Z., X. Yang, Y. Fu, K. Du, *Ultrathin molybdenum diselenide nanosheets anchored on multi-walled carbon nanotubes as anode composites for high performance sodium-ion batteries,* Journal of Power Sources, 296 (2015) 2-9

 doi:10.20944/preprints202510.1895.v1

71. Wang, S., F. Gong, S. Yang, J. Liao, M. Wu, Z. Xu, C. Chen, X. Yang, F. Zhao, B. Wang, *Graphene oxide-template controlled cuboid-shaped high-capacity VS4 nanoparticles as anode for sodium-ion batteries,* Advanced Functional Materials, 28 (2018) 1801806
72. Sun, R., Q. Wei, Q. Li, W. Luo, Q. An, J. Sheng, D. Wang, W. Chen, L. Mai, *Vanadium sulfide on reduced graphene oxide layer as a promising anode for sodium ion battery,* ACS applied materials & interfaces, 7 (2015) 20902-20908
73. Zhang, Y., N. Wang, P. Xue, Y. Liu, B. Tang, Z. Bai, S. Dou, *Co9S8@ carbon nanospheres as high-performance anodes for sodium ion battery,* Chemical Engineering Journal, 343 (2018) 512-519
74. Pan, Y., X. Cheng, Y. Huang, L. Gong, H. Zhang, *CoS2 nanoparticles wrapping on flexible freestanding multichannel carbon nanofibers with high performance for Na-ion batteries,* ACS Applied Materials & Interfaces, 9 (2017) 35820-35828
75. Freitas, F.S., A.S. Gonçalves, A. De Morais, J.E. Benedetti, A.F. Nogueira, *Graphene-like MoS2 as a low-cost counter electrode material for dye-sensitized solar cells,* J. NanoGe J. Energy Sustain, 1 (2012) 11002-11003
76. Kim, K., *Unveiling the Unique Phase Transformation Behavior and Sodiation Kinetics of 1D van der Waals Sb2S3 Anodes for Sodium Ion Batteries Shanshan Yao, Jiang Cui, Ziheng Lu, Zheng-Long Xu, Lei Qin, Jiaqiang Huang, Zoya Sadighi, Francesco Ciucci,* and Jang,*
77. Xiong, X., G. Wang, Y. Lin, Y. Wang, X. Ou, F. Zheng, C. Yang, J.-H. Wang, M. Liu, *Enhancing sodium ion battery performance by strongly binding nanostructured Sb2S3 on sulfur-doped graphene sheets,* ACS nano, 10 (2016) 10953-10959
78. Dong, S., C. Li, X. Ge, Z. Li, X. Miao, L. Yin, *ZnS-Sb2S3@ C core-double shell polyhedron structure derived from metal–organic framework as anodes for high performance sodium ion batteries,* Acs Nano, 11 (2017) 6474-6482
79. Ge, P., X. Cao, H. Hou, S. Li, X. Ji, *Rodlike Sb2Se3 wrapped with carbon: the exploring of electrochemical properties in sodium-ion batteries,* ACS applied materials & interfaces, 9 (2017) 34979-34989
80. Luo, W., A. Calas, C. Tang, F. Li, L. Zhou, L. Mai, *Ultralong Sb2Se3 nanowire-based free-standing membrane anode for lithium/sodium ion batteries,* ACS Applied Materials & Interfaces, 8 (2016) 35219-35226
81. Xiong, X., C. Yang, G. Wang, Y. Lin, X. Ou, J.-H. Wang, B. Zhao, M. Liu, Z. Lin, K. Huang, *SnS nanoparticles electrostatically anchored on three-dimensional N-doped graphene as an active and durable anode for sodium-ion batteries,* Energy & Environmental Science, 10 (2017) 1757-1763
82. Lin, Y., Z. Qiu, D. Li, S. Ullah, Y. Hai, H. Xin, W. Liao, B. Yang, H. Fan, J. Xu, *NiS2@ CoS2 nanocrystals encapsulated in N-doped carbon nanocubes for high performance lithium/sodium ion batteries,* Energy Storage Materials, 11 (2018) 67-74
83. Ma, L., S. Wei, H.L. Zhuang, K.E. Hendrickson, R.G. Hennig, L.A. Archer, *Hybrid cathode architectures for lithium batteries based on TiS 2 and sulfur,* Journal of Materials Chemistry A, 3 (2015) 19857-19866
84. Chung, S.-H., L. Luo, A. Manthiram, *TiS2–polysulfide hybrid cathode with high sulfur loading and low electrolyte consumption for lithium–sulfur batteries,* ACS Energy Letters, 3 (2018) 568-573
85. Tang, W., *Electrical, electronic and optical properties of MoS2 & WS2,* (2017)
86. Chen, L., R. Wang, N. Li, Y. Bai, Y. Zhou, J. Wang, *Optimized Adsorption–Catalytic Conversion for Lithium Polysulfides by Constructing Bimetallic Compounds for Lithium–Sulfur Batteries,* Materials, 17 (2024) 3075
87. Wang, M., L. Fan, X. Sun, B. Guan, B. Jiang, X. Wu, D. Tian, K. Sun, Y. Qiu, X. Yin, *Nitrogen-doped CoSe2 as a bifunctional catalyst for high areal capacity and lean electrolyte of Li–S battery,* ACS Energy Letters, 5 (2020) 3041-3050
88. Fan, X., M. Tebyetekerwa, Y. Wu, R.R. Gaddam, X.S. Zhao, *Magnesium/lithium hybrid batteries based on SnS2-MoS2 with reversible conversion reactions,* Energy Material Advances, (2022)
89. Han, X., J. Yang, Y.-W. Zhang, Z.G. Yu, *Molecular engineering on a MoS 2 interlayer for high-capacity and rapid-charging aqueous ion batteries,* Nanoscale Advances, 5 (2023) 2639-2645
90. Alshammari, G.M., M.A. Mohammed, A. Al Tamim, M.A. Yahya, A.E.A. Yagoub, *Changes in nutrients, heavy metals, residual pesticides, bioactive compounds, and anti-oxidant activity following germination and fermentation of Sudanese and Yemeni sorghums,* International Journal of Food Science and Technology, 60 (2025) vvaf069
91. Pang, B., L. Xiang, K. Wang, S. Zeng, J. Guo, N. Li, *Interlayer-expanded 1T-phase MoS2 as a cathode material for enhanced capacitive deionization,* Desalination, 593 (2025) 118211

92. Fan, C., R. Yang, Y. Yang, Y. Yang, Y. Huang, Y. Yan, L. Zhong, Y. Xu, *Cubic CoSe2@ carbon as polysulfides adsorption-catalytic mediator for fast redox kinetics and advanced stability lithium-sulfur batteries,* Journal of Colloid and Interface Science, 660 (2024) 246-256
93. Liu, X., Y. Zheng, M. Zhang, S. Qi, M. Tan, R. Zhao, M. Zhao, *Surface-Dependent Electrocatalytic Activity of CoSe2 for Lithium Sulfur Battery,* Advanced Materials Interfaces, 10 (2023) 2202205
94. Liu, G., Q. Zeng, Z. Fan, S. Tian, X. Li, X. Lv, W. Zhang, K. Tao, E. Xie, Z. Zhang, *Boosting sulfur catalytic kinetics by defect engineering of vanadium disulfide for high-performance lithium-sulfur batteries,* Chemical Engineering Journal, 448 (2022) 137683
95. Tagliaferri, S., G. Nagaraju, M. Sokolikova, R. Quintin-Baxendale, C. Mattevi, *3D printing of layered vanadium disulfide for water-in-salt electrolyte zinc-ion batteries,* Nanoscale Horizons, 9 (2024) 742-751
96. Roy, A., S. Dey, G. Singh, *MoS2, WS2, and MoWS2 flakes as reversible host materials for sodium-ion and potassium-ion batteries,* ACS omega, 9 (2024) 24933-24947
97. Bissett, M.A., S.D. Worrall, I.A. Kinloch, R.A. Dryfe, *Comparison of two-dimensional transition metal dichalcogenides for electrochemical supercapacitors,* Electrochimica Acta, 201 (2016) 30-37
98. Al-Tahan, M.A., Y. Dong, A.E. Shrshr, X. Liu, R. Zhang, H. Guan, X. Kang, R. Wei, J. Zhang, *Enormous-sulfur-content cathode and excellent electrochemical performance of Li-S battery accouched by surface engineering of Ni-doped WS2@ rGO nanohybrid as a modified separator,* Journal of Colloid and Interface Science, 609 (2022) 235-248
99. Jing, P., S. Stevenson, H. Lu, P. Ren, I. Abrahams, D.H. Gregory, *Pillared Vanadium Molybdenum Disulfide Nanosheets: Toward High-Performance Cathodes for Magnesium-Ion Batteries,* ACS Applied Materials & Interfaces, 15 (2023) 51036-51049
100. Zhang, J., X. Lu, J. Zhang, H. Li, B. Huang, B. Chen, J. Zhou, S. Jing, *Metal-ions intercalation mechanism in layered anode from first-principles calculation,* Frontiers in Chemistry, 9 (2021) 677620
101. Wang, Q., X. Wei, M. Li, Y. Zhang, Y. Yang, Y. Tian, Z. Li, S. Wei, L. Duan, *TiS2/VS2 heterostructures: A DFT study unveiling their potential as high-performance anodes for Li/Na/K-ion batteries,* Materials Today Communications, 41 (2024) 111037
102. Sotoudeh, M., M. Dillenz, A. Groß, *Mechanism of magnesium transport in spinel chalcogenides,* Advanced Energy and Sustainability Research, 2 (2021) 2100113
103. Gong, K., K. Yang, C.E. White, *Density functional modeling of the binding energies between aluminosilicate oligomers and different metal cations,* Frontiers in Materials, 10 (2023) 1089216
104. Mizanuzzaman, M., M.A. Chowdhury, R. Ahmed, M.A. Mahmud, M.A. Kowser, *DFT based investigation of Se doped MgMo6S8-ySey as promising cathode materials for Mg-ion battery application,* Scientific Reports, 15 (2025) 30817
105. Imran, S., G.N. Shao, H. Kim, *https://www. sciencedirect. com/science/article/abs/pii/S092633731500346X,* (2016)
106. Paul, A., M. Pandey, P. Johari, *Computational study of adsorption of magnesium polysulfides on VS4 magnesium sulfur batteries,* Materials Today: Proceedings, 76 (2023) 352-358
107. Kheralla, A. ,N. Chetty, *A review of experimental and computational attempts to remedy stability issues of perovskite solar cells,* Heliyon, 7 (2021)
108. He, Q., B. Yu, Z. Li, Y. Zhao, *Density functional theory for battery materials,* Energy & Environmental Materials, 2 (2019) 264-279
109. Wu, J., Z. Yu, Y. Yao, L. Wang, Y. Wu, X. Cheng, Z. Ali, Y. Yu, *Bifunctional catalyst for liquid–solid redox conversion in room-temperature sodium–sulfur batteries,* Small Structures, 3 (2022) 2200020
110. Song, H., Y. Li, X.L. Li, Y. Li, D.s. Li, D. Wang, S. Huang, H.Y. Yang, *Recent progress in heterostructured materials for room-temperature sodium-sulfur batteries,* Interdisciplinary Materials, 3 (2024) 565-594
111. Salvatore, K.L., J. Fang, C.R. Tang, E.S. Takeuchi, A.C. Marschilok, K.J. Takeuchi, S.S. Wong, *Microwave-assisted fabrication of high energy density binary metal sulfides for enhanced performance in battery applications,* Nanomaterials, 13 (2023) 1599
112. Shen, M., S. Xu, X. Wang, Y. Zhang, Y. Feng, F. Xing, Y. Yang, Q. Gao, *Modification and Functionalization of Separators for High Performance Lithium–Sulfur Batteries,* International Journal of Molecular Sciences, 25 (2024) 11446

113. Wang, L., S. Riedel, J. Drews, Z. Zhao-Karger, *Recent developments and future prospects of magnesium–sulfur batteries,* Frontiers in Batteries and Electrochemistry, 3 (2024) 1358199
114. Du, S., Y. Yu, X. Liu, D. Lu, X. Yue, T. Liu, Y. Yin, Z. Wu, *Catalytic engineering for polysulfide conversion in high-performance lithium-sulfur batteries,* Journal of Materials Science & Technology, 186 (2024) 110-131
115. Li, T., Z. Wang, J. Hu, H. Song, Y. Shi, Y. Jiang, D. Zhang, S. Huang, *Manipulating polysulfide catalytic conversion through edge site construction, hybrid phase engineering, and Se anion substitution for kinetics-enhanced lithium-sulfur battery,* Chemical Engineering Journal, 471 (2023) 144736
116. Puntambekar, U., S. Veliah, R. Pandey, *Point-defects in magnesium sulfide,* Journal of materials research, 9 (1994) 132-134
117. Chen, T., G. Sai Gautam, P. Canepa, *Ionic transport in potential coating materials for Mg batteries,* Chemistry of Materials, 31 (2019) 8087-8099
118. Lu, J., T. Wu, K. Amine, *State-of-the-art characterization techniques for advanced lithium-ion batteries,* Nature Energy, 2 (2017) 1-13
119. Islam, M.S. ,C.A. Fisher, *Lithium and sodium battery cathode materials: computational insights into voltage, diffusion and nanostructural properties,* Chemical Society Reviews, 43 (2014) 185-204
120. Oganov, A.R., C.J. Pickard, Q. Zhu, R.J. Needs, *Structure prediction drives materials discovery,* Nature Reviews Materials, 4 (2019) 331-348
121. Vincent, S., J.H. Chang, P. Canepa, J.M. García-Lastra, *Mechanisms of electronic and ionic transport during Mg intercalation in Mg–S cathode materials and their decomposition products,* Chemistry of Materials, 35 (2023) 3503-3512
122. Rajput, N.N., X. Qu, N. Sa, A.K. Burrell, K.A. Persson, *The coupling between stability and ion pair formation in magnesium electrolytes from first-principles quantum mechanics and classical molecular dynamics,* Journal of the American Chemical Society, 137 (2015) 3411-3420
123. Zhang, Z., Z. Cui, L. Qiao, J. Guan, H. Xu, X. Wang, P. Hu, H. Du, S. Li, X. Zhou, *Novel design concepts of efficient Mg-Ion electrolytes toward high-performance magnesium–selenium and magnesium–sulfur batteries,* Advanced Energy Materials, 7 (2017) 1602055
124. DeWitt, S., N. Hahn, K. Zavadil, K. Thornton, *Computational examination of orientation-dependent morphological evolution during the electrodeposition and electrodissolution of magnesium,* Journal of The Electrochemical Society, 163 (2015) A513
125. Chadwick, A.F., G. Vardar, S. DeWitt, A.E. Sleightholme, C.W. Monroe, D.J. Siegel, K. Thornton, *Computational model of magnesium deposition and dissolution for property determination via cyclic voltammetry,* Journal of The Electrochemical Society, 163 (2016) A1813
126. Latz, A. ,J. Zausch, *Thermodynamic consistent transport theory of Li-ion batteries,* Journal of Power Sources, 196 (2011) 3296-3302
127. Drews, J., P. Jankowski, J. Häcker, Z. Li, T. Danner, J.M. García Lastra, T. Vegge, N. Wagner, K.A. Friedrich, Z. Zhao-Karger, *Modeling of Electron-Transfer Kinetics in Magnesium Electrolytes: Influence of the Solvent on the Battery Performance,* ChemSusChem, 14 (2021) 4820-4835
128. Krauskopf, T., F.H. Richter, W.G. Zeier, J.r. Janek, *Physicochemical concepts of the lithium metal anode in solid-state batteries,* Chemical reviews, 120 (2020) 7745-7794
129. Richter, R., J. Häcker, Z. Zhao-Karger, T. Danner, N. Wagner, M. Fichtner, K.A. Friedrich, A. Latz, *Degradation effects in metal–sulfur batteries,* ACS Applied Energy Materials, 4 (2021) 2365-2376
130. Zhao, Q., R. Wang, Y. Zhang, G. Huang, B. Jiang, C. Xu, F. Pan, *The design of Co3S4@ MXene heterostructure as sulfur host to promote the electrochemical kinetics for reversible magnesium-sulfur batteries,* Journal of Magnesium and Alloys, 9 (2021) 78-89
131. Yang, Y., W. Fu, D. Zhang, W. Ren, S. Zhang, Y. Yan, Y. Zhang, S.-J. Lee, J.-S. Lee, Z.-F. Ma, *Toward high-performance Mg-S batteries via a copper phosphide modified separator,* ACS nano, 17 (2022) 1255-1267
132. Ladha, D.G., *A review on density functional theory–based study on two-dimensional materials used in batteries,* Materials Today Chemistry, 11 (2019) 94-111
133. Miao, W., H. Peng, S. Cui, J. Zeng, G. Ma, L. Zhu, Z. Lei, Y. Xu, *Fine nanostructure design of metal chalcogenide conversion-based cathode materials for rechargeable magnesium batteries,* Iscience, 27 (2024)

 doi:10.20944/preprints202510.1895.v1

134. Liu, J., T. Shen, J.-C. Ren, S. Li, W. Liu, *Role of van der Waals interactions on the binding energies of 2D transition-metal dichalcogenides,* Applied Surface Science, 608 (2023) 155163
135. Giuffredi, G., T. Asset, Y. Liu, P. Atanassov, F. Di Fonzo, *Transition metal chalcogenides as a versatile and tunable platform for catalytic CO2 and N2 electroreduction,* ACS Materials Au, 1 (2021) 6-36
136. Liu, Y., B.V. Merinov, W.A. Goddard III, *Origin of low sodium capacity in graphite and generally weak substrate binding of Na and Mg among alkali and alkaline earth metals,* Proceedings of the National Academy of Sciences, 113 (2016) 3735-3739
137. Gu, G.H., J. Noh, I. Kim, Y. Jung, *Machine learning for renewable energy materials,* Journal of Materials Chemistry A, 7 (2019) 17096-17117
138. Agrawal, A. ,A. Choudhary, *Perspective: Materials informatics and big data: Realization of the "fourth paradigm" of science in materials science,* Apl Materials, 4 (2016)
139. Gabardi, S., E. Baldi, E. Bosoni, D. Campi, S. Caravati, G. Sosso, J. Behler, M. Bernasconi, *Atomistic simulations of the crystallization and aging of GeTe nanowires,* The Journal of Physical Chemistry C, 121 (2017) 23827-23838
140. Herring, P., C.B. Gopal, M. Aykol, J.H. Montoya, A. Anapolsky, P.M. Attia, W. Gent, J.S. Hummelshøj, L. Hung, H.-K. Kwon, *BEEP: A python library for battery evaluation and early prediction,* SoftwareX, 11 (2020) 100506
141. Sulzer, V., S.G. Marquis, R. Timms, M. Robinson, S.J. Chapman, *Python battery mathematical modelling (PyBaMM),* Journal of Open Research Software, 9 (2021)
142. Liu, X., X.-Q. Zhang, X. Chen, G.-L. Zhu, C. Yan, J.-Q. Huang, H.-J. Peng, *A generalizable, data-driven online approach to forecast capacity degradation trajectory of lithium batteries,* Journal of Energy Chemistry, 68 (2022) 548-555
143. Lombardo, T., M. Duquesnoy, H. El-Bouysidy, F. Årén, A. Gallo-Bueno, P.B. Jørgensen, A. Bhowmik, A. Demortiere, E. Ayerbe, F. Alcaide, *Artificial intelligence applied to battery research: hype or reality?,* Chemical reviews, 122 (2021) 10899-10969
144. Liu, X., H.J. Peng, B.Q. Li, X. Chen, Z. Li, J.Q. Huang, Q. Zhang, *Untangling degradation chemistries of lithium-sulfur batteries through interpretable hybrid machine learning,* Angewandte Chemie International Edition, 61 (2022) e202214037
145. Orikasa, Y., T. Masese, Y. Koyama, T. Mori, M. Hattori, K. Yamamoto, T. Okado, Z.-D. Huang, T. Minato, C. Tassel, *High energy density rechargeable magnesium battery using earth-abundant and non-toxic elements,* Scientific reports, 4 (2014) 5622
146. Chen, W., Z. Lin, X. Zhang, H. Zhou, Y. Zhang, *AI-driven accelerated discovery of intercalation-type cathode materials for magnesium batteries,* Journal of Energy Chemistry, 108 (2025) 40-46
147. Jain, A., S.P. Ong, G. Hautier, W. Chen, W.D. Richards, S. Dacek, S. Cholia, D. Gunter, D. Skinner, G. Ceder, *Commentary: The Materials Project: A materials genome approach to accelerating materials innovation,* APL materials, 1 (2013)
148. Batzner, S., A. Musaelian, L. Sun, M. Geiger, J.P. Mailoa, M. Kornbluth, N. Molinari, T.E. Smidt, B. Kozinsky, *E (3)-equivariant graph neural networks for data-efficient and accurate interatomic potentials,* Nature communications, 13 (2022) 2453